ENERGY LEVELS IN Sm^{151}

ENERGY LEVELS IN SAMARIUM 151

by

DENNIS GARTH BURKE, M.Sc.

A Thesis

Submitted to the Faculty of Graduate Studies

in Partial Fulfilment of the Requirements

for the Degree

Doctor of Philosophy

McMaster University

May, 1963

DOCTOR OF PHILOSOPHY (1963) McMASTER UNIVERSITY

(Physics) Hamilton, Ontario

TITLE: Energy Levels in Sm^{151}

AUTHOR: Dennis Garth Burke, B.E. (University of Saskatchewan)
M.Sc. (University of Saskatchewan)

SUPERVISOR: Professor M. W. Johns

NUMBER OF PAGES: x, 123

SCOPE AND CONTENTS:

The energy levels of Sm^{151} populated in the beta decay of Pm^{151} have been studied with the aid of magnetic spectrometers. The internal and external conversion spectra were examined with a $\pi\sqrt{2}$ spectrometer of 50 cm radius. A Gerholm-type double lens coincidence spectrometer was used to perform electron-beta, electron-electron, electron-gamma and gamma-beta coincidence experiments. In addition, precise measurements of the transition energies obtained by Geiger and Graham (1962) with the Chalk River $\pi\sqrt{2}$ iron-free spectrometer are included. A decay scheme based on these results is proposed and speculations are made concerning the possible interpretation of the levels on the basis of the Nilsson model. The results are also compared with other recently published data on this decay.

ACKNOWLEDGEMENTS

I wish to express my gratitude to Professor M. W. Johns for encouragement and understanding during my years in his research group. His influence, both as a scientist and an individual, has formed attitudes which I hope to keep for a lifetime.

I should also like to thank the members of my supervisory committee, Dr. M. W. Johns, Dr. C. C. McMullen and Dr. G. L. Keech, for the interest which they have shown.

Assistance from other members of the Beta- and Gamma-Spectroscopy Group, in the form of technical advice, data collection and inspiring discussions, is gratefully acknowledged. In particular, I should like to thank Dr. M. E. Law for selecting the problem and performing some of the early experiments.

Thanks are also due the Chalk River Beta Spectroscopy Group for helpful advice and for the communication of data prior to publication.

Financial assistance from the National Research Council in the form of studentships is gratefully acknowledged.

I should also like to express my appreciation to my wife for her understanding attitude during my years as a student and for typing the manuscript of this thesis.

Finally, I wish to thank Mrs. Marion Tweedley for typing the final draft.

TABLE OF CONTENTS

LIST OF FIGURES

LIST OF TABLES

PREFACE

One of the principal aims in nuclear physics is the development and experimental verification of models and theories which explain the properties of the nucleus in terms of fundamental particles and forces. It is obvious that some of these properties must be determined before models can be proposed, and when theories have been developed they must be tested by further measurements. One of the most fruitful approaches to the experimental study of nuclear structure has been nuclear spectroscopy -- i.e. a study of the radiations absorbed or emitted when a nucleus undergoes transitions from one state to another. Stable nuclei can be induced to undergo such transitions or unstable nuclei can be created which decay spontaneously.

During the past half century, a great deal of information about the properties of many different nuclear species has been accumulated. It has been found that many nuclei behave as though all the nucleons act individually, whereas others show pronounced collective effects. For instance, nuclei in the mass region $150 < A < 190$ have a non-spherical shape and the energy level spectra indicate that collective rotations occur.

In an attempt to learn something of the nuclear properties in the transition region between spherical nuclei and highly deformed ones, a study of the energy levels in Sm^{151} has been carried out. The results of this investigation will be presented in Chapter 4 of this

thesis. However, before the experimental work is described, a short discussion of the theoretical concepts necessary for an understanding of the experiments is given in Chapters 1 and 2. Chapter 3 is devoted to a description of the instruments and techniques used for the measurements. The appendices describe a method of preparing thin beta sources and a Geiger counter designed for low-energy electrons.

CHAPTER 1

THEORETICAL ASPECTS OF NUCLEAR SPECTROSCOPY

Introduction

One of the aims of the experimentalist in nuclear spectroscopy is to learn as much as he can about the properties of the various energy levels in nuclei. Examples of the properties of interest may be the spin, parity and energy of the state. Most excited states are too short-lived to determine quantities such as spin and parity by studying the nucleus while it is in that particular state. However, in many cases, these properties can be deduced from a study of the transitions between the level in question and other levels for which the spins and parities are known.

The purpose of this chapter is to discuss the theoretical aspects of various types of transitions encountered in radioactive decay. These concepts are essential for an understanding of the implications of the experimental measurements to be discussed later.

1.1 Properties of Nuclear Levels

As mentioned above, some of the most commonly studied properties of nuclear levels are the energy, spin and parity. It will be seen later that there are also other important characteristics. However, as these have meaning only in terms of a particular model, they will be deferred until the next chapter.

For the purpose of decay scheme studies, the energy of a nuclear level is not determined absolutely, but is measured in

relation to some other level, usually the ground state or lowest energy level for the particular nuclide. The energies of levels can be determined most readily by observing the amounts of energy emitted or absorbed as the nucleus undergoes transitions. The study of transition energies to determine the energy differences of levels is still one of the most fruitful approaches to the determination of level schemes.

"Spin" is a term commonly used to signify the intrinsic angular momentum of a particle. In nuclear spectroscopy the term is used also for the vector sum of the intrinsic angular momenta and orbital angular momenta of all the nucleons in the nucleus. Thus the spin of a state means the resultant angular momentum of all the nucleons when the nucleus is in that state. For nucleons, the intrinsic momentum is $\frac{1}{2}\hbar$ ($\hbar = \frac{h}{2\pi}$ where h is Planck's Constant, 6.625×10^{-27} erg.sec). The orbital angular momentum of nucleons must be an integral multiple of $\hbar$. Therefore, the spin of a nucleus with an even number of nucleons must have an integral value (in units of $\hbar$), whereas a nucleus with an odd number of nucleons has a half-integral spin.

The prediction of spins is simplified considerably by the fact that the individual protons and neutrons tend to pair off and cancel each others' spins. The most striking evidence for this is the fact that the ground states of all even-even nuclei have zero spins. However, in spite of this tendency, the prediction of spins is not a simple task and no one nuclear model is successful for all nuclides.

The parity of a state is a property of the wave function which describes the state. If the sign of the wave function changes upon a reflection of the spatial co-ordinates through the origin, the parity is odd. If the sign of the wave function does not change upon such a reflection, the parity is even.

Thus $\psi(-x,-y,-z,\text{spin}) = \psi(x,y,z,\text{spin})$ for even parity

$\psi(-x,-y,-z,\text{spin}) = -\psi(x,y,z,\text{spin})$ for odd parity

1.2 Beta Decay

At present, there are four known types of physical forces: nuclear forces (arising from the π-meson field), electromagnetic forces, weak interactions and gravitational forces, in order of decreasing strength. The weak interactions are interactions whereby two fermions (particles with spin $\frac{1}{2}\hbar$) are converted into two different fermions, the most common pairs being the neutron $\rightleftharpoons$ proton and electron $\rightleftharpoons$ neutrino. Historically, three of the possible nuclear reactions among these particles and their antiparticles have become classed as beta decay:

$n \longrightarrow p^+ + e^- + \bar{\nu}$

a neutron decaying into a proton, an electron and an anti-neutrino. This reaction describes the beta decay of all neutron-rich nuclei, including the free neutron.

$p^+ \longrightarrow n + e^+ + \nu$

a proton decaying into a neutron, a positron and a neutrino. This reaction describes the positron decay of proton-rich nuclei. It cannot take place with free protons because of energy considerations.

$p^+ + e^- \longrightarrow n + \nu$

a proton and an electron interact to form a neutron and a neutrino. This reaction is observed when atomic electrons interact with protons in the nucleus.

In the first two cases shown above the excess energy of the reaction is shared statistically between the electron and the neutrino; hence, the distribution in energy for each particle is a continuum.

As the neutrino interacts so weakly with matter, it was observed only during the last decade after long and careful experiments (Reines and Cowan (1953,1959)). It would not have been possible in the first quarter of the present century to discover this particle with the techniques then available. Therefore, while early workers found the continuous energy distribution of the electrons, they could not see the complementary energy which was carried away by the neutrino. For several years it was not decided whether the actual decay energy was represented by the average beta energy or by the beta end-point energy. Sargent (1925) cleared up this point by showing that the end-point energy of the beta spectrum was the decay energy. Physicists at this time were in a dilemma because it appeared that energy was conserved only for the very few events where the beta particle was emitted with the maximum energy. Furthermore, since the number of nucleons does not change, the spin of the nucleus remains integral for even-A or half-integral for odd-A during a beta decay. Since the electrons' angular momentum is half-integral, the law of conservation of angular momentum also appeared to break down. In order to preserve these cherished laws of physics, Pauli(1934) suggested that beta-decay processes were accompanied by the emission of

a new particle with spin $\frac{1}{2}\hbar$, no charge or mass, and a very low cross section for interaction with matter. This particle, called the neutrino, had to wait almost twenty-five years for the improved techniques required for its experimental verification.

Fermi (1934) incorporated Pauli's hypothesis into the first successful theory of beta decay. This theory was so comprehensive in scope that it has withstood the test of time and has been only sharpened by the recent parity upset. Fermi's original theory was constructed in analogy with that for electromagnetic interactions. From the perturbation theory, the probability for the interaction may be written

$$\lambda = \frac{2\pi}{\hbar}\left|\langle\psi_f^*\varphi_f^*|H_\beta|\psi_i\varphi_i\rangle\right|^2 \rho_e$$

where ψ_i and ψ_f represent initial and final nuclear states, φ_i and φ_f are initial and final lepton states. H_β is the interaction Hamiltonian and ρ_e is the density of final states. The form of H_β has been the subject of much discussion. In addition to the operators which are obviously necessary to convert neutrons into protons, neutrinos into electrons, etc., there may be still other operators, O_x, present. Konopinski and Uhlenbeck (1941) discuss the five different forms that O_x can take and still satisfy the conditions of Lorentz invariance, conservation of momentum and of angular momentum. These five forms are called the scalar, pseudo scalar, vector, axial vector and tensor interactions and are denoted by S,P,V,A and T, respectively. As parity is not conserved in beta decay (Wu et al.(1957)) each of these types of operator can enter the Hamiltonian through one term which conserves parity and another which does not conserve parity. Thus, there are

ten constants to be determined. Goldhaber et al. (1958) have shown that the neutrinos found in beta decay have negative helicity. This fact can be used to show that the parity-conserving terms have the same coefficients as the ones which do not conserve parity. Hence, the problem reduces to five unknown constants. From the work of Wu et al. (1957), it is known that beta particles have negative helicity. Since the S, T and P interactions would produce negatrons with a positive helicity, these forms can be ruled out, leaving only the A and V interactions. It had been known for some time that at least two types of interaction must exist because two sets of selection rules for the change in angular momentum had been found experimentally. The V interaction is the one which was first used by Fermi and results in the so-called Fermi selection rules. The A interaction yields the Gamow-Teller selection rules. A brief listing of the most common selection rules for spin and parity (π) is shown below.

Type of Transition	Fermi or Vector		Gamow-Teller or Axial Vector	
Allowed	$\Delta I=0$	$\Delta\pi$ = No	$\Delta I=0,\pm1$	$\Delta\pi$ = No
First Forbidden	$\Delta I=0,\pm1$	$\Delta\pi$ = Yes	$\Delta I=0,\pm1,\pm2$	$\Delta\pi$ = Yes
Second Forbidden etc.	$\Delta I=\pm2$	$\Delta\pi$ = No	$\Delta I=\pm2,\pm3$	$\Delta\pi$ = No

Both types of interaction consist of a term due to the charge density of the nucleons plus a much smaller term due to the currents caused by the moving nucleons. If the effects of the atomic electrons are ignored, the lepton wave functions are plane waves and can be expanded as a series in which each term is much larger than the following one. The product of the largest nuclear term and the largest leptonic

term results in the matrix element for allowed beta decay. If this term happens to be zero, decay can still take place through various products of the smaller terms, resulting in the so-called forbidden transitions with the degree of forbiddenness depending on how many terms it is necessary to consider.

By integrating the transition probabilities over all the unobserved quantities, the momentum distribution of the beta particles is found to be

$$N'(p) = C|M|^2 F(Z,E)p^2(E_o - E)^2 S_n$$

where C is a constant, M is the nuclear matrix element, F(Z,E) is the Fermi function which corrects for effects of the atomic electrons, p is the electron momentum, E is electron energy and E_o is the maximum beta energy. The shape factor, S_n, is a constant for most allowed and first forbidden transitions except the first forbidden unique ($\Delta I = \pm 2$) case and will be ignored from here on.

From the above expression, it is seen that a plot of $\left[N'(p)/p^2F\right]^{\frac{1}{2}}$ against energy should result in a straight line which intercepts the energy axis at $E = E_o$. Such a plot is called a Fermi plot and is useful in the determination of beta end point energies.

If one integrates the probability of decay over all momenta, it is seen that the total probability of decay is

$$\lambda = \frac{\ln 2}{T_{\frac{1}{2}}} = C|M|^2 f(Z,E_o)$$

where $T_{\frac{1}{2}}$ is the half-life and $f = \int F(Z,E)p^2(E_o - E)^2 dp$. Values of the integral $f(Z,E_o)$ have been tabulated (Feenberg (1950)) and hence the product $fT_{\frac{1}{2}}$ can be found. The values of $fT_{\frac{1}{2}}$ involve the nuclear matrix

elements and vary over a wide range. In practice it is found that $\log_{10}(fT_{\frac{1}{2}})$ is in the region 3 to $\sim$6 for allowed transitions, $\sim$ 6 to $\sim$9 for first forbidden transitions, and so on. Thus, the $\log(fT_{\frac{1}{2}})$ value can give a rough indication of the degree of forbiddenness of a transition.

1.3 Electromagnetic Transitions

An excited state of a nucleus may lose its excess energy by the emission of electromagnetic radiation. This radiation is classified as being of multipole order λ when the quantum carries away λ units of angular momentum. There is a further classification into electric (E) or magnetic (M) transitions, depending on whether a parity change is involved. For electric transitions $\Delta\pi = (-1)^{\lambda}$, while for magnetic transitions $\Delta\pi = (-1)^{\lambda+1}$. In this notation $\Delta\pi = 1$ means that there is no parity change, whereas $\Delta\pi = -1$ means that the parity does change. The names for these classes of radiation are carried over from classical theory where Eλ and Mλ are the types of radiation emitted from oscillating electric and magnetic 2^{λ} poles, respectively. There is a selection rule on the possible initial and final values of the nuclear spin, I_i and I_f for a given λ. They must obey the triangle relation $|I_i - I_f| \leq \lambda \leq I_i + I_f$ Transitions for which $I_i = I_f = 0$ are forbidden and no transitions occur with $\lambda = 0$.

The transition probability for emission of a photon of energy $\hbar\omega$ ($\omega = c\,k$), with the nucleus going from state i to state f, is (Preston 1962)

$$T(\sigma\lambda) = \frac{8\pi(\lambda+1)}{\lambda[(2\lambda+1)!!]^2} \frac{k^{2\lambda+1}}{\hbar} B(\sigma\lambda)$$

where

$$B(\sigma\lambda) = (2J_i + 1)^{-1} \sum_{M_i, M_f} |\langle f | O_{\lambda\mu} | i \rangle|^2$$

is the so-called reduced matrix element. σ refers to the type of transition, electric or magnetic, and $O_{\lambda\mu}$ is the appropriate electric or magnetic multiple operator for the transition.

From this expression it is seen that the transition probability decreases rapidly as λ increases. Thus, for either electric or magnetic transitions, only the lowest multipole order allowed by angular momentum and parity considerations will be present with appreciable intensity. However, there can be competition between electric and magnetic transitions because the latter are slower than the former by a factor of approximately $R\left(\frac{Mc}{\hbar}\right)^2$ where R is the radius of the nucleus and M is the mass of a nucleon. Such competition is found most often between M1 and E2 transitions because collective effects in deformed nuclei enhance the E2 transition probability to such an extent that it can be comparable with that for M1 transitions.

Since the nuclear wave functions are not known, values for $T(\sigma\lambda)$ cannot be calculated unless some model is assumed for the nucleus. The earliest calculations were for single particle transitions in the shell model (Weisskopf(1951)). The probabilities for electric and magnetic transitions were found to be (Preston (1962))

$$T_w(E\lambda) = \frac{2(\lambda+1)}{\lambda\left[(2\lambda+1)!!\right]^2}\left(\frac{3}{\lambda+3}\right)^2\frac{e^2}{\hbar c}\left(\frac{\omega R}{c}\right)^{2\lambda}\omega \text{ sec}^{-1}$$

$$T_w(M\lambda) = \frac{2(\lambda+1)}{\lambda\left[(2\lambda+1)!!\right]^2}\left(\frac{3}{\lambda+2}\right)^2\frac{e^2}{\hbar c}\left(\frac{\hbar/Mc}{R}\right)^2\left(\mu_p\lambda - \frac{\lambda}{\lambda+1}\right)^2\left(\frac{\omega R}{c}\right)^{2\lambda}\text{sec}^{-1}$$

where μ_p is the proton magnetic moment. These values are found to agree with experiment within an order of magnitude for most cases. The most striking exception is for the case of E2 transitions in deformed nuclei

where collective effects enhance the transition probability by several orders of magnitude. It has become a common practice to use the single particle estimates as standards to which experimental results and the predictions of other models are compared.

1.4 Internal Conversion

A mode of decay which always competes with gamma emission is internal conversion. In this process, the excitation energy of the nucleus is transferred by the electromagnetic fields to one of the atomic electrons. The electron is then ejected from the atom with a kinetic energy $E_k = E_o - E_B$ where E_o is the transition energy (equivalent to the energy of the competing gamma ray) and E_B is the binding energy of the electron in the atom. Since both quantities on the right-hand side have definite values, the conversion electrons appear as line spectra in contrast with the continuous distribution of the electrons in beta decay. For any given gamma transition, several competing conversion lines will appear, corresponding to internal conversion of electrons from the K, L_1, L_2, L_3 etc. shells.

The internal conversion process can be classified according to multipolarities in the same way as for the competing electromagnetic transitions. If the finite size of the nucleus is neglected, the transition probability for internal conversion involves the same matrix elements as that for the competing gamma ray. Thus, the ratio of the transition rates for the two processes is independent of the detailed motions of the nucleons and can be calculated quite accurately. This ratio is called the internal conversion coefficient α_i

$$\alpha_i = \frac{\text{Probability of internal conversion in the ith shell}}{\text{Probability of the competing gamma ray}}$$

The total conversion coefficient $\alpha = \sum_i \alpha_i$. A measurement of α_K can often lead to a unique determination of the multipolarity of a transition. Other ratios which are also useful in this respect are $\alpha_K : \alpha_L$, $\alpha_{L_1} : \alpha_{L_2} : \alpha_{L_3}$ etc. Rose et al. (1951) have calculated conversion coefficients assuming the nucleus to be a point charge. In actual fact, the finite size of the nucleus does have an appreciable effect in some cases. There are two effects. The electronic wave function is different in the case of a point nucleus to what it is for a nucleus of finite size. A correction for this effect has been made in more recent calculations by Rose (1958) and Sliv and Band (1956,1958). Also, with a nucleus of finite size, the electrons can spend a portion of their time inside the nucleus, and in this case the form of the matrix elements is no longer the same as for the corresponding electromagnetic transitions. The correction for this effect is small unless the competing gamma transition happens to be forbidden as, for example, in the case of E0 transitions.

CHAPTER 2

NUCLEAR MODELS

Introduction

No general theory or model of the nucleus presently available will explain all the experimentally observed properties of nuclei under different conditions and in different mass regions. However, several different models have had success in describing phenomena restricted to certain energy regions or to certain classes of nuclei. For instance, the shell model and collective model are useful in describing the properties of the ground states and low energy levels of most nuclei, whereas the optical model and statistical model are more convenient for describing higher energy processes such as nuclear reactions. As the present work involves relatively low energy decay processes, the only models which will be considered further are those applicable to low energy phenomena.

2.1 The Shell Model

The shell model, introduced independently by Mayer (1948, 1949, 1950) and Haxel, Jensen and Suess (1949,1950), began with no theoretical justification but is surprisingly useful, due to its successes in predicting nuclear properties pertaining to magic numbers. The "magic numbers" are found empirically to be 2, 8, 14, 20, 28, 50, 82 and 126. The model assumes that each nucleon moves in the average potential of all the other nucleons in the nucleus and that the total

internal motion can be obtained by summing these independent motions. Each nucleon in this potential can be described by its own set of quantum numbers which determine its nuclear level. The order of filling of the levels is dictated by the level energy and the Pauli exclusion principle. If there happens to be a relatively large energy region with no levels, then "closed shell" effects are expected when all the levels up to this energy region have been filled.

Using this procedure, the magic numbers 2 and 8 appear quite naturally as the closing of the 1s and 1p shells, using almost any reasonable form for the potential. However, on this simple picture, there was no reason to predict any of the other magic numbers. Mayer (1948) and Haxel, Jensen and Suess (1949) overcame this difficulty by postulating a strong coupling between the spin of a nucleon and its orbital angular momentum. This adds another term to the potential of the form $f(r)\ \underline{l}.\underline{s}$ where $f(r)$ describes the radial dependence and $\underline{l}$ and $\underline{s}$ are the orbital and spin angular momenta. The effect of the spin-orbit force is to separate the levels with the two possible j-values for each $\underline{l}$-value by an amount of energy proportional to $\underline{l}$. As the effect is more important for larger values of $\underline{l}$, the strength of the interaction can be chosen so as to depress the levels with high angular momentum down to the next shell. When this is done, it turns out that the closing of major shells can be made to occur for nucleon numbers which correspond to the observed magic numbers.

According to this model, nucleons in closed shells should couple their angular momenta in such a way that the resultant for the entire shell is zero. If there is one particle outside of a closed

shell the only contribution to the total spin is from that particle. Similarly, nuclei which are one particle short of a closed shell have a spin contribution from the single "hole." Cases with several nucleons outside of closed shells are more complicated. The measured spins of nuclei near closed shells agree very well with those predicted by this model.

Another success of the shell model is the explanation of the "Islands of Isomerism." These are values of N or Z near which many nuclides with relatively long-lived isomeric states are found. These are readily explained by the existence of the high angular momentum state which has been depressed by the $\underline{l} \cdot \underline{s}$ force into a lower shell with many states of lower angular momenta. The low transition probability for electromagnetic transitions with large angular momentum changes results in long half-lives.

The model just described is often called the extreme single particle model, and the term, "single particle model," includes extensions of the simple case described above. A great deal of work has been done to extend this model to the case of several nucleons outside closed shells. For instance, by including the interactions between particles outside closed shells, better agreement with the observed order of levels is obtained. Such corrections are also useful in explaining the deviations of the magnetic moments from the "Schmidt limits" which are predicted by the simple theory.

There are other nuclear properties, however, for which the shell model does not work so well. For instance, the large electric

quadrupole moments and the fast E2 transitions for nuclei not near magic numbers cannot be explained by this model. We shall see in the next section that a theory which includes the collective motions of the nucleons predicts these properties in a natural way.

2.2 Collective Motions

Collective motions in nuclei are of two types: vibrations and rotations. Vibrations are oscillations in the shape of the nucleus; rotations constitute a rotation of nuclear matter about some axis in the nucleus. The whole nucleus need not rotate as does a rigid body; instead, the process may be thought of as the motion of a surface wave around a spherical core.

In order to discuss these effects, we shall at first neglect any intrinsic nuclear spin (e.g. assume an even-even nucleus) and also assume that the excited states due to collective motions have lower energies than the next particle state. Interactions of particle levels with collective levels will be discussed later.

To consider vibrations, it is usual to assume a non-spherical nucleus with a "surface" given in polar co-ordinates by

$$R(\theta,\varphi) = R_o\left[1 + \sum_{\lambda\mu} \alpha_{\lambda\mu} Y_{\lambda\mu}(\theta,\varphi)\right]$$

R_o is the radius of an equivalent spherical nucleus, $Y_{\lambda\mu}(\theta,\varphi)$ are spherical harmonics of order λ,μ and the $\alpha_{\lambda\mu}$ are the deformation parameters. The $\alpha_{\lambda\mu}$ vary with time, of course, if the nuclear shape is changing. Assuming that the nuclear matter behaves somewhat like a fluid, it is possible to set up expressions for the kinetic and

potential energies and obtain relationships for the frequency of vibration of the surface, ω_λ. These vibrations are called phonons, of order λ, and have associated with them an angular momentum λ, parity $(-1)^\lambda$ and an energy $\hbar\omega_\lambda$. The frequency ω_λ increases quite rapidly with λ so we need consider only the low values of λ since we are interested only in the low energy nuclear levels. Terms with $\lambda = 0$ and $\lambda = 1$ can be ignored, as they represent density oscillations of a spherical nucleus and vibrations of the mass center, respectively. Thus, the first mode of vibration would be a phonon with $\lambda = 2$ and therefore would result in a 2+ state in an even-even nucleus. The next mode of vibration as one increases the energy would be either one $\lambda = 3$ phonon or two $\lambda = 2$ phonons. The latter case of coupling two $\lambda = 2$ phonons together would give a 0+, a 2+ or a 4+ level at about twice the energy of the first 2+ level. There should be no crossover transition from the second 2+ level to the ground state, as only one phonon can be destroyed at a time. These predictions are found to agree well with experiment as many nuclides have been found near closed shells with a 2+ level as the first excited state and with 0+, 2+, and 4+ levels at about twice this energy. In such cases, the ground state transition from the second 2+ state is absent or weak. Some 3- states assumed to be due to the presence of a $\lambda = 3$ phonon have also been observed.

For deformations with $\lambda = 2$ it is convenient to describe the nucleus by two parameters β and γ which are simply related to the $\alpha_{2\mu}$'s by $\alpha_{20} = \beta \cos\gamma$ and $\alpha_{22} = (1/\sqrt{2})\beta \sin\gamma$. Then β is a measure of the total deformation of the nucleus and γ determines whether the

nucleus has a symmetry axis. If $\gamma = 0$ or a multiple of 30°, there is a symmetry axis; otherwise, the nucleus is an ellipsoid with three unequal axes. If we have a beta vibration (where β changes with time), the symmetry axis can be retained but the eccentricity changes. If the nucleus undergoes gamma vibrations (γ varies with time), it loses its axial symmetry.

If the nucleus has a large permanent deformation, the equations of motion show that there may be oscillations in the shape (vibrations) or changes in the orientation of the nucleus (rotations). The motions can be separated and the energy associated with the rotational part can be written:

$$E_R = \frac{\hbar^2}{2}\left[\frac{J(J+1)-K^2}{\mathcal{I}_1} + \frac{K^2}{\mathcal{I}_3}\right]$$

for the case of axial symmetry. $\mathcal{I}_3$ and $\mathcal{I}_1$ are the moments of inertia about axes along and perpendicular to the symmetry axis, respectively. J is the total angular momentum and K is its component along the symmetry axis. These and other important angular momentum quantum numbers are shown in Figure 1. The moment of inertia about a symmetry axis is zero so that, for low energies, K=0 and the rotational energy is simply $E_R = \frac{\hbar^2}{2\mathcal{I}_1}J(J+1)$. Since there is a plane of symmetry perpendicular to the symmetry axis, J can take on even values only, for K=0. Thus, the energies of the first, second, third and fourth excited levels in a rotational band should appear in the ratio 1: 10/3: 7:12. The observed level spacings in some well deformed even-even nuclei agree well with this prediction. For example, according to the Nuclear Data Sheets (1959) the observed

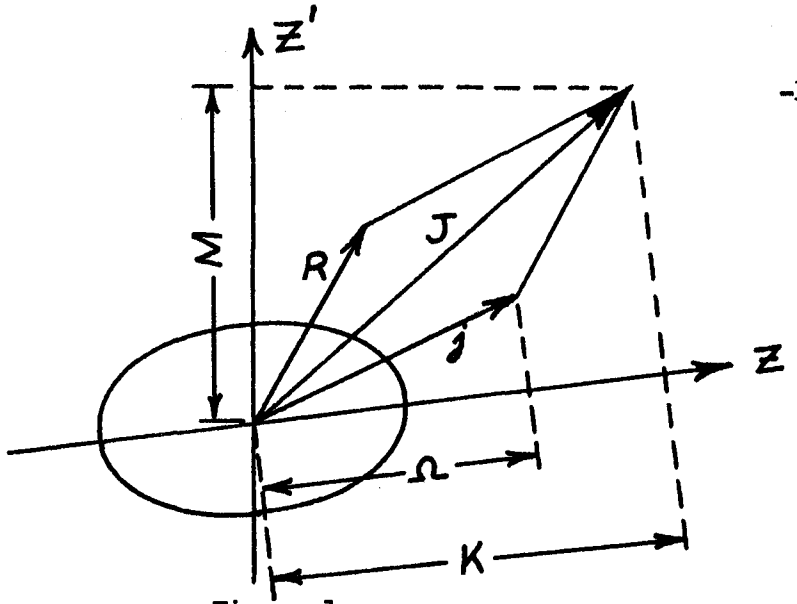

Figure 1

ratios of the first levels in Hf^{180} are 1: 3.32: 6.89: 11.67. The deviations from the expected values can be explained as due to other perturbations. For the case where K does not equal zero, J takes on the values K, K+1, K+2, etc.

For odd nuclei, the intrinsic spin is non-zero and it becomes necessary to consider the coupling of the collective motions with the particle motions. If one assumes that the nucleus is well deformed, the so-called "strong coupling" case, the energy of a state can be written

$$\frac{\hbar^2}{2\mathcal{I}}\left[J(J+1) - K^2-\Omega^2\right] + \frac{\hbar^2}{2\mathcal{I}_3}\left[K-\Omega\right]^2 + \text{RPC} + \epsilon_\Omega$$

where Ω is the component of the particle angular momentum (j) along the symmetry axis (see Figure 1). Since $\mathcal{I}_3 = 0$, we see that $K = \Omega$ for low-lying states. The quantity ϵ_Ω involves particle motions only, whereas the rotational particle coupling term (RPC) is analagous to a Coriolis term and involves both particle and core motions. The RPC energy is negligible except in two special cases. If a nucleus has two closely spaced particle states differing by one

unit in K, important perturbations can result. Kerman (1956) attributes the disturbed order of the band structure in W^{183} to this effect. The other case where the RPC term is important is in a rotational band for which $\Omega = \frac{1}{2}$. In this case it takes the value

$$RPC = \frac{\hbar^2}{2\mathcal{J}} a(-1)^{J+\frac{1}{2}}(J + \tfrac{1}{2})$$

where a is a constant called the decoupling parameter. Hence, the rotational energy for states in a given band is

$$E_R = \frac{\hbar^2}{2\mathcal{J}} \left[J(J + 1) - 2K^2 + \delta_{K,\frac{1}{2}}\, a(-1)^{J+\frac{1}{2}}(J + \tfrac{1}{2}) \right]$$

For bands with $K=\frac{1}{2}$, the Coriolios term can be sufficiently large that some state other than the one with $J=\frac{1}{2}$ may appear as the ground state.

2.3 The Unified Model

The existence of large deformations for even-even nuclei in regions not near closed shells suggested the possibility that the particle states might be affected by the distortion. Nilsson (1955) calculated the single particle energies for axially-symmetrical ellipsoidal potentials of various eccentricity. For ease of calculation, he chose a simple harmonic oscillator potential and, in order to make a closer approximation to reality, added terms which were essentially proportional to $\underline{l}\cdot\underline{s}$ and $\underline{l}^2$. The strengths of these terms were adjusted so that the calculations yielded the observed level spacings for spherical nuclei. The results are presented in the form of graphs showing the energy of

the various particle states as a function of deformation and tables giving the wave functions of the states. For example, using Nilsson's notation, a wave function may be expressed as

$$\psi = \sum a_{\ell\Lambda} \left| N\ell\Lambda\Sigma \right\rangle$$

Here N is the total number of oscillator quanta, ℓ is the particle's orbital angular momentum and Λ is its component along the symmetry axis. Σ is the component of spin along the symmetry axis and thus $\Omega = \Lambda + \Sigma$. The $a_{\ell\Lambda}$ are the quantities which are found in Nilsson's tables. For large deformations, it is common to refer to a state using its asymptotic quantum numbers $\left[N\, n_3 \Lambda\right]$ where n_3 is the number of oscillator quanta along the symmetry axis.

In order to see which state this model predicts for any nuclide, one simply counts up the orbitals at the appropriate deformation, placing two particles in each. Thus, for an odd-Z nucleus, the last proton would go into an orbital which would not be filled and the total proton contribution to the spin would be just that of the last orbital. Spins predicted in this manner agree very well with those observed for a large number of nuclides in the three well-known regions of deformed nuclei $A \sim 25$, $150 < A < 190$ and $220 < A$ (Mottelson and Nilsson (1959)). Of course it is possible to build rotational and vibrational bands on each particle state, as discussed in the last section. Vibrational structure cannot be identified as easily as in spherical nuclei, however, because the level density is so great that several particle states are usually found below the excitation energy required for vibrations.

The equilibrium shape of a given nucleus can also be predicted from the model by adding up all the single particle energies for different deformations and finding the deformation for which this total energy is minimized. Mottelson and Nilsson (1959) have made such calculations for many nuclei and find that their results agree well with the observed values obtained from measurements of electric quadrupole moments. Better agreement with experiment is obtained if one extends the model by including the effects of pairing forces. When this is done, the sudden change in deformation which occurs, for example, between N = 88 and N = 90 is explained quite naturally. An interaction between the quadrupole moment of a given particle and the total nuclear quadrupole moment tends to distort the nucleus. At the same time, the pairing forces tend to produce a spherical shape. Belyaev (1959) shows that as the number of nucleons is increased a value is reached for which the net effect of these two forces changes sign, leading to a rapid change in deformation.

Nilsson's model has also had much success in predicting transition rates between levels in distorted nuclei. Alaga (1955, 1957) gives the selection rules for the quantum numbers N, n_3, Λ and K which characterize a state in the limit of large deformations. Mottelson and Nilsson (1959) have compiled tables which show that beta and gamma transitions which disobey these asymptotic selection rules are hindered with respect to transitions which are allowed by the selection rules.

The model also predicts correctly the main variations of such quantities as nuclear magnetic moments and decoupling parameters for bands with $K = \frac{1}{2}$. Thus it is seen that the successes of the collective model have been combined with the shell model which worked so well near magic numbers. The result is a picture of the nucleus which explains an enormous body of experimental detail pertaining to low energy states and transitions.

2.4 Asymmetric Nuclei

Davydov et al. (1958,1959) have calculated the energies for rotational states of nuclei which do not possess axial symmetry. Their treatment is a generalization of that discussed in the last section with β and γ assumed to have stable non-zero values. Since the nucleus now has unequal moments of inertia about the three axes, a greater variety of rotations is possible and hence there is a larger number of rotational levels. In the limit of axial symmetry, the predictions are the same as in the last section, of course, because the new levels rapidly rise to an infinite energy due to the factor $\mathcal{I}_3$ which tends to zero in the denominator. The levels which are present for axial symmetry are not strongly affected by a large permanent value of γ.

According to this model, the levels classed as vibrational states in the last section, and the rotational bands based on them, are interpreted as being the new rotational levels brought in by the asymmetry. For instance, Preston (1962) points out that the 3+ and 5+ levels observed in some even-even nuclei can be explained

either by the asymmetric rotator model or by vibrations and rotations of an axial nucleus. It is a difficult task to determine experimentally which of these pictures is correct, as they give similar predictions for many nuclear properties. Actually, both are simplified pictures of the same physical behaviour and perhaps a combination of the two would be closer to reality. One model assumes that γ undergoes oscillations about the value zero, whereas the other assumes γ to be fixed at some non-zero value. It is not surprising that rotational bands based on vibrations of rms value γ_o are similar to rotations of a nucleus with an asymmetry corresponding to γ_o. The asymmetrical model has the advantage that, as one goes through transition regions from spherical nuclei to deformed nuclei, the observed levels are all explained by rotations. Thus, it is not necessary to make calculations of rotation-vibration interaction, etc.

Newton (1960) has extended Nilsson's calculations to the asymmetric case and has found that the predicted values for γ are usually small or zero, indicating that the Nilsson model is valid in most cases. More experimental data are still required in order to test fully the predictions of the asymmetric rotator model.

CHAPTER 3

INSTRUMENTS AND TECHNIQUES

Introduction

Over the years many different types of instruments have been used to study the radioactive decay of nuclei. The most useful of those used in present-day research provide an indication not only of the presence of radiation but also of its energy. There are two commonly used methods for obtaining the energy selection: the radiation can be absorbed and the amount of energy it gives up measured, or charged particles can be subjected to an electromagnetic field and their deflection observed. Solid state detectors and scintillation counters utilize the first principle, whereas the magnetic spectrometers fall into the second category. By the use of coincidence techniques it is also possible to determine the spatial and temporal relationships, if any, between different radiations from a nucleus. Such information is very useful when a complex spectrum is being studied.

The work to be described in this thesis was done with the aid of scintillation spectrometers, a Siegbahn-type beta spectrometer and an electron-electron coincidence spectrometer of the Gerholm type. This chapter is devoted to a description of these instruments and how they may be used to carry out various measurements.

3.1 The Scintillation Spectrometer

This instrument makes use of the fact that certain materials fluoresce when struck by energetic photons or charged particles.

The light is usually guided to the photocathode of a photomultiplier, and hence a pulse of current is obtained for each particle detected. If the gain of the system is constant, the size of the output pulse is proportional to the amount of energy lost to the phosphor. Thus, radiations which are totally absorbed yield output pulses proportional to the incident energies and with the use of a pulse height analyser these energies can be determined.

It is possible to build detectors of this type which are very efficient for gamma rays because large masses of solid or liquid phosphor can be made. Sodium iodide crystals activated with thallium are probably the most popular scintillators at present for gamma ray spectroscopy. This material can be grown into large crystals and has other desirable properties for a radiation detector, e.g., high specific gravity, relatively fast rise and decay time, high light output, etc. The scintillators used in the present work were thallium-activated sodium iodide crystals, 1 3/4 inches in diameter by 2 inches long.

In actual practice, one does not have the ideal situation outlined above. A monoenergetic source of gamma rays does not yield a series of pulses all of the same height, but instead one finds a large peak at the end of a continuous distribution of pulse heights, as seen in Figure 2. The peak, usually called the photopeak, is due to photons which have been totally absorbed by the crystal. Its shape, which is approximately Gaussian, results from the fact that only a finite number of photoelectrons are ejected from the photocathode. The peak width at half height ΔE, divided by the energy E, is defined to be the

resolution, R. This parameter is a measure of the instrument's ability to resolve gamma rays of different energies. The variation of the resolution with energy can be expressed roughly by

$$R = a + b/\sqrt{E}$$

where a and b are constants and the last term is the most important

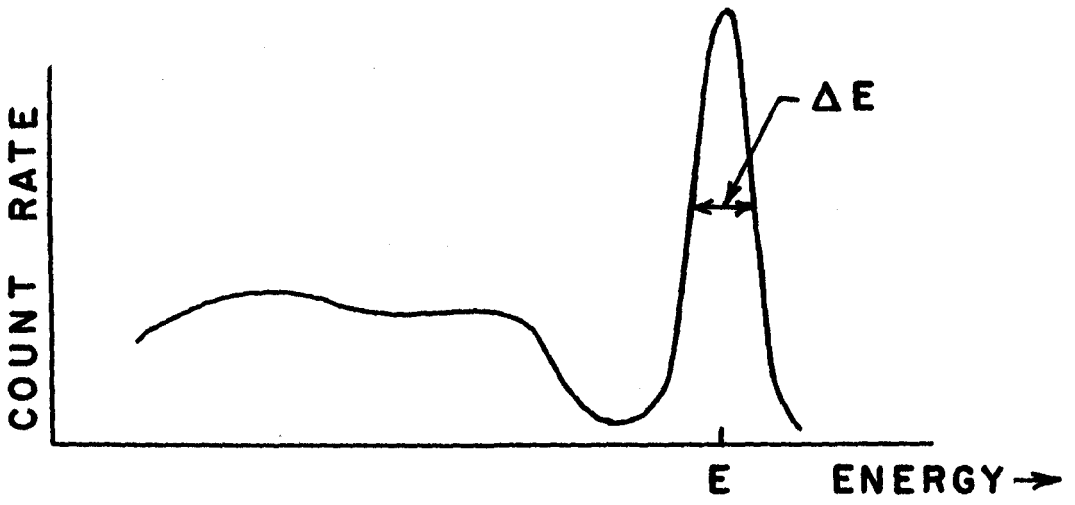

Figure 2

one for energies less than 1 Mev. Typical values for the resolution are 8% to 10% for the 662 kev transition in the decay of Cs^{137}.

The continuous distribution of pulse heights shown below the photopeak in Figure 2 results from gamma rays which lose only part of their energy in the crystal. This can happen if the photon suffers a Compton scattering in the crystal and the scattered photon escapes, or if a photon Compton scattered from some nearby object is absorbed in the crystal. Various other processes also occur which can result in peaks which are not true photopeaks. For instance, if two gamma

rays are detected within the resolving time of the phosphor, summing of pulse heights occurs. Also, if the gamma energy, E, is greater than 1.02 Mev, pair production can take place. One then sees peaks at energies $E - 2m_oc^2$, $E - m_oc^2$ and E, corresponding to the escape from the crystal of both, one, or none of the resultant annihilation quanta. The photopeak efficiency, defined to be the probability that an incoming photon will result in an output pulse in the photopeak, varies with energy for a scintillation counter. From an experimental viewpoint, the value which is usually of interest is the product of this efficiency with the solid angle subtended at the source by the detector. This quantity can be determined for a given energy by counting a source of known strength. As the efficiency varies smoothly with energy, measurements such as this at several different energies provide an adequate calibration of the instrument. Miller et al. (1958) have calculated the photopeak efficiency as a function of gamma ray energy for various geometries. The fact that efficiencies measured in this laboratory follow the same trends as the theoretical values gives one confidence in interpolating a calibration curve from several experimental points.

This type of detector has the advantage of a high efficiency for gamma rays. Also, by means of a multi-channel pulse height analyser, the entire energy spectrum may be measured at once. Unfortunately, the relatively poor resolution limits its usefulness for complex spectra. In the next section we shall see how a beta spectrometer can be used to measure photon intensities and energies with much better resolution but with low efficiency.

3.2 The Siegbahn $\pi\sqrt{2}$ Beta Spectrometer

This instrument falls into the category of the "flat" spectrometers because the electron trajectories remain approximately in a plane, thus differing from the helical trajectories in a lens-type spectrometer. If the electron paths are described in cylindrical co-ordinates, r, θ, z, a central trajectory would follow $r = r_o$, $z = o$. If a uniform magnetic field is used, it is possible to get some radial focusing for $\theta = 180^o$. However, the use of shaped magnetic fields can result in higher-order radial focusing as well as focusing in the z direction. The instrument used in the present work employs a shaped magnetic field and the electrons are focused in both the z and r directions after travelling through an angle $\theta = \pi\sqrt{2}$ radians. The design of this instrument is due to Siegbahn and Svartholm (1946) and the construction details are described by Johns et al. (1953). The main features can be seen in Figure 3. The nominal radius of the electron orbits is 50 cm.

In a magnetic spectrometer, the momentum of electrons being focused is proportional to the magnetic field. If a source of monoenergetic electrons is observed and the count rate is plotted against magnetic field strength, a peak with a finite width will result because the source and detector are not infinitely narrow. It is common to define the resolution of the spectrometer to be the width in momentum of such a peak at half-height divided by the momentum of the peak. For the instrument being discussed, it is possible to use a resolution as low as 0.3%. However, better count rates are obtained if one uses a broader source and opens the baffles slightly. Under normal operation, a resolution of 0.5% to 1.0% is typical. The transmission or effective solid

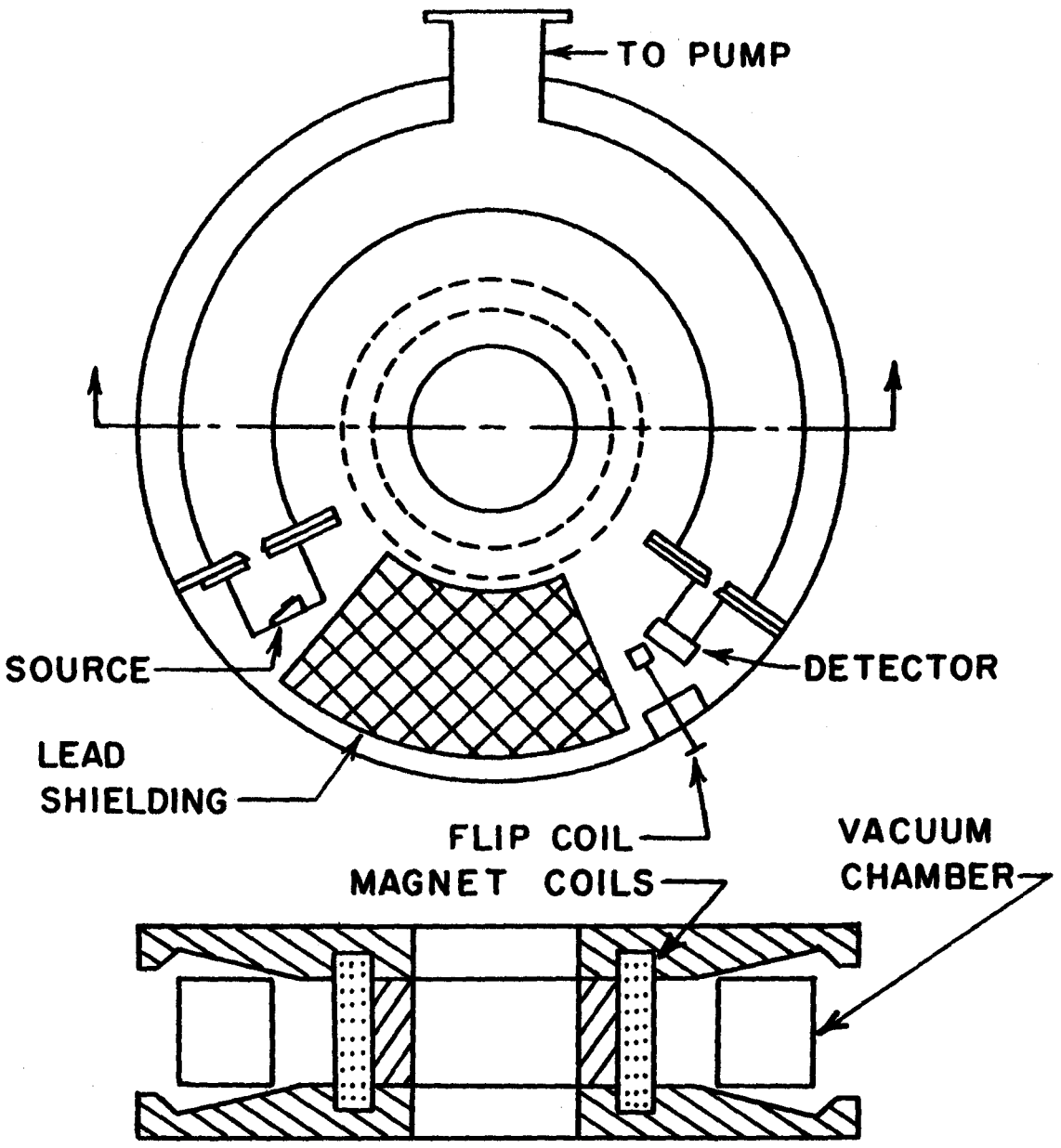

SIEGBAHN $\pi\sqrt{2}$ BETA SPECTROMETER

FIGURE 3

angle of the instrument with such operation is of the order of 0.1%.

For the present work, the detector was an anthracene crystal 2.5 cm long x 1.0 cm wide x 0.4 cm thick, coupled to a Dumont 6291 photomultiplier. The output pulses were fed through an amplifier and lower level discriminator to a scaler. A measure of the magnetic field strength was obtained by means of a flip coil and ballistic galvanometer. Absolute values of the field strength were not required as momentum calibrations were obtained using conversion lines of known energy.

Several different types of experiments have been performed with this instrument, including measurements of beta spectra, internal conversion electron energies and intensities, photon energies and intensities by means of external conversion, and internal conversion coefficients. The techniques and procedure for each of these experiments will be discussed individually.

3.2.1 Beta Spectra

In order to study the continuous distribution of beta particles, high resolution is not necessary, so the baffles are normally opened wide to give a greater transmission. It is very desirable to have a thin source in order that the electrons do not lose an appreciable amount of energy in escaping from the source material. Methods used in the present work to prepare thin sources are described in Appendix A. For the Siegbahn spectrometer, the beta sources were approximately 0.5 cm wide by 2.5 cm long. The procedure was to take counts for different values of momentum until the entire spectrum had been scanned.

If one assumes 100% detection efficiency, the count rate when the instrument is set to focus momentum p is:

$$N = \int_0^\infty N_o \varphi(q)\, \omega\, g(p,q)\, dq$$

g(p,q) is the probability that an electron of momentum q will be counted when the instrument is set to momentum p. ω is the transmission of the instrument. $\varphi(q)$ is the probability that an electron in the spectrum being measured will have momentum q and thus

$$\int_0^\infty N_o \varphi(q)\, dq = N_o$$

where N_o is the source strength.

g(p,q) is obviously related to the resolution of the instrument and is zero if p differs greatly from q. Also, if the magnetic field shape is constant for all field strengths, it follows that g(p,q) depends only on the ratio p/q and not on their absolute values. Hence

$$\int_0^\infty g(p,q)\, dq = \eta\, p$$

where η is a constant. We shall see later that η is equivalent to our definition of the resolution in the case of an ideal peak.

In our expression for the count rate above, we can replace $\varphi(q)$ by $\varphi(p)$ since $q \approx p$ for $g(p,q) \neq 0$ and $\varphi(q)$ varies slowly with q. Thus:

$$N = N_o \varphi(p)\, \omega\, \eta\, p$$

and

$$\int_0^\infty \frac{N}{p}\, dp = N_o \eta\, \omega$$

This means that the area under a plot of N/p vs. p gives $N_o \eta \omega$ and if one knows the resolution and transmission of the instrument, the source strength can be determined.

In order to determine whether the spectrum is simple or contains more than one beta group, one usually constructs a Fermi plot. From section 1.2 we recall that this is a plot of $\left[N'(p)/p^2F\right]^{\frac{1}{2}}$ against energy. However, $N'(p)$ is the number of beta particles per unit of momentum and is proportional to N/p because the spectrometer counts the events in a window which is proportional to p. The combined Fermi functions of the National Bureau of Standards (1952) were used in the present work. These tables actually list f(Z,p) which is equivalent to p^2F. Thus, to construct a Fermi plot, one plots $\left[N/pf\right]^{\frac{1}{2}}$ against energy.

If several beta groups are present, they can often be separated by peeling off successive straight line portions from the Fermi plot. The groups can then be plotted in the form N/p against p and by measuring the areas under these curves one can obtain the branching ratios and hence the log ft values.

3.2.2. Internal Conversion Spectra

To study internal conversion lines, which appear as peaks superposed on the beta continuum, one uses the same methods of source preparation and experimental set-up as for beta spectra. However, a better resolution is usually necessary to resolve the various lines. To measure the energy of the conversion line, one scans carefully over the peak and finds the magnetic field strength corresponding to the centre of the peak. Calibration of the field

strength is carried out by repeating this procedure for several conversion lines whose energies are well known. (e.g., the 411.772 kev transition in Au^{198}.) The area under the peak can be used to obtain a measure of the intensity of the conversion line. If a transition has a probability per decay of f and a probability $\mathcal{K}$ for internal conversion in a given shell, then there are $N_o f\mathcal{K}$ electrons per second in the conversion line. N_o is again the source strength. Using the same nomenclature as in the previous section, the count rate when the spectrometer is set to focus momentum p will be

$$N = N_o \; f\mathcal{K}\omega \; g(p,q)$$

q is the momentum of the conversion electrons in this case.

The area under the peak when N/p is plotted against p is

$$\int_o^\infty \frac{N}{p}\, dp = N_o f\mathcal{K}\omega \int_o^\infty \frac{g(p,q)}{p}\, dp$$

When good resolution is used, g(p,q) is negligible unless $p \approx q$. Thus, the range of integration is so small that the p in the denominator can be taken out as a constant, in which case the remaining integral is η p. Thus, the area is $N_o f\mathcal{K}\omega\eta$. If one notes that the peak counting rate is $N_o f\mathcal{K}\omega$, it is seen that η is the ratio of the peak area to the peak height. In the ideal case of a symmetric triangular peak, it is obvious that the resolution $\Delta p/p$ is also the ratio of the peak area to peak height and thus η is the resolution. For a given transition, the K:L, L:M, L_1:L_2:L_3, etc. conversion ratios can be

obtained readily and used to gain an indication of the transition multipolarity. Also, the ratio of the area under a peak to that under the total beta continuum is the product $f\mathcal{K}$. If $\mathcal{K}$ can be found by measuring the actual conversion coefficient, the branching ratio for the transition is obtained.

3.2.3 External Conversion Spectra

As mentioned earlier, it is possible to study gamma ray spectra with a beta spectrometer by means of a process called external conversion. The photons are allowed to strike a thin foil of material called a radiator and the photoelectrons ejected from the foil pass through the spectrometer in the normal manner. The radiator is usually a high Z material such as gold or uranium in order to get a high photoelectric cross-section. The radiator must be thick enough to produce an appreciable number of events but must not be too thick, or the photoelectrons will lose too much energy in escaping from the foil. Usually, the thickness is chosen to suit various experimental factors such as the energy region being studied, whether resolution is to be improved at the expense of counting rate, etc. In practice, a beta stopper made of a low Z material is placed between the source and the radiator to reduce the continuum and thus provide better counting statistics on the conversion peaks.

In general, for each gamma transition there will appear several peaks, corresponding to conversion in the K, L_1, L_2, L_3, etc. shells of the radiator material. If the L lines from one transition interfere with the K line from another transition, it is possible to

separate them by choosing a different radiator material because the separation of the K and L peaks for any given transition will be different. Similarly, radiators of different atomic numbers also give an indication as to whether a peak is a K or L line. In the present work, gold radiators with thicknesses of 0.4 to 4.2 mg/cm^2 and uranium radiators with thicknesses of 1.4 to 3.3 mg/cm^2 were used.

The measurement of the energy of an external conversion line is similar to that described for an internal conversion line. However, the momentum of the inflection point on the high energy side of the peak is used instead of the momentum of the centre of the peak, because the latter varies with radiator thickness.

The measurement of photon intensities by this method is complicated by the fact that the over-all efficiency of the conversion process varies in a complex manner with energy and radiator thickness. Artna (1961) has measured relative peak heights for cascade gamma rays of different energy whose relative intensities are well known. These results are consistent with the semi-empirical relation for the photon intensity

$$I_\gamma = K \frac{n}{p\beta^3 \gamma} \left[C^2 + \left(\frac{Rp\beta^3}{t} \right)^2 \right]^{\frac{1}{2}}$$

where K is a geometry-dependent constant

n is the observed peak height

γ is the photoelectric cross-section

R is the instrumental resolution

t is the radiator thickness

β is v/c for the electrons

$C = I\beta^3$ where I is the stopping power of the material, dp/dt.

The work of Artna (1961) has resulted in empirical curves for the expression

$$\left[C^2 + \left(\frac{Rp\beta^3}{t}\right)^2\right]^{\frac{1}{2}}$$

for each of the radiators used in the present work. These values were used to convert all measured peak heights to relative photon intensities.

This method of studying gamma ray spectra makes use of the high resolution of a beta spectrometer and thus has an advantage over the scintillation spectrometer. In the present work, resolutions of 0.8% to 1% were obtained, as compared with ten times these values for NaI(Tl) detectors. However, the external conversion method has a much poorer efficiency and requires many hours of scanning for even a rough spectrum.

3.2.4 Measurement of Internal Conversion Coefficients

The internal conversion coefficient of a transition can be determined experimentally by measuring its peaks in both internal and external conversion. From section 3.2.1, the number of conversion electrons emitted by a source is $N_e = K_1 A$ where K_1 is a geometry dependent constant and A is the peak area. If the source is now covered with a beta stopper and a radiator is installed, the number

of photons emitted is given by $N_\gamma = K_2 I_\gamma$ where I_γ can be found as described in the previous section. K_2 is another geometry-dependent constant.

By definition, the internal conversion coefficient is

$$\alpha = \frac{N_e}{N_\gamma} = \frac{K_1 A}{K_2 I_\gamma} = k\left(\frac{A}{I_\gamma}\right)$$

where k depends on geometries only. The value of k can be determined by repeating the experiment with the same geometry, using a source with a transition for which α is well known.

Once α is known for one transition, it can be readily found for any other transition in the decay by taking intensity ratios of the peaks in internal and external conversion. This information is helpful in the assignment of multipolarities. Also, as pointed out in section 3.2.2, a value for a conversion coefficient, when combined with other information, gives a measurement of the probability per decay that any transition will occur. These quantities are obviously very important contributions to any decay scheme.

3.3 Double Lens Coincidence Spectrometer

3.3.1 Description of the Instrument

The instrument to be described in this section is the one on which the majority of the work for this thesis was performed. It consists essentially of two beta spectrometers which count electrons from the same source and whose outputs are fed into coincidence circuitry. The original design was due to Gerholm (1956) and a

detailed description of the instrument is given by Habib (1961).

A cross-sectional view of one end of the instrument can be seen in Figure 4. The source S is located at the geometrical centre of the cylinder containing the two spectrometers whose axes are collinear. Current in the magnet coils produces an axial magnetic field which causes the electrons to travel through the spectrometer along trajectories which somewhat resemble helices. Electrons of the desired momentum which pass through the exit baffle are detected by an anthracene crystal coupled to a photo-multiplier tube by means of a light guide.

The magnetic field is not uniform but varies along the axis as shown in the graph in Figure 4. This field shape is produced by the contours of the pole faces and has certain desirable features. The ring focus produced at the position of the exit baffle results in better resolution for the same transmission than for various other simple field shapes. Also, the magnetic field at the source position is small or zero, which reduces interference between the fields in the two spectrometers. As can be seen from Figure 4, the two spectrometers are magnetically independent and the field from one should not affect the other. In actual fact a small amount of interference is present but this is negligible in most cases. It was observed only once when an 18 kev conversion line was found to shift slightly as the field in the other spectrometer was increased to focus 1 Mev electrons.

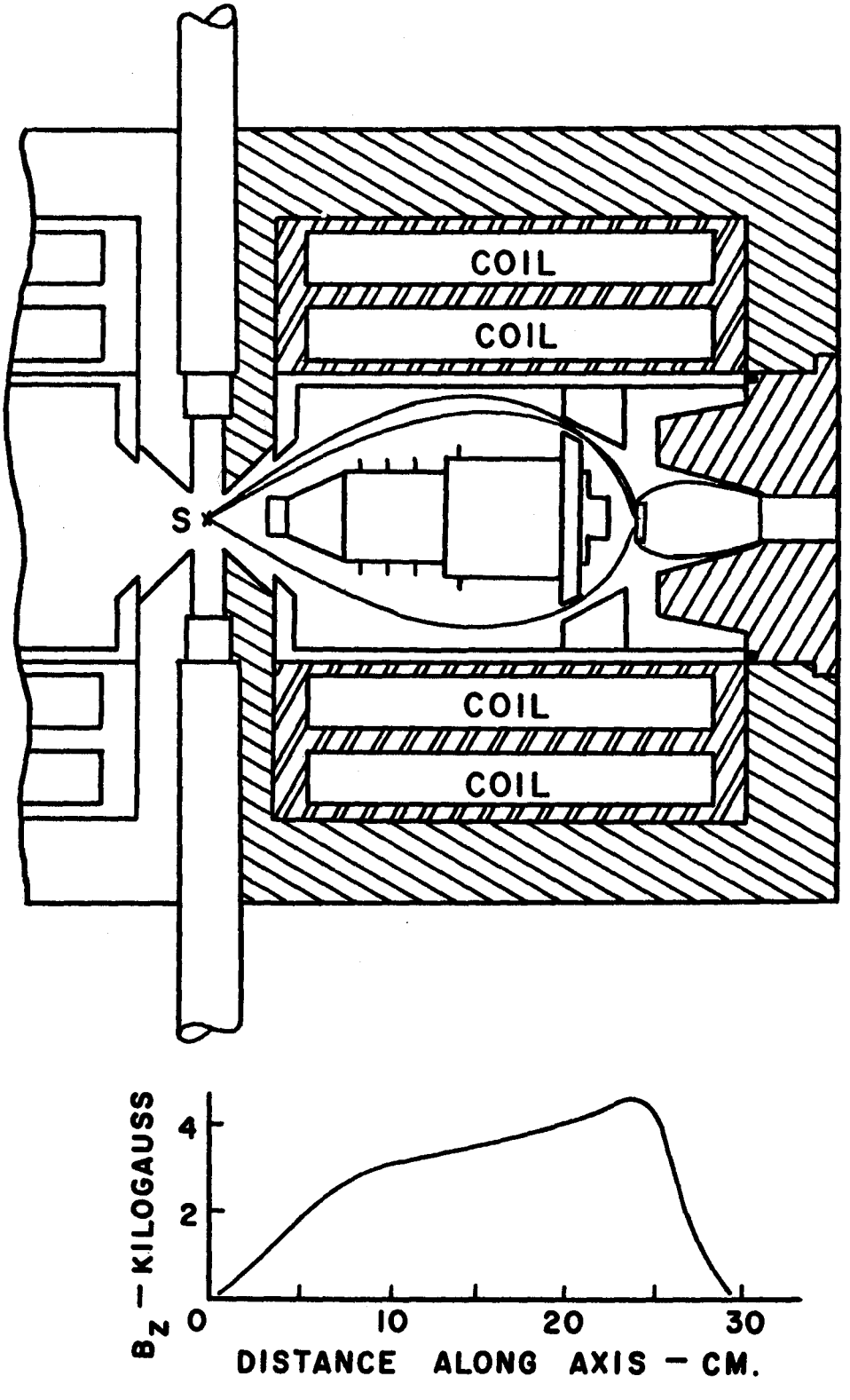

DOUBLE LENS COINCIDENCE SPECTROMETER

FIGURE 4

Along the axis of each spectrometer is a lead slug which prevents direct beta and gamma radiation from reaching the detector. The small fins which can be seen on this slug have been found to be very useful in preventing scattered electrons from reaching the detector. When the instrument was first constructed, counts were always obtained when the spectrometer was set to energies above the end point of the beta spectrum. The first problem undertaken in the present work was to determine the cause of this undesirable effect and to eliminate it. The counts were found to be due to electrons which hit the central slug and were scattered with the right energy and in the right direction to get through the exit baffle. The addition of the small fins has reduced the intensity of the scattered electrons to a negligible value.

The entrance baffle limits the maximum transmission which can be obtained. The exit baffle is movable and is adjusted to suit the needs of a particular experiment. By changing the setting of this baffle, smooth variation from a resolution of 1% at 1% transmission to a resolution of 3½% at 3½% transmission can be obtained with a source 0.2 cm in diameter.

The magnet current for each spectrometer is provided by a 4.7 kilowatt D.C. generator stabilized by a chopper-amplifier feedback system. In normal use the stability is better than one part in two thousand. The current through the magnet coils is used as a measure of the magnetic field. This is an acceptable procedure, as the reluctance of the iron constitutes only a small fraction of the total reluctance of the magnetic circuit. Experimental

justification of this practice exists in that the electron momentum is found to be proportional to the field current without hysteresis effects for energies as low as 3 kev.

The photomultiplier tubes used in this spectrometer are Philips 56 AVP's. These tubes are noted for their small variation in electron transit time which is desirable for coincidence work. They also have a high gain. A standard fast-slow coincidence circuit of the type described by Bell et al.(1952) is used. The essential features of this circuit are shown in the top half of Figure 5. Fast pulses from the photomultiplier anode are fed to a fast coincidence circuit which is relatively easy to build with a small resolving time, provided energy selection is not required. Pulses from the eleventh dynodes of the photomultipliers are fed through slow (~1 microsecond) amplifiers and discriminators and are used to trigger the slow triple coincidence circuit, if the event was of the desired type. It is seen that this circuit provides the good resolving time of the fast coincidence circuit and allows side channel discrimination and monitoring without involving the use of fast amplifiers and discriminators. The fast resolving time is desirable in order to reduce the rate of accidental coincidences -- that is, the rate at which events, not necessarily related, happen to be detected within the resolving time of the circuitry.

Details of the fast coincidence circuit are shown in Figure 6. Pulses from the photomultiplier anode are fed to the grid of a 404A pentode which is conducting about 10 to 20 milliamperes.

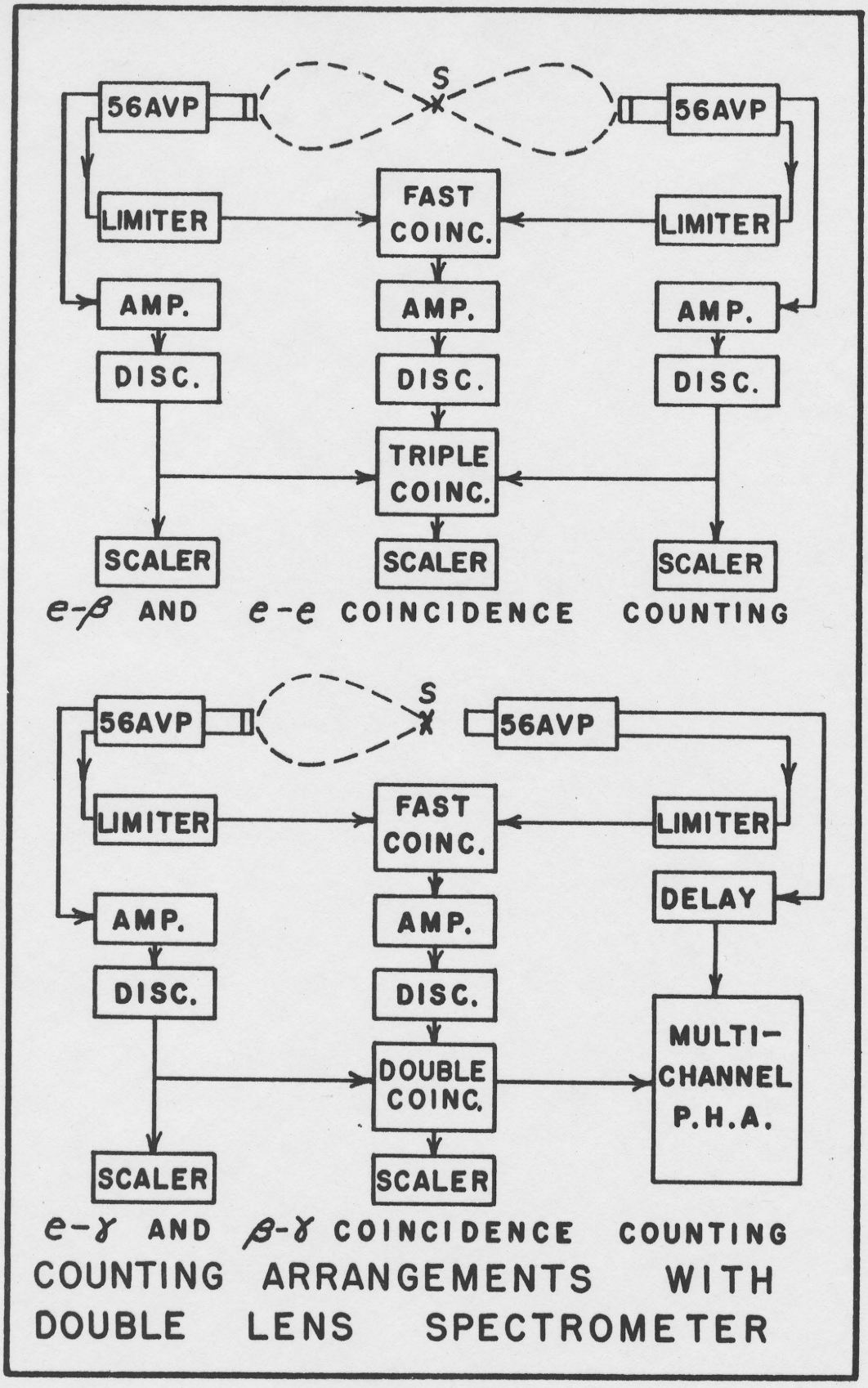
S
56AVP
56AVP
LIMITER
FAST COINC.
LIMITER
AMP.
AMP.
AMP.
DISC.
DISC.
DISC.
TRIPLE COINC.
SCALER
SCALER
SCALER
e-β AND e-e COINCIDENCE COUNTING
S
56AVP
56AVP
LIMITER
FAST COINC.
LIMITER
DELAY
AMP.
AMP.
DISC.
DISC.
MULTI-CHANNEL P.H.A.
DOUBLE COINC.
SCALER
SCALER
e-γ AND β-γ COINCIDENCE COUNTING
COUNTING ARRANGEMENTS WITH DOUBLE LENS SPECTROMETER

FIGURE 5

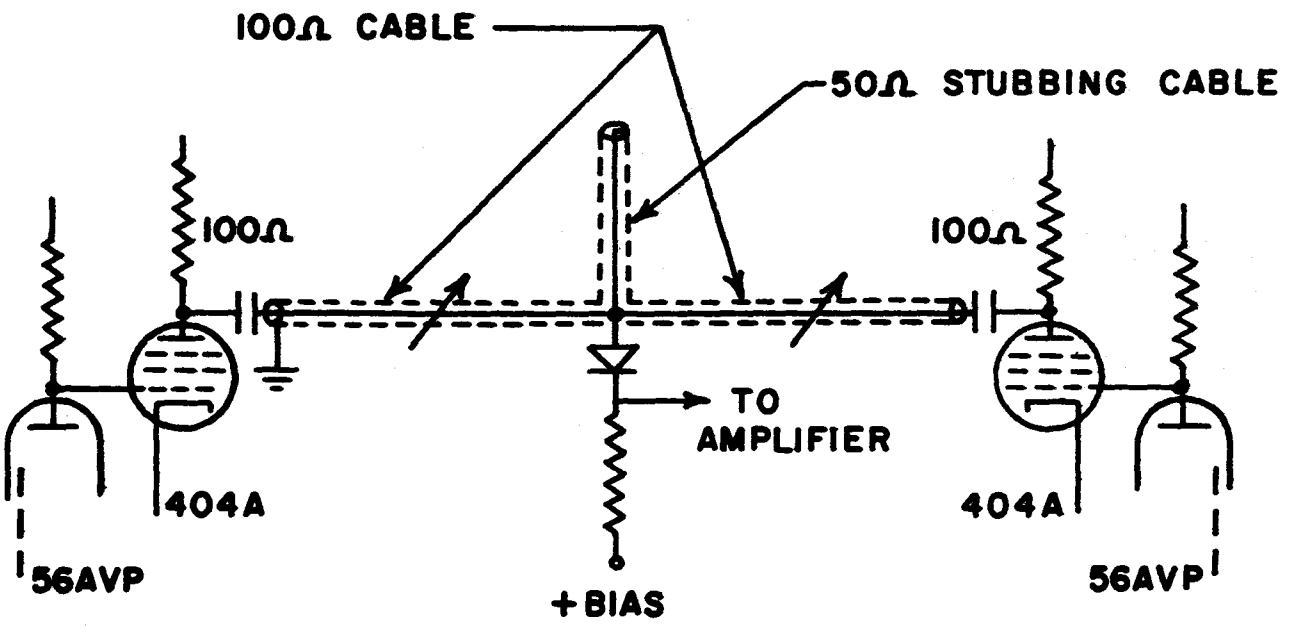

DETAILS OF FAST COINCIDENCE CIRCUIT

FIGURE 6

The tube is quickly cut off, producing a fast-rising pulse 1 to 2 volts high across the 100 ohm load resistor. This pulse travels down the 100 ohm cable to the point where the 50 ohm stubbing cable is attached. When the pulse reaches the shorted end of the stubbing cable, it is reflected with a change in polarity. If the time taken to travel down the stubbing cable and back is τ, then all of the original pulse except the portion which occurs in the first τ seconds is cancelled out. In this manner, pulses which are τ seconds wide are obtained from each detector. The diode is biased to reject all pulses caused by an event in one detector only. However, if there is an event in both detectors within the time 2τ, a larger pulse is produced which overcomes the diode bias. The resulting pulse is amplified and fed to the triple coincidence circuit.

Variable delays consisting of lengths of 100 ohm cable can be placed between the 404A limiter and the fast coincidence circuit. These are useful for cancelling out inherent delays due to differences in cable lengths, etc., as well as for imposing an artificial delay in one side for measuring lifetimes and chance coincidence rates.

The procedure for setting up the instrument for an experiment is as follows: Assuming the circuitry has had time to "warm up," the source is placed in position and the magnetic fields are adjusted to focus electrons of the desired momentum. The side channel amplifiers and discriminators are then set to count as many true events as possible without counting photomultiplier noise etc.

The currents through the 404A limiter tubes are adjusted so that singles pulses from both detectors are cut off for the same value of diode bias. The coincidence rate is then measured as a function of diode bias and a value of the bias is chosen on the plateau just above the value where singles counts have been discriminated against. A typical bias curve is shown in the top half of Figure 7 where the operating point is indicated by an arrow. Using this value of bias, the coincidence rate is then measured for different delays imposed in both sides of the fast coincidence circuit. This is done to correct for differences in transit times for the two spectrometers, differences in cable lengths, etc. Variations in electron transit time with energy when scanning over a beta continuum are usually small compared with the resolving time and can be ignored. For instance, since the spectrometer is about 30 cm long, the variation in transit time from 100 kev to 1 Mev is only one or two nanoseconds, whereas the resolving time is usually about fifteen nanoseconds. For proper operation, a flat-topped curve, such as than shown in Figure 7, should be obtained when the coincidence rate is plotted for different artificial delays. For large delays in either side, the chance rate only is observed. The width of the flat-topped operating region containing the true coincidences is roughly equal to 2τ at half height and is called the resolving time. A delay corresponding to the centre of this plateau is chosen and the instrument is then ready for the experiment to begin.

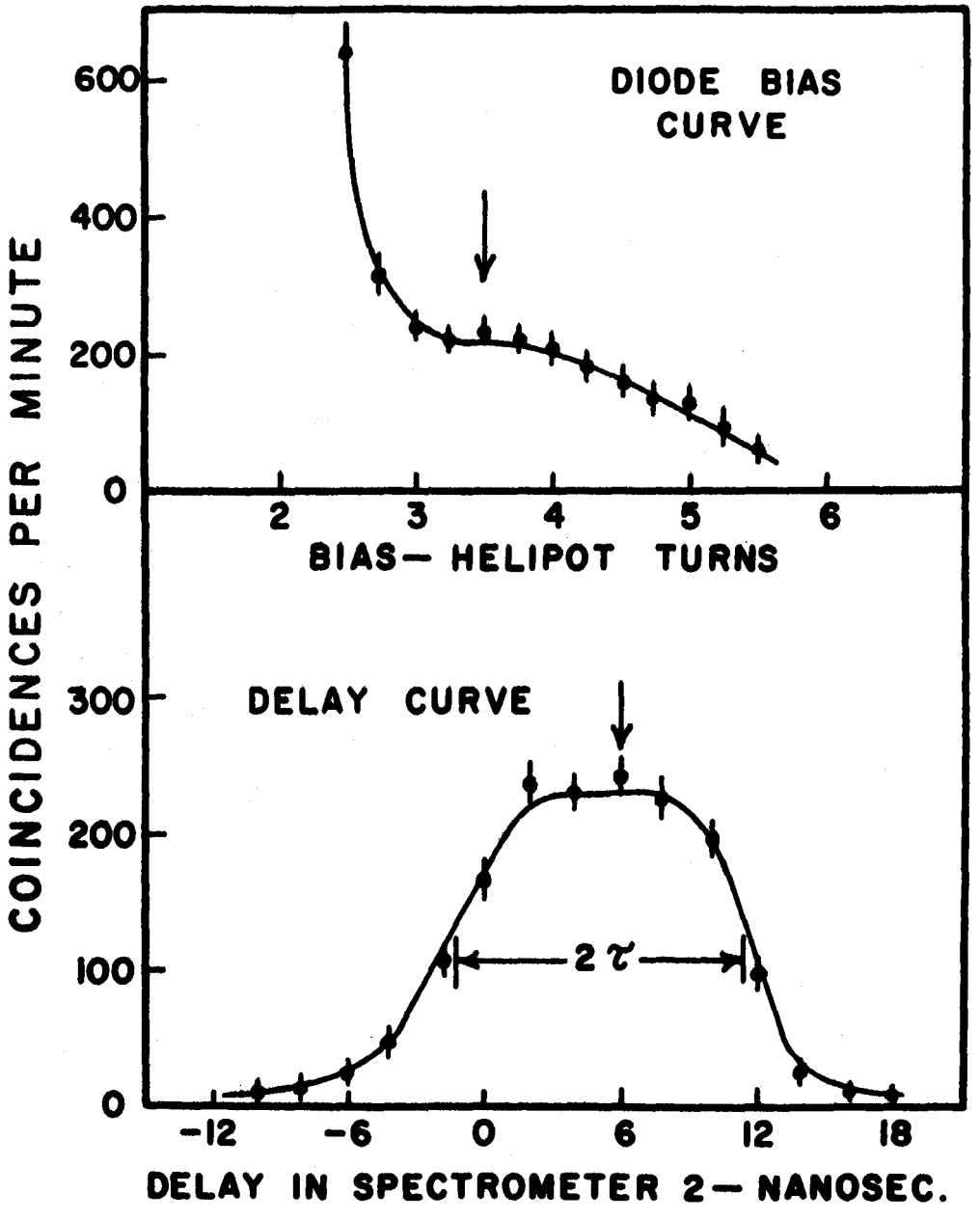

TYPICAL CENTRE CHANNEL DIODE BIAS AND DELAY CURVES

FIGURE 7

As described thus far, the spectrometer can be used for electron-electron or electron-beta coincidence experiments. By removing the baffles from one end of the spectrometer and inserting a NaI(Tl) crystal with photomultiplier, electron-gamma and beta-gamma experiments can also be performed. In this mode of operation, the slow pulses from the gamma detector are fed directly to a multichannel pulse height analyzer which is gated on by the output pulse from the slow coincidence circuit, as shown in the lower half of Figure 5. The multichannel analyzer thus accumulates the gamma spectrum which is in coincidence with the electrons being focused in the other end of the instrument.

The gamma spectra that one obtains in this manner are not as good as can be obtained with the detector outside the instrument. This is partly due to the detection of photons which are Compton-scattered from the magnet pole faces, coils, etc. This undesirable effect has been reduced considerably by the addition of lead shielding and collimators, but has not been completely eliminated.

For the experiments with low energy electrons, the anthracene detectors were of no use because the output pulses were completely masked by photomultiplier noise. Therefore, a thin window Geiger counter was constructed for these measurements. The details of this detector are described in Appendix B.

The remainder of this chapter will be devoted to an outline of how several types of coincidence experiments can be carried out with this spectrometer and how the results may be used.

3.3.2 Examples of Typical Experiments

In order to establish the level order of a decay scheme, electron-beta and beta-gamma experiments are very useful, as they give the end point energy of the beta group or groups feeding the various transitions. These data, combined with energy measurements of the gamma transitions, often determine a level scheme uniquely. Electron-electron and gamma-gamma experiments may confirm the picture or add to it. For instance, in the simple case shown in Figure 8, e-β or β-γ experiments would show that transitions f_1 and f_2 are fed by δ_1,

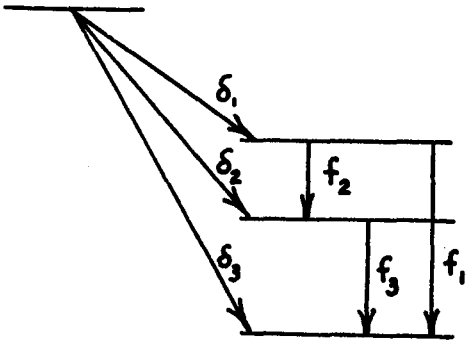

Figure 8

whereas f_3 is fed by δ_1 and δ_2. This is a very simple decay scheme which can be solved with only a few experiments. However, it will be useful as an example to show how branching ratios and conversion coefficients can be determined by the coincidence method. In the discussion which follows, δ's and f's will be used to denote the branching ratios (i.e. the probabilities per decay) for the respective transitions shown in Figure 8 and the nomenclature will be the same as that used in section 3.2.

If one spectrometer (say, number 1) is set to focus a conversion line from f_2 in Figure 8 and the other (number 2) scans the beta continuum, using the results of 3.2., the following statements can be made. The area under the single spectrum conversion peak in end number 1 is

$$\int \frac{N_1}{p}\, dp = N_o f_2 \kappa_2 \omega_1 \eta_1 \qquad (1)$$

(Subscripts on ω and η refer to the spectrometer number.) The area under the single spectrum beta continuum in end number 2 is

$$\int \frac{N_2}{p}\, dp = N_o \omega_2 \eta_2 \qquad (2)$$

The area under the coincidence beta spectrum is found by similar arguments to be

$$\int \frac{N_c}{p}\, dp = N_o f_2 \kappa_2 \omega_1 \omega_2 \eta_2 \qquad (3)$$

This result, and others to be derived later, are based on the assumption that the coincidence circuit is operating with an efficiency of 100%. Separate experiments performed for calibration purposes indicate that this assumption is valid for the results to be presented in this thesis.

The ratio $\frac{(3)}{(2)} = f_2 \kappa_2 \omega_1$ and thus, if ω_1 is known, the product $f_2 \kappa_2$ is obtained. In general, the solid angles are dependent on the source

geometry. However, the maximum solid angle, obtained with the baffle wide open, is independent of source geometry and can be obtained by a separate experiment with a source of known strength. The fraction of the maximum solid angle being used with any source and any baffle setting can be found by measuring the ratio of peak heights of a conversion line with the baffle in two positions -- at the position used for the experiment and wide open.

Suppose now that spectrometer number 1 is set on a conversion line from transition f_3. The area under this conversion peak is, of course

$$\int \frac{N_1}{p}\, dp = N_o f_3 \mathcal{K}_3 \omega_1 \eta_1 \qquad (4)$$

The coincident beta continuum will now have two groups, δ_1 and δ_2, with areas $N_o f_2 \mathcal{K}_3 \omega_1 \omega_2 \eta_2$ and $N_o \delta_2 \mathcal{K}_3 \omega_1 \omega_2 \eta_2$, respectively. By taking ratios of these areas with expression (4), the ratios of the intensities of δ_2, f_2 and f_3 can be determined.

More information can now be obtained by performing electron-electron coincidence experiments. To do this, one might set spectrometer number 1 on f_3 and spectrometer number 2 on f_2. The area under the peak in number 1 is given by (4) above, and that in number 2 is

$$\int \frac{N_2}{p}\, dp = N_o f_2 \mathcal{K}_2 \omega_2 \eta_2 \qquad (5)$$

The coincidence counting rate will have contributions from four effects: coincidences between (a) conversion lines of f_2 and f_3,

(b) line of f_2 and continuum under line of f_3

(c) line of f_3 and continuum under line of f_2

(d) continua under the two lines

The rate due to (d) is small as it is caused only by accidental coincidences or electrons scattered from a conversion line. By taking a count with spectrometer number 1 still on the line but with number 2 just off the line of f_2, the sum of effects (c) and (d) is observed. Similarly, the sum of effects (b) and (d) can be obtained. By appropriate additions and subtractions, effect (a), which is the desired coincidence rate between the two conversion lines, can be found. This rate is given by

$$N_c = N_o f_2 \mathcal{K}_2 \omega_1 \mathcal{K}_3 \omega_2 \qquad (6)$$

The ratio of the quantities (6) and (5) is

$$\frac{(6)}{(5)} = \frac{\omega_1 \mathcal{K}_3}{\eta_2}$$

so the internal conversion coefficient for f_3 can be found, since ω_1 and η_2 are known. This information could also be found from the ratio

$$\frac{(6)}{(3)} = \frac{\mathcal{K}_3}{\eta_2}$$

without having to rely on solid angle measurements. Since the product $f\mathcal{K}$ can easily be found for any conversion line, the experiment also yields the branching ratios for the transitions.

From the above discussion, it is seen that the coincidence method offers an alternate means to that discussed in section 3.2 for obtaining conversion coefficients and branching ratios. In spite of

this apparent rivalry, the two instruments actually complement each other because the Siegbahn spectrometer is capable of better resolution. Also, it is desirable to have two or more independent means of measuring a quantity.

Electron-gamma and beta-gamma experiments can also be used to determine conversion coefficients and branching ratios. These experiments result in better count rates, especially for weakly converted transitions, and the whole gamma spectrum can be studied at the same time. However, the resolution is not as good so that in many cases the results can be ambiguous. The expressions for the count rates are derived in a manner similar to those outlined above, so will not be given in detail here. The most important difference is that the photopeak efficiency of the NaI(Tl) detector varies with energy and must be taken into consideration.

3.3.3 Accidental Coincidences

When performing coincidence experiments, it is always necessary to know what fraction of the counts are due to accidental coincidences. These are counts caused when two unrelated radiations happen to trigger the detectors within the resolving time of the coincidence circuitry. The chance rate is given by

$$N_{chance} = 2\tau N_1 N_2$$

where 2τ is the resolving time and N_1 and N_2 are the side channel counting rates. When doing an experiment, the chance rate is usually determined in two ways. The resolving time can be found from a time

resolution curve such as that in Figure 7 and N_{chance} calculated from the above expression. The other method is to insert a delay in one side of the coincidence circuit to destroy the time relationship. The observed rate is then the chance rate. Two or three such counts are usually taken during each experiment and used to calculate the chance rate for all the data. The ratio of true coincidences to chance varies inversely with both the source strength and the resolving time. Hence, for a given resolving time, the true to chance ratio may limit the strength of source which can be used. When performing electron-beta and gamma-beta coincidence experiments, the true to chance ratio may become quite poor near the end points of partial beta spectra. Fortunately, the end point energy can usually be determined from a Fermi plot without having to rely heavily on the data near the end point. In addition, these data carry very little weight in the determination of beta intensities.

3.3.4 Lifetime Measurements

If a nuclear state has an appreciable lifetime, the radiations from this state will be delayed with respect to those feeding it. Thus, if a circuit were set up to record prompt coincidences, certain events may not be counted. If an artificial delay were placed in the side of the circuit which was detecting the first radiation, some of these events would be counted. The coincidence rate varies with the amount of artificial delay, as shown in Figure 9. Curve A is obtained from prompt coincidences, i.e., radiations whose intermediate state

has a negligible lifetime. Curve B shows the coincidences delayed due to the lifetime.

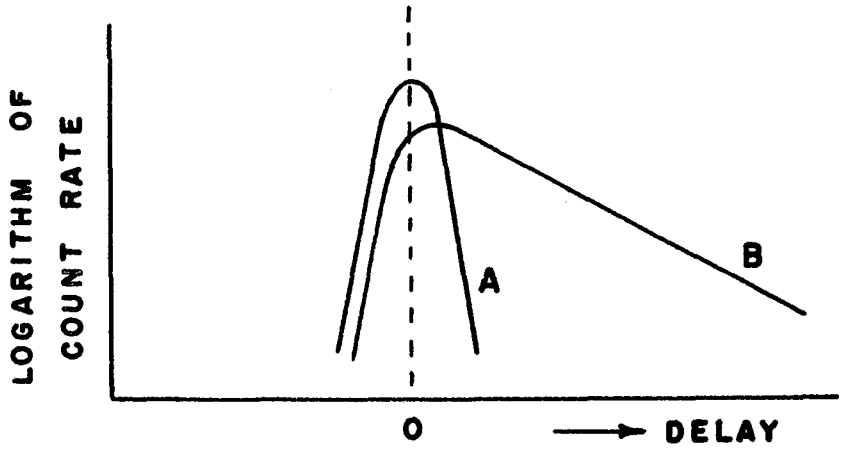

Figure 9

Van Name (1949) has shown that the slope of the tail on curve B is equal to λ, the decay constant for the intermediate state. Hence, a measurement of this slope is sufficient to determine the lifetime of the state. If the lifetime is shorter than, or comparable to, the resolving time of the circuit, the effect is not so noticeable as in Figure 9 and the lifetime cannot be measured accurately by the slope method. From Figure 9, it can be seen that the centroid of the area under curve B is shifted along the time axis with respect to that under the prompt curve. Bay(1950) has shown that the amount of this shift is equal to the mean life of the intermediate state. This method can be used even when the resolving time is considerably longer than the lifetime. In this case it is important that the prompt curve be carefully determined, preferably for the same energy as the radiation whose lifetime is being measured, as most detectors have a response time which is energy-dependent.

CHAPTER IV

THE STUDY OF THE DECAY OF Pm^{151}

4.1 Historical Survey

The decay of 27.5 hour Pm^{151} has been studied by many workers. Rutledge et al. (1952) studied the internal conversion lines with a magnetic spectrograph. Their work resulted in good energy measurements for the strong transitions and, on this basis, two possible decay schemes were proposed.

Coincidence experiments using scintillation spectrometers were performed by Hans et al. (1955). Unfortunately, the results obtained by pulse height analysis from scintillation counters are difficult to interpret because the resolution is not adequate to resolve the closely spaced transitions in this decay. In spite of this shortcoming, these experiments removed some of the ambiguities and an improved decay scheme was given.

Burson and Schmid (1958) examined the beta spectrum with a 180° magnetic spectrometer. They have separated this spectrum into five partial spectra, the most energetic of which has an end-point energy of 1.53 Mev. Scintillation counters were used to search for gamma-gamma and gamma-beta coincidences. For the latter, the end-point energies of the beta groups were determined by absorption in aluminum. No decay scheme was proposed as this was an interim report.

A recent report by Chery (1962) describes another investigation carried out with scintillation counters. This work includes beta-gamma, gamma-gamma and angular correlation experiments, together with lifetime measurements for some of the levels. A better picture of the decay has resulted from these experiments, but the lack of good resolution makes some of the data difficult to interpret.

In order to eliminate some of the uncertainties in this decay, a series of experiments was undertaken in this laboratory with an electron-electron coincidence spectrometer of the Gerholm type. Additional measurements of line intensities in internal and external conversion and of the beta continuum were also carried out, with the Siegbahn-type double focusing beta spectrometer. During the course of this work, Geiger and Graham (1962) of the Chalk River Laboratories have also examined the internal conversion spectrum using the high resolution Chalk River iron-free $\pi\sqrt{2}$ beta-spectrometer. This has resulted in precise energy measurements for the transitions. The measurements from this laboratory and the data obtained from Geiger and Graham have been published in a recent report by Burke et al. (1963).

Since the above article was submitted for publication, a report by Harmatz et al. (1962), including a study of the Pm^{151} decay, has appeared in the literature. The internal conversion spectrum was measured with a high resolution magnetic spectrograph and a decay scheme was formulated which was interpreted on the basis of Nilsson's model.

Ewan (1962) of the Chalk River Laboratories has also studied this decay while at Copenhagen. Electron-gamma and beta-gamma coincidence experiments were performed, in addition to studies of the conversion spectra at high resolution. These data are not yet published, but some preliminary information has been obtained by means of a private communication.

This chapter will include the presentation of the already published results obtained from the work in this laboratory and the energy measurements of Geiger and Graham. The significance of these results will then be discussed in the light of the data published by Harmatz et al. (1962).

4.2 EXPERIMENTAL MEASUREMENTS

4.2.1 Internal and External Conversion Spectra

The investigation was begun by scanning the Pm^{151} spectrum in both internal and external conversion. Methods used for the preparation of sources for these experiments are described in Appendix A. The external conversion spectrum as seen with gold radiators is shown in Figures 10 and 11. Most of the transitions have also been studied with uranium radiators. However, with the exception of special cases, these data do no more than confirm the information obtained with gold radiators and hence are not shown. One exception can be seen in the insert of Figure 11, where evidence for a 0.345 Mev transition converted in uranium is found. When a gold radiator is used, the K-conversion peak of this transition is obscured by the L lines of the 0.275 Mev transition.

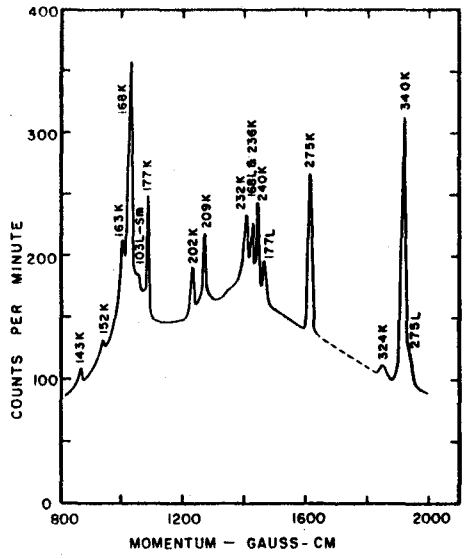

Figure 10. The low-energy external conversion spectrum taken with a 1.2-mg/cm^2 gold radiator.

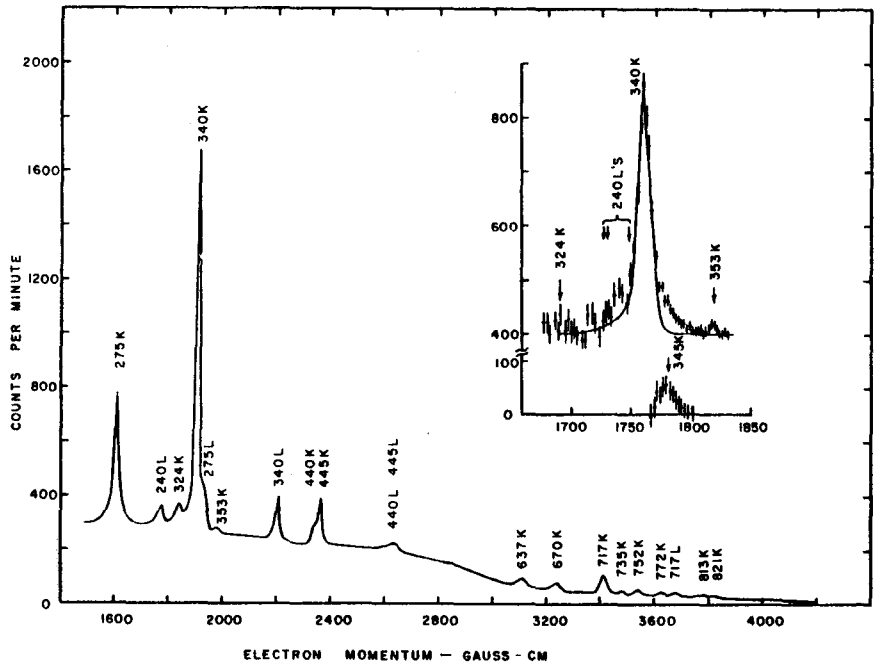

Figure 11. The high-energy external conversion spectrum taken with a 4.4-mg/cm^2 gold radiator. The insert shows the region of the 340 K peak taken with a 1.4-mg/cm^2 uranium radiator. The expected profile for the 340 K peak, obtained from the shape of the 308 K peak in Er^{171}, is shown as a solid line. The difference between the experimental and expected profiles is attributed to the presence of a 345-kev transition.

Figures 12 to 14 show the various regions of the internal conversion spectrum. The measurements made with the Siegbahn spectrometer at a resolution of 0.7% for electron momenta from 1000 to 2600 gauss-cm are shown in Figure 12. As it was impossible to scan the entire spectrum with any one source, the strong K-conversion lines of the 0.177 Mev doublet (not resolved in this spectrometer) were scanned in each source and used for normalization. The spectrum for electron momenta from 450 to 1100 gauss-cm, as measured with the Gerholm instrument at a resolution of 1.3%, is shown in Figure 13.

The decay scheme proposed in the present work postulates a level at an excitation energy of 4.8 kev with a strong ground-state transition. In order to verify this directly, the low energy electron spectrum was measured to search for the M and N conversion electrons from the 4.8 kev transition. The thin window Geiger counter used to detect these electrons is described in Appendix B. The spectrum is shown in Figure 14 where the conversion electrons are found to be superposed on a complex of L-Auger electrons.

Most of the peaks shown in these spectra have been scanned several times in order to check that they decay with the correct half-life for Pm^{151}. This is particularly important for the external conversion peaks as the sources used for these measurements were not subjected to the ion-exchange separation.

The measurements of photon energies as determined from the above data are given in Table I where the values obtained by Rutledge et al. and Burson and Schmid are shown for comparison. Also shown

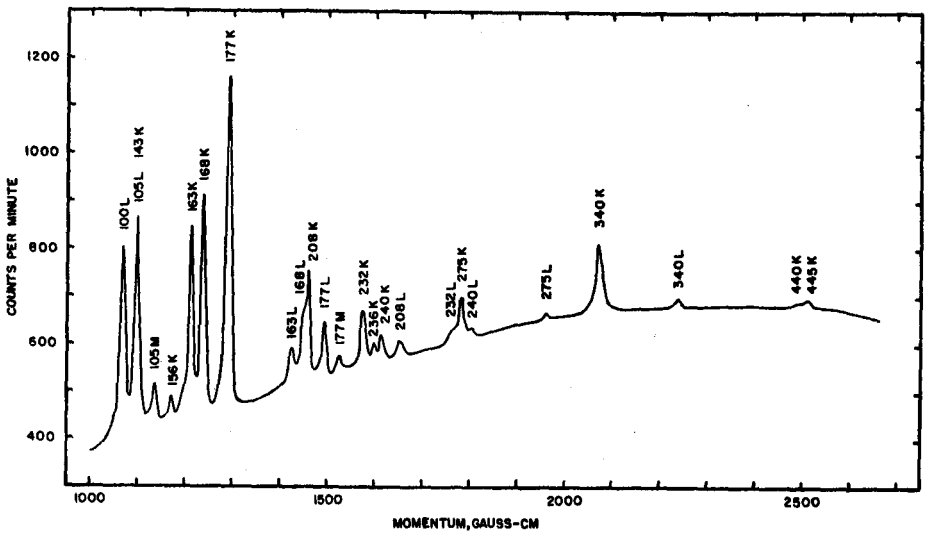

Figure 12. Internal conversion spectrum from 1000 to 2600 gauss-cm taken with a resolution of 0.7% in momentum.

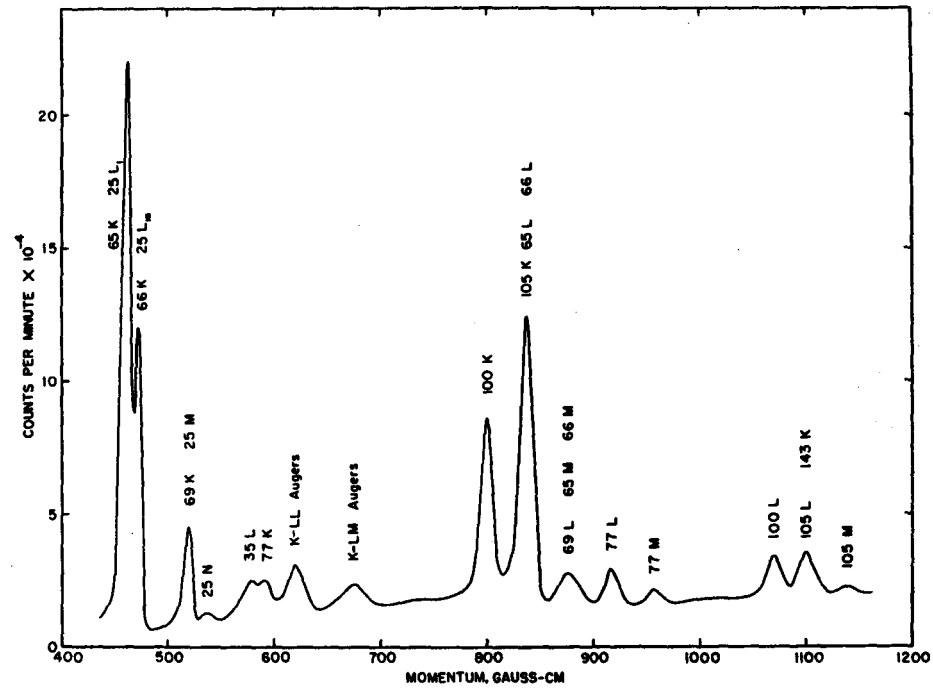

Figure 13. Internal conversion spectrum from 450 to 1100 gauss-cm at a resolution of 1.4%.

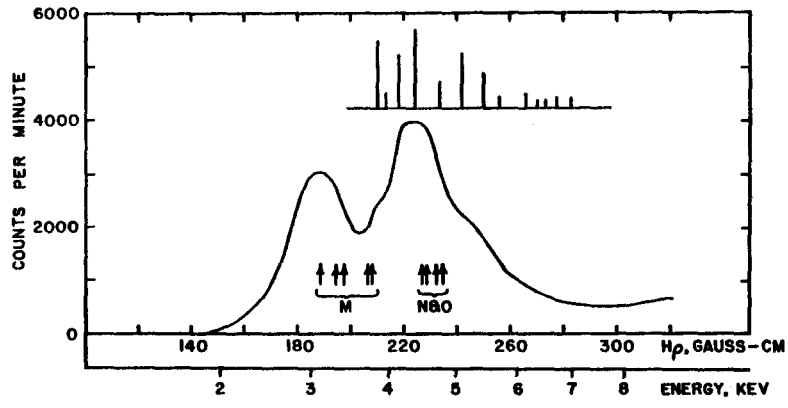

Figure 14. Low-energy internal conversion spectrum showing the M and N conversion electrons from the 4.8-kev transition superposed on the L-Auger spectrum. The arrows indicate where the conversion lines would be expected for a transition energy of 4.82 kev. The vertical lines above the spectrum show the expected energies and intensities of L-Auger electrons by analogy with those measured in Er^{171}.

in Table I are the more recent and much more precise values obtained by Geiger and Graham (1962). It is seen that some new transitions have been found and also some transitions found by previous workers were not observed in the present work. These differences will be discussed later.

The intensities of the K and L conversion peaks of some of the transitions are presented in columns 3 and 4 of Table II. In column 2 are shown the photon intensitics of the transitions as determined by external conversion. These photon intensities have been corrected for effects due to radiator thickness, photo-electric cross-section etc., using the empirical data of Artna (1961) as described in Chapter 3. The intensities given in Table II have been normalized to probabilities per decay in a manner which will be explained in the next section.

TABLE I

Energy measurements for transitions in Sm^{151}
(all values are expressed in Mev)

Rutledge *et al.*	Burson and Schmid	Present work	Geiger and Graham[a]
		0.0048±0.0001[b]	0.004817
		0.025±0.001[c]	0.02570
		0.035±0.001[c]	0.03512
			0.06101
			0.06291
0.0647		0.065±0.001[c]	0.06488
0.0658		0.066±0.001[c]	0.06582
0.0696		0.069±0.001[c]	0.06969
		0.077±0.001[c]	0.07620
			0.09804
			0.09869
0.1000		0.0999±0.0004	0.10000
			0.10190
		0.105±0.001	0.10482
0.1162			
			0.13929
0.1440		0.1434±0.0004[d]	0.14316
		0.1522±0.0004[d]	
		0.1563±0.0003	0.15619
		0.1636±0.0004	0.16291
			0.16357
		0.1680±0.0003	0.16773
			0.16838
		0.1771±0.0003	0.17651
			0.17716
		0.2018±0.0003[d]	
0.2083		0.2088±0.0003	0.20898
0.2319		0.2323±0.0003	0.23240
		0.2365±0.0004	
0.2399		0.2399±0.0004	0.24008
0.2752	0.275	0.2749±0.0003	0.27520
		0.3242±0.0004[d]	
0.3402	0.340	0.3399±0.0003	0.34008
		0.345±0.0001[d]	
		0.3529±0.0004[d]	
		0.4394±0.0015	
	0.445	0.4445±0.0005	
	0.545		
	0.642	0.637±0.002[d]	
		0.670±0.002[d]	
0.715	0.715	0.717±0.002	
		0.735±0.002[d]	
		0.752±0.002[d]	
	0.765	0.772±0.002[d]	
		0.813±0.002[d]	
		0.821±0.002[d]	
	0.945	0.952±0.005[d]	

[a]Values in this column were obtained by taking differences of the level energies in Fig. 20. Refer to this figure for errors on the measurements.
[b]This value was obtained assuming most of the *M* conversion to be in the *M*1 subshell.
[c]This energy measurement is from the Gerholm spectrometer.
[d]This value was obtained from external conversion measurements only.

TABLE II

Photon and conversion electron intensities in the decay of Pm^{151}

Transition energy, Mev	Photons/decay, $\times 10^2$	Conversion electrons/decay: K-shell, $\times 10^2$	L-shell, $\times 10^2$	Transition probability, $\times 10^2$	α_K, $\times 10^2$	K/L§	Multipolarity
0.0048		Strong $M+N$ shell groups		35*			
0.0257			3.0†	3.7†			
0.0351			0.7†	0.8†			
0.0649		9.4†	2.2†	14.0†			
0.0658		5.6†	1.2†	8.3†			
0.0697		2.0†	0.4†	2.9†			
0.0762		0.7†	0.6†	1.6†			
0.1000		3.9±0.6	0.8±0.1	7.6±1.1		4.9±0.5	$M1+E2$ or $M2$
0.1048		2.5†	0.6†	5.0†			
0.1432	0.8±0.3						
0.1522	0.4±0.2						
0.1562		0.06±0.02					
0.1629	2.4±0.9	0.51±0.06	0.12±0.03	3.0±1.0	21±0.7‡	4.0±0.4‡	$M1+E2$‡
0.1635							
0.1677	11±3	0.56±0.05	0.07±0.02	12±3	5±1.5‡	7.8±1.6‡	$E1$‡
0.1684							
0.1765	5.2±1.2	0.92±0.09	0.15±0.04	6.3±1.2	18±5‡	6.5±0.5‡	$M1+E2$‡
0.1771							
0.2018	1.3±0.5			1.5			
0.2090	1.8±0.4	0.30±0.03	0.04±0.01	2.1±0.4	17±6	8.0±1.5	$M1+E2$
0.2324	1.4±0.4	0.12±0.02	0.04±0.01	1.6±0.4	8±3	3.2±0.5	$M1+E2$
0.2365	1.4±0.8	0.04±0.01		1.5±0.8	2.9±1.7		
0.2401	3.0±1.3	0.05±0.008	0.02±0.003	3.1±1.3	1.7±0.6	2.4±0.4	$E1$
0.2752	6.3±1.2	0.10±0.02	0.01±0.003	6.4±1.2	1.6±0.6	8.4±1.5	$E1$
0.3240	0.9±0.4			0.9±0.4			
0.3401	21±4	0.19±0.02	0.02±0.004	21±4	0.90±0.14	6.9±0.6	$E1$
0.3449	1.5±0.7			1.5±0.7			
0.3529	0.5±0.2			0.5±0.2			
0.4394	0.9±0.3	0.006±0.002		0.9±0.3	0.7±0.4		$E1$
0.4445	3.3±1.0	0.016±0.004		3.3±1.0	0.5±0.2		$E1$
0.637	1.2±0.4			1.2±0.4			
0.670	1.2±0.4			1.2±0.4			
0.717	3.5±0.8	0.005±0.002		3.5±0.8	0.14±0.06		$E1$
0.735	0.8±0.3			0.8±0.3			
0.752	1.0±0.3			1.0±0.3			
0.772	0.6±0.3			0.6±0.3			
0.813	0.4±0.2			0.4±0.2			
0.821	0.4±0.2			0.4±0.2			
0.95	0.6±0.3			0.6±0.3			

*This value involves an estimate of the Geiger counter efficiency based on the intensity of the L Auger electrons.
†These values were estimated in the rather arbitrary manner described in the text.
‡Values obtained by treating these unresolved doublets as single lines.
§These ratios were obtained from internal conversion spectra and are more precise than the values deduced from columns 3 and 4.

4.2.2 Measurement of α_K and Total Transition Probability for the 0.340 Mev Transition

In order to relate the internal and external conversion intensity scales, the K-conversion coefficient for the 0.340 Mev transition was measured directly by comparing the number of K-conversion electrons with the photon intensity from the same

source. A strong beta source was prepared and the number of internal conversion electrons in the peak was measured. The source was then covered with a radiator and the external conversion peak height determined. Under these circumstances, it was shown in Chapter 3 that

$$\alpha_K = k\left(\frac{A}{I_\gamma}\right)$$

where A is the area under the internal conversion peak, I_γ is the photon intensity corrected for radiator efficiency, and k is a factor which depends only on the geometry of the instrument, baffles, source-holder, detector etc.

The value of k was determined by performing the experiment with a Au^{198} source of the same dimensions placed in the same geometry and using the value of 0.028 for α_K for the 0.4118 Mev transition in this decay (Frey et al.(1962)).

In this manner the measured values of α_K for the 0.340 Kev transition were 0.0088 ± 0.0015 and 0.0093 ± 0.0018 using gold and uranium radiators, respectively. The average value of 0.0090 ± 0.0014, indicates that this is an E1 transition (Rose, 1958).

The probability per decay for a transition to occur can easily be found once its internal conversion coefficient is known. The ratio of the area under the K-conversion peak to the area under the total beta spectrum is fK where f is the probability per decay for the transition measured and K is the probability of K-conversion

for this transition. From the definition of α_K, it is seen that $K = \alpha_K/(1 + \alpha_T)$. For the 0.340 Mev transition, these experiments lead to 0.0019 $\pm$ 0.0002 K-conversion electrons per disintegration and a photon intensity of 0.21 $\pm$ 0.04. From these two values, the probabilities per decay for conversion electron and photon emission for the other transitions can be evaluated from the relative intensities directly measured. These are shown in columns 2, 3 and 4 of Table II.

For any given transition, the sum of the entries in columns 2, 3 and 4 of Table II is the total transition probability (except for low energy transitions where higher order internal conversion becomes appreciable). This quantity is shown in column 5 of Table II. For some of the transitions above 0.30 Mev, the K or L peak intensities were too weak to be measured in internal conversion. In such cases the transition intensity was taken to be the same as the photon intensity measured in external conversion. The error introduced in this way is probably small in comparison with the experimental error on the photon intensity measurements. On the other hand, for some of the low energy transitions it was not possible to perform external conversion experiments and therefore the photon intensity could not be measured directly. In most of these cases the intensities could be estimated from the internal conversion work alone on the assumption that the photon contribution is small.

For each transition, the ratio of the entries in columns 2 and 3 of Table II gives the internal K-conversion coefficient which is tabulated in column 6. This value is not available for all of

the transitions as it requires a clean measurement of the transitions in both internal and external conversion.

The value of α_K for the 0.275 Mev transition was also measured directly using the same method as described for the 0.340 Mev transition. This measurement was complicated by the fact that the internal K conversion line of the 0.275 Mev transition was not completely separated from the L lines of the 0.232 and 0.240 Mev transitions and also was mixed with the L lines of the 0.236 Mev transition whose existence was not realized until later. Hence, this experiment is regarded mainly as a check. However, the value of $\alpha_K = 0.021 \pm 0.0055$ obtained directly agrees, within experimental error, with the value of 0.016 ± 0.006 quoted in Table II.

4.2.3 Beta Spectrum Measurement

The beta spectrum was scanned on two occasions and the results were subjected to Fermi analyses. At first, before the order of levels and transitions in the decay scheme was known, the Fermi analyses were carried out without regard to where the end-points of the various sub-groups might be. This work suggested the presence of six partial spectra with end-point energies and intensities of 1.20 Mev (11%), 1.10 Mev (18%), 0.96 Mev (9%), 0.84 Mev (40%), 0.725 Mev (12%) and 0.435 Mev (10%).

Coincidence experiments performed later showed that the situation was more complex than the above data predicted. Several of the above partial spectra were found to be two or more groups with end-point energies differing by a relatively small amount. Thus,

when the level scheme had been determined, the Fermi analyses were repeated, the partial spectra being drawn in with end points determined from coincidence experiments and the level scheme. Unfortunately, the levels in Sm^{151} are too closely spaced to determine by this method the beta intensity feeding each level. Several of the beta groups obtained are not actually single groups but feed more than one level. The results of this second analysis yielded partial spectra with energies and intensities 1.20 Mev (11%), 1.13 Mev (13%), 1.03 Mev (12%), 0.85 Mev (44%), 0.75 Mev (11%) and 0.425 Mev (9%) in reasonable agreement with the first analysis with its larger number of degrees of freedom.

4.2.4 Coincidence Experiments

As mentioned earlier, coincidence experiments were undertaken in an attempt to resolve some of the ambiguities in the possible decay schemes based on previous work. Different types of coincidence experiments were performed, depending upon the properties of the different transitions studied.

First, the beta spectra in coincidence with the conversion electrons of various transitions were measured. This was accomplished by focusing the conversion electrons in one end of the spectrometer and scanning the beta continuum with the other end. The baffle in the conversion electron end of the instrument was usually set to give a resolution of 1.5% to 2% in momentum, while the baffle in the beta end was opened wider to give a greater transmission where high resolution was not necessary. Fifteen-minute counts were taken

at points spaced about 50 kev apart on the beta continuum, up to about 100 kev higher than the end-point energy of the partial spectra being measured. Care was taken to avoid setting the beta spectrometer on any internal conversion peaks. This "scanning" was then repeated six to eight times and the points were averaged after being corrected for decay and for accidental coincidences. Typical results are shown in Figures 15 and 16. Figure 15 shows Fermi plots of the partial beta spectra in coincidence with the K-conversion lines of the 0.168 and 0.177 Mev doublets. Figure 16 shows the Fermi plots of beta spectra in coincidence with the K-conversion lines of the 0.100 and 0.340 Mev transitions. The end-point energies of partial beta spectra in coincidence with various conversion lines are summarized in column four of Table III.

By removing the baffles in one end of the spectrometer and installing a NaI(Tl) crystal, coincidences between conversion electrons and gamma rays could be measured. First, the electron spectrometer was focused on the desired conversion line and the coincident gamma spectrum collected in the multi-channel pulse

TABLE III

Summary of conversion-electron coincidence experiments

Conversion electrons focused, Mev	Coincident gammas, Mev	Coincident electrons, Mev	Coincident beta end points, Mev
0.0048 *M*	0.340, 0.275, 0.100		
0.065 *K*	0.275, gammas in 0.65–0.75 region		0.85, 1.13
0.100 *K* and *L*	0.240, gammas in 0.65–0.75 region		0.85, 1.09
0.105 *L*			0.85, > 1.05
0.163 *K* doublet	Photopeak at 0.17 Mev	0.177 *K* doublet No. 0.163 or 0.168 *K* doublet	
0.168 *K* doublet	Photopeak at 0.17 Mev	0.177 *K* doublet No. 0.163 *K* doublet	0.85, 1.03
0.177 *K* doublet	Photopeak at 0.17 Mev	0.163 *K* and 0.168 *K* doublets	0.85
0.340 *K*			0.85

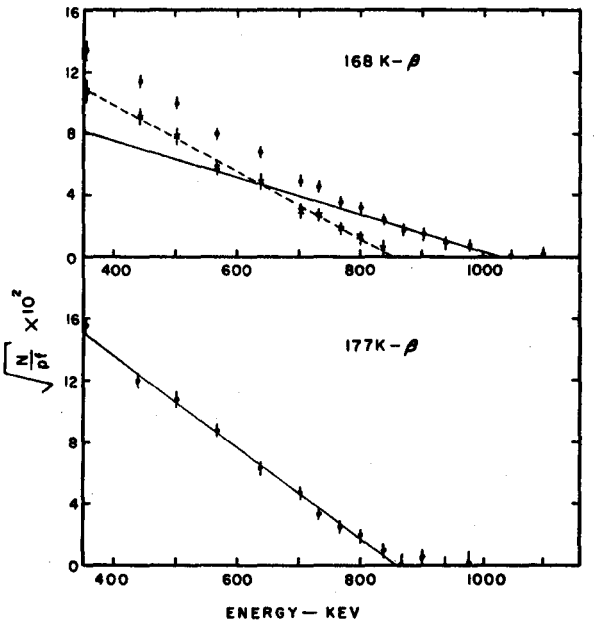

Fig. 15. Fermi plots of beta spectra in coincidence with the 168 K and 177 K conversion lines. These data, when combined with electron-electron coincidence results, first suggested the existence of the level at 4.8 kev.

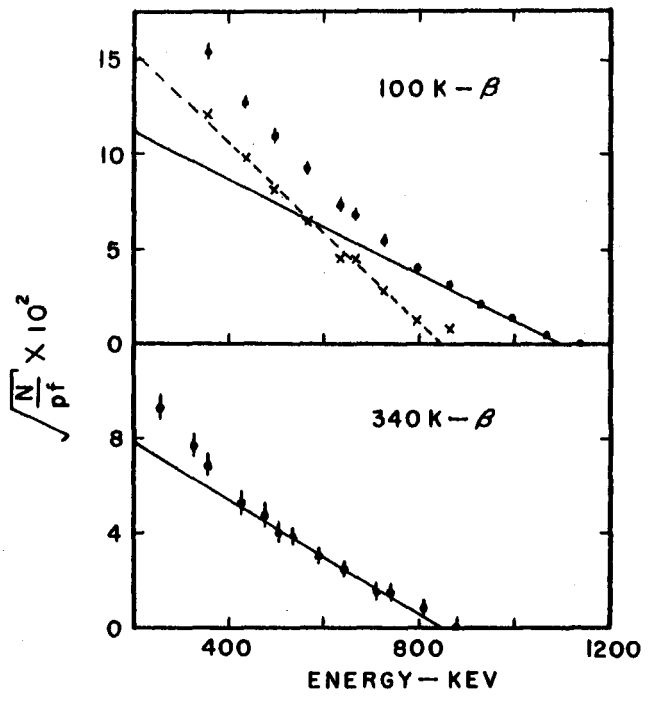

Fig. 16. Fermi plots of beta spectra in coincidence with the 100 K and 340 K conversion lines.

height analyzer. The electron spectrometer was then set just off the conversion line and the experiment repeated to determine the contribution of the underlying beta continuum to the coincidence gamma spectrum. The results of such experiments are given in the second column of Table III, and some typical coincidence spectra are shown in Figure 17.

Using the same experimental arrangement, the gamma spectra in coincidence with various points on the beta continuum were measured and Fermi plots made for each of the photopeaks in the gamma spectrum. As explained in Chapter 3, such gamma-beta experi-

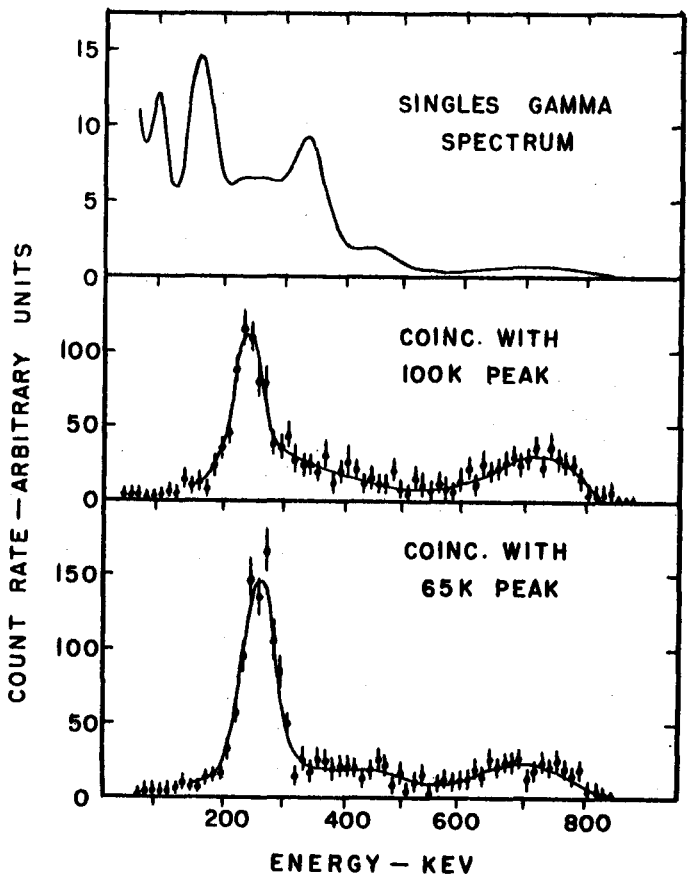

Fig. 17. Results of conversion electron-gamma coincidence experiments with the 100 K and 65 K peaks. The top curve is a singles gamma spectrum for calibration.

ments are easier to do than electron-beta experiments for high energy transitions, but the analysis is complicated by the fact that the transitions are not all resolved. Typical results can be seen in Figure 18 which shows Fermi plots of the partial spectra in coincidence with the photopeaks at 0.170, 0.340 and 0.445 Mev. The deviations from linearity for beta energies below about 300 kev in these plots result from source thickness, as this was an early experiment for which the source was not prepared by the sublimation technique.

Coincidence experiments were also performed between different pairs of conversion lines. As discussed in section 3.3.2, these

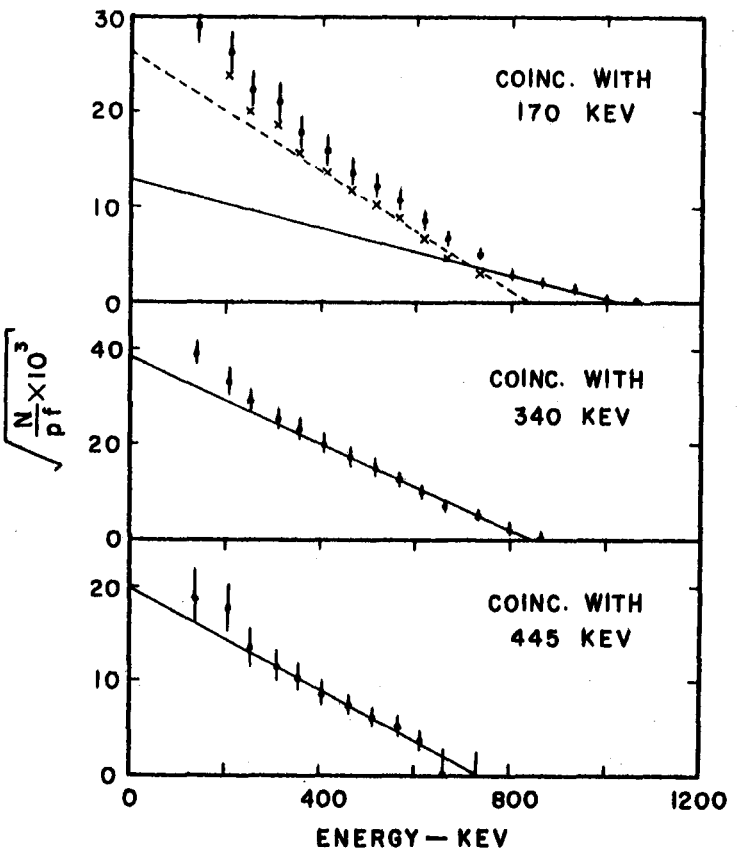

Fig.18. Fermi plots of beta spectra in coincidence with photopeaks at 170, 340 and 445 kev.

electron-electron experiments require a series of counts with each of the spectrometers on and off the conversion line in order to make a correction for the coincidences caused by the underlying beta continua. In this way the coincidence rates between the K-conversion lines of the "0.163, 0.168 and 0.177 Mev transitions" were determined.

Coincidences between	"163K"- "177K"	"168K"- "177K"	"163K"-"168K"
Coincidence Rate (counts/hr)	170 ± 36	257 ± 37	-5 ± 31

These data show that the "0.163 Mev" and "0.168 Mev" transitions are both in coincidence with the "0.177 Mev" transition but not with each other. It was later learned from the experiments of Geiger and Graham (1962) that each of these lines was actually a doublet. That is, the "0.163, 0.168 and 0.177 Mev transitions" are actually the unresolved pairs of transitions 0.16291 and 0.16357, 0.16773 and 0.16838, 0.17651 and 0.17716 Mev, respectively. Fortunately, this does not change any of the arguments based on these experiments.

4.2.5 Formulation of Decay Scheme

The above results are sufficient to determine a unique order for the strongest transitions in this decay. The various energy sums from coincidence work and the beta spectrum measurements indicate that the total decay energy is 1.195 ± 0.010 Mev. This differs from predictions of 1.5 Mev and 1.8 Mev based on previous work. The value of 1.8 Mev was obtained by Rutledge *et al.* (1952) using coincidence methods with aluminum absorption techniques to measure

the beta energy. They concluded that a 1.1 Mev beta group was in coincidence with the 0.715 Mev transition. The beta-gamma coincidence measurements in the present work indicate that the beta group in coincidence with the 0.715 Mev transition has an end point energy of 0.390 $\pm$ 0.020 Mev. This is consistent with a Q-value of 1.2 Mev.

Other evidence for a decay energy greater than 1.2 Mev is that Hans et al. (1955) report a gamma transition of about 1.5 Mev with a half life of 27.5 hours. Also, Burson and Schmid (1958) report a weak beta-group with an end-point energy of 1.5 Mev. It should be pointed out that none of the previous workers performed an ion exchange separation on the source before measurements were taken and therefore various impurities were probably present. As mentioned earlier, among the impurities separated out by the ion exchange process in the present work were 9-hour Eu^{152m} and 72-day Tb^{160}. Both of these nuclides have beta groups of about 1.8 Mev and gammas of about 1.4 Mev.

In the present work, energy sums of coincidences with all the strong transitions add up to about 1.2 Mev; for example, the 0.340 Mev transition is in coincidence with a 0.850 Mev beta group, the 0.065 Mev transition is in coincidence with a 1.14 Mev beta group and also with a 0.275 Mev transition and an 0.850 Mev beta group, and so on. No sums greater than 1.2 Mev have been observed in the present work and all the strong transitions take part in coincident sums adding up to this value. Thus it is concluded that this value represents the decay energy.

It was realized by early workers that several pairs of transitions had energy sums of 0.340 Mev; e.g.: 0.275 + 0.065, 0.240 + 0.100, 0.163 + 0.177 and, of course, the 0.340 Mev transition itself. Hence, these were usually considered to be competing modes of decay from a 0.340 Mev level. Electron-gamma and electron-electron coincidence experiments in the present work verify that each of the above pairs is actually a pair of coincident transitions. Also, the electron-beta experiments show that the 0.065, 0.100, 0.163, 0.177 and 0.340 Mev transitions all have a coincident beta spectrum with an end-point energy of 0.850 Mev. Furthermore, since the first three of these transitions also have coincident beta spectra with end-point energies of 1.13, 1.09 and 1.03 Mev, respectively, they must be the lower members of the cascades. In all previous work, it was assumed that the level fed by these cascades was the ground state. However, the electron-electron and electron-beta coincidence experiments show that the 0.177 Mev transition feeds both the strong 0.168 Mev and the 0.163 Mev transitions. This leads one to postulate a level structure as shown in the decay scheme of Figure 19 where the 0.340 Mev transition and the cascades mentioned above feed a level at an excitation energy of 4.8 kev. As several strong transitions feed this low energy level, an intense 4.8 kev transition to the ground state should exist. Experiments which resulted in the identification of this transition and a measurement of the lifetime of the 4.8 kev level will be discussed in the next section.

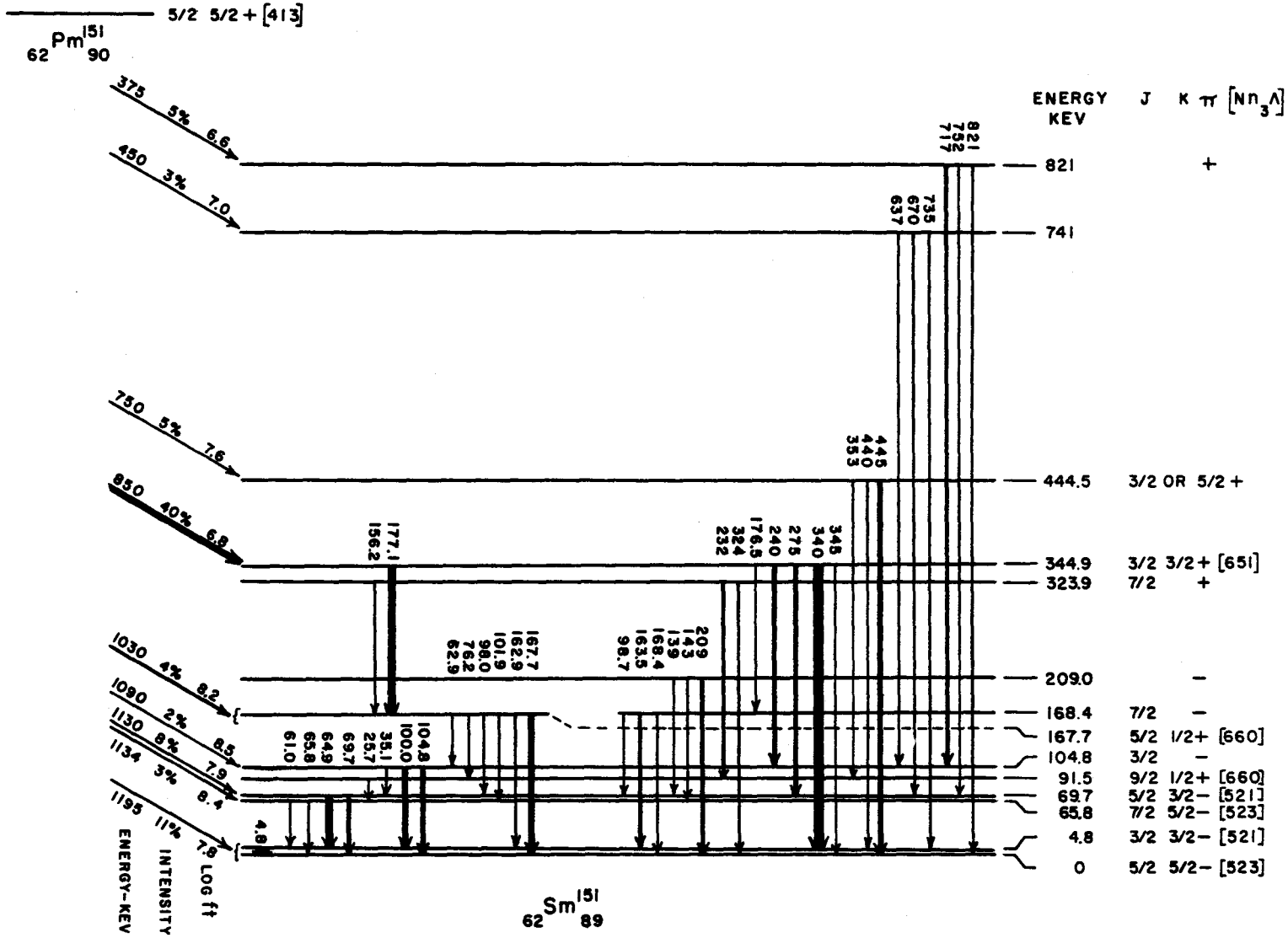

FIGURE 19 — PROPOSED LEVEL SCHEME FOR SAMARIUM — 151

The existence of this low energy level immediately explains the nature of several pairs of transitions differing in energy by 4.8 kev. For example, the 0.440 and 0.445 Mev transitions feed the 4.8 kev level and ground state, respectively, from a level at 0.445 Mev. This is substantiated by beta-gamma coincidence work, which shows a beta group with end-point energy of 0.750 Mev in coincidence with the photopeak containing the 0.440 Mev and 0.445 Mev transitions (see Figure 18). Similarly, the 0.0648 Mev and 0.0696 Mev transitions feed the two lowest levels from a level at 0.0696 Mev, while the 0.1000 and 0.1048 Mev transitions depopulate a level at 0.1048 Mev. The 0.1048 Mev transition was not seen clearly in the present work or in the internal conversion work of Rutledge et al. Its K-conversion line was mixed with the L lines of the 0.0648 and 0.0658 Mev transitions, while its L conversion lines were under the K peak of the 0.143 Mev transition. However, the K/L ratio for the internal conversion peaks of the 0.143 Mev transition had an unrealistic value of greater than 10 in the present work, indicating that there was probably another peak mixed with its K-conversion line. The 0.143 Mev transition itself is well verified as it has been seen in external conversion. Postulating a 0.1048 Mev cross-over transition explains this abnormally high K/L ratio as well as the weak peak at about 0.104 Mev electron energy, which is attributed to the M-conversion electrons. This conclusion was later verified by Geiger and Graham (1962) who could resolve the lines in internal conversion. Also, their precise energy measurements confirm and add to the structure of the decay scheme for the levels below 0.345 Mev

as can be seen from Figure 20. There are several transitions of medium intensity which had not been placed by coincidence work

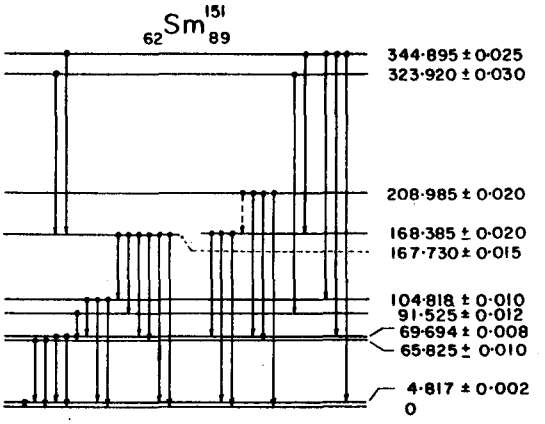

FIG. 20 This Sm^{151} level scheme results from studies of the Pm^{151} conversion-electron spectrum made with the Chalk River beta spectrometer by Geiger and Graham (1962). The level sequence has been deduced from energy sum considerations. The level energies are based on a momentum value for the *K*-conversion line of the 411.772-kev transition in Hg^{198} of 2222.399±0.044 gauss-cm (Murray *et al.* 1962). The uncertainties in the level energies are estimated standard deviations in their absolute values.

before their results became available. These include the 0.076 Mev, 0.143 Mev, 0.209 Mev, 0.232 Mev and 0.323 Mev transitions. In addition, the work of Geiger and Graham has revealed several weak transitions not found by any other workers (see Table I and Figure 20). The precise energy measurements for these transitions are sufficient to determine uniquely their position in the decay scheme.

Several higher energy transitions have been seen in external conversion. These can be seen in Figure 11 which shows the external conversion spectrum taken with a gold radiator in the region from 1500 to 4200 gauss cm. There are peaks corresponding to transitions with energies 0.637 Mev, 0.670 Mev, 0.717 Mev, 0.735 Mev, 0.752 Mev, 0.772 Mev, 0.813 Mev and 0.821 Mev. The

conversion peaks from the first five of these transitions decay with a half life appropriate for Pm^{151}. The conversion peaks from the last three transitions are weaker and therefore it is more difficult to obtain a measure of their half-lives. However, from the measurements which have been made, it is known that the half-lives for these peaks are greater than 8 hours and less than 60 hours. As none of the known impurities with half-lives in this range have gamma rays with these energies, it is assumed that all of these transitions are in the decay of Pm^{151}.

From electron-gamma coincidence work, it is known that some of the transitions between 0.60 and 0.85 Mev are in coincidence with the conversion lines of the 0.0648 Mev and 0.1000 Mev transitions (see Figure 17). The individual photopeaks were not resolved in the NaI(Tl) detector used for this work but in each case the coincident gamma spectrum contained a peak in this region which was too wide to be one photopeak. Hence, more than one of the high energy gammas is in coincidence with each of the above conversion lines. On the basis of these measurements, the beta-gamma results for the high energy transitions, and energy fit, six of the high energy transitions are placed in the decay scheme as shown, depopulating levels at 0.741 Mev and 0.821 Mev.

The remaining two of these transitions, with energies of 0.772 Mev and 0.813 Mev, have not been placed in the decay scheme shown in Figure 19. Similarly, the 0.952 Mev transition, which has

been observed in external conversion with a uranium radiator has not been placed in the decay scheme. The presence of these weak transitions indicates that the level structure is more complex at high energies than is shown in Figure 19.

The 0.116 Mev transition reported by Rutledge et al. has not been found. The internal conversion peak which was formerly thought to be the 0.116 Mev K peak has been found to be the L conversion lines to a 0.076 Mev transition. The reason for this change is that peaks corresponding to the 0.076 Mev K and 0.076 Mev M conversion lines have also been found. What was formerly called the L conversion lines to the 0.116 Mev transition is actually the K conversion line of the 0.1562 Mev transition.

In view of the fact that the 0.340 Mev transition is one of the strongest in the decay, it was interesting to note that no 0.345 Mev cross-over transition to the ground state had yet been seen. This region of the spectrum was examined more carefully using a uranium radiator with external conversion. The data are shown in the insert of Figure 11, where the 0.345 Mev K peak would be expected to be in the tail on the high energy side of the strong 0.340 Mev K peak. The solid line in this spectrum is the expected peak shape for this energy with the Siegbahn instrument obtained by examining the 0.308 Mev transition in Er^{171}. It is seen that a small peak appears to be present at 0.345 Mev with an intensity of 0.07 ± 0.04 relative to the 0.340 Mev K peak.

The improved statistics obtained on the nearby continuum while performing the search described above show the presence of

another weak peak with an electron energy of about 0.238 Mev. This is interpreted as being the K conversion peak (in uranium) of a 0.353 Mev transition which would have the correct energy to fit between the levels at 0.0915 Mev and 0.4445 Mev.

A transition with an energy of 0.2365 Mev has been observed in internal conversion and also in external conversion, using a uranium radiator. No observations could be made from external conversion with a gold radiator as the 0.2365 Mev K peak would be mixed with the 0.168 Mev L peak. This transition does not have the proper energy to fit between any pair of the levels shown in Figure 19.

From the values of α_K in column 6 of Table II, and the theoretical conversion coefficients of Rose (1958), it is possible to determine the multipolarities of some of the transitions. The 0.715 Mev, 0.445 Mev, 0.340 Mev, 0.275 Mev and 0.240 Mev transitions are all E1. The 0.208 Mev and 0.232 Mev transitions would appear to be either E2 or M1 or some mixture of these. The 0.1677 Mev and 0.1684 Mev transitions were not resolved in the present work but the ratio of the sum of the K conversion electron intensities to the sum of photon intensities is 0.054 ± 0.015. As this is about the value of α_K expected for an E1 transition and all other multipolarities would have a larger conversion coefficient, it is assumed that at least one of these transitions is E1 in character. It will be seen later that the 4.8 kev transition is predominantly M1. From these results it can be concluded that the 0.0048, 0.0696, 0.1048 and 0.2090 Mev

levels all have the same parity as the ground state, while the 0.821, 0.4445, 0.3449 Mev levels and one of the levels at about 0.168 Mev have opposite parity.

In order to make a check on the balance of the intensities feeding into and out of each level, it was necessary to make estimates of the intensities of the strong transitions depopulating the 0.0658 Mev, 0.0696 Mev and 0.1048 Mev levels. In the present work, none of the conversion lines from these transitions was completely separated from other lines. Therefore, the values which are obtained must be regarded as estimates only and should be used with caution. The K and L conversion peaks of the 0.1000 Mev transition could contain contributions from the 0.0980 Mev, 0.0987 Mev and 0.1019 Mev transitions. As these lines would have been resolved in the spectrum taken with the Siegbahn instrument, the fact that they were not seen indicates that they were probably weak compared with the 0.1000 Mev conversion lines. This assumption would appear to be justified by the fact that the gamma spectrum in coincidence with the 0.1000 Mev K conversion peak does not show the 0.177 Mev radiation which would be expected if the conversion electrons from the other three transitions were contributing strongly.

The strong 0.0648 Mev and 0.0658 Mev K conversion peaks are resolved from each other but are both mixed with the 0.025 Mev L lines. The 0.0257 Mev transition must have an intensity of at least 0.03 per decay as it is the only mode of depopulation for the 0.0915 Mev level. If there is a beta group feeding the 0.0915 Mev level, the 0.0257 Mev

transition would have to be still more intense. If at first one neglects the presence of such a beta group, estimates can be made of the K-conversion electron intensities for the 0.0648 and 0.0658 Mev transitions. These are found to be 0.094 and 0.056 per decay, respectively. It is noted that if the intensity of the 0.0257 Mev transition were twice the value assumed above, the 0.0648 and 0.0658 Mev K conversion intensities would be affected only 15 to 20 per cent. Similar crude calculations were made for the other conversion lines and small corrections applied for photon contribution assuming E2 + M1 admixtures. The final estimates obtained in this fashion are entered in Table II with a dagger. It should be clear that these values have been arrived at in a rather arbitrary manner and that they could be in error by as much as 50 to 100 per cent.

The intensities of the beta groups shown in Figure 19 have been deduced from the decay scheme, using the criterion that the total number of decays going to any level must be the same as the number leaving that level. Exceptions to this are the 1.20 Mev beta group whose intensity was obtained from the Fermi analysis and the 1.095 and 1.03 Mev groups which will be discussed later. It is seen that the beta intensities shown in Figure 19 are in reasonable agreement with the values obtained by Fermi analysis of the beta continuum. It is not known whether the 1.20 Mev beta group feeds the ground state or the 0.0048 Mev level, or whether it is actually two groups feeding both of these levels. Similarly, the 1.03 Mev group could feed either one or both of the levels at 0.168 Mev.

4.2.6 Experiments with Low Energy Electrons

One of the major changes in the structure of the level scheme brought about by this work is the prediction of a strongly fed level at 4.8 kev. It was felt that this structure could be verified by finding the conversion electrons from the 4.8 kev transition to the ground state. A thin source was prepared and mounted in the Gerholm spectrometer and a thin window Geiger counter, as described in Appendix B, was used as a detector. The spectrum obtained for electron energies from 3 to 8 kev is shown in Figure 14. The arrows in this figure show where the various M and N conversion electrons from the 4.8 kev transition would be expected. Low energy calibration was accomplished by mounting an electron gun in the spectrometer in the position normally occupied by the source. By applying different accelerating voltages to this gun, calibration points were taken between 1.5 and 3.0 kev. Points at electron energies 18 kev and higher were obtained from the known lines in the decay of Pm^{151}. When the electron momentum was plotted against the spectrometer current required to focus that momentum, the points obtained with the electrons from 1.5 to 3.0 kev were collinear with those at 18 kev and higher. Hence, it was assumed that the momentum of electrons focused by the spectrometer was linear with current for the entire region of interest. It was noticed, however, that the resolution of the instrument started to become poorer below about 20 kev until at 3 or 4 kev the resolution was about 5%, regardless of the baffle settings. It is felt that this effect may be the result of a change in the shape of the magnetic field as one goes to lower currents. No evidence for hysteresis in the iron

could be found at electron energies down to 3 kev as the peaks were found at the same current setting whether scanned with increasing or decreasing current.

The low energy electron spectrum shown in Figure 14 shows evidence for the existence of a 4.8 kev transition in that peaks are found in the places expected. However, it is not considered to be a proof because the intense L-Auger electrons are expected to lie in this energy region also and the resolution is not good enough to separate the conversion electrons from them.

Although it is energetically possible to have L-Auger electrons from 3.1 to 7.5 kev, analogy with nearby nuclides for which the L-Auger spectra have been measured (Tm^{171}, Hatch and Boehm (1957); Lu^{171}, Valentin (1962)) indicates that in Sm^{151} few or no L-Auger electrons should be found below about 3.8 kev, provided the various electronic transitions have roughly the same relative intensities in the Auger spectra of the different nuclides in this region. This would tend to indicate that the low energy peak at 3 kev in Figure 14 is due to M-conversion electrons, while the spectrum from 4 to 7 kev is due to a mixture of Auger and N and O conversion electrons.

This assumption has been verified by measuring the gamma spectrum in coincidence with each of the two peaks seen at 3 kev and at 4.4 kev in Figure 14. Auger electrons are produced by the re-arrangement of the atomic electrons following internal conversion. Therefore, in coincidence with Auger electrons one would expect to find the gamma rays which are in coincidence with strongly converted lines. The

0.0648 Mev transition is strongly converted and therefore the 0.275 Mev transition should be found in coincidence with the Auger lines. On the other hand, gamma-gamma coincidence experiments in the present work and also by Burson and Schmid (1958) have found no gammas in coincidence with the 0.340 Mev transition. Therefore, there should be no L-Auger electrons in coincidence with the 0.340 Mev gammas. However, it is seen from the decay scheme that the 0.340 Mev transition is expected to be found in coincidence with the 4.8 kev transition, provided the lifetime of the 4.8 kev level is shorter than or comparable to the resolving time of the coincidence circuitry.

The gamma spectra in coincidence with the electron peaks at 3 kev and 4.4 kev are shown in Figure 21, which also shows a single channel gamma spectrum for calibration. The difference between the two coincidence spectra constitutes the proof of the existence of the 4.8 kev transition. The spectrum in coincidence with the 3 kev electrons shows a strong 0.34 Mev peak as expected for conversion electrons and which would not be present if the 3 kev electrons were Auger electrons. On the other hand, the spectrum in coincidence with the 4.4 kev electrons shows some 0.34 Mev radiation but also a stronger peak of 0.275 Mev gammas. This is caused by the fact that there are Auger electrons as well as conversion electrons in this peak.

From the results of this experiment it is therefore possible to say that the existence of the 4.8 kev level has been confirmed and that the lifetime of this level is less than or comparable to the resolving time of the circuit (in this case, 300 nanoseconds).

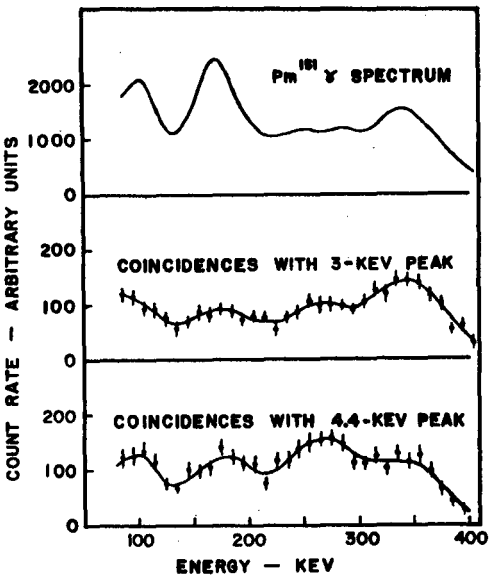

Fig. 21. Gamma spectra in coincidence with low energy conversion electrons. The difference between the two coincidence spectra verifies the existence of the 4.8 kev transition. The poor peak-to-valley ratio observed in these spectra is caused by radiation scattered from the pole pieces and other parts of the magnetic spectrometer which surrounded the NaI(Tl) detector.

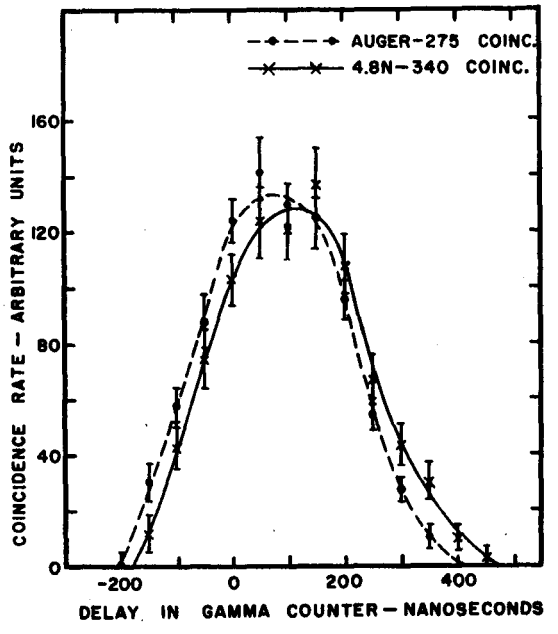

Fig. 22. Measurement of the lifetime of the 4.8 kev level by the method of delayed coincidences.

At about the same time, Geiger and Graham (1962) had independently verified the existence of the 4.8 kev level by resolving the various M, N and O conversion lines and separating them from the Auger lines. From the relative intensities of the M subshell conversion lines Geiger et al. (1963) conclude that the 4.8 kev transition is M1 with an E2 admixture of $\sim$0.07%.

An attempt has also been made in the present work to determine the lifetime of the 4.8 kev level, using the method of delayed coincidences. With the electron spectrometer set on the Auger and conversion electrons at 4.4 kev, coincident gamma spectra were measured for different values of artificially inserted delay in the two sides of the coincident circuit. The counts under the 0.34 Mev peaks in these spectra were all due to coincidences between conversion electrons and 0.340 Mev gammas and were used to plot the delayed coincidence curve shown in Figure 22. The counts under the 0.275 Mev peaks in the same spectra were due partly to coincidences with Auger electrons and partly to coincidences with conversion electrons. The latter contribution was subtracted from each spectrum, using the ratio of 0.275 Mev counts to 0.340 Mev counts from the spectrum coincident with the 3 kev conversion electrons. After subtracting this portion, the remaining contribution, which was due to coincidences between Auger electrons and 0.275 Mev gammas, was plotted as the dashed curve in Figure 22. The curves in this diagram have been normalized so that the area under each is the same. The difference in centroid positions along the time axis for the

areas under these two curves is the mean life of the 4.8 kev level minus the mean lives of the 0.0697 Mev level and of the electronic levels resulting in the Auger transitions. From Figure 22 this difference is found to be 28 ± 15 nanoseconds. It is seen from the work of Ramburg and Richtmyer (1937) that the electronic states leading to L-Auger transitions have level widths of the order of a few electron volts for $Z \approx 60$. Using the uncertainty relationship $\Delta E \, \Delta t \approx \hbar$, it is concluded that the lifetimes of the electronic levels are of the order of 10^{-15} seconds. As this is several orders of magnitude shorter than the centroid shift in Figure 22, it can be ignored in this work. From the work of Chery (1962), it is concluded that the lifetime of the 0.0697 Mev transition is $\leq 5 \times 10^{-10}$ sec, which is also negligible compared with 28 ± 15 nanoseconds. Hence, the dashed curve is considered to be a prompt curve for this particular electron energy.

It has been observed that the collection time of the Geiger counter was dependent upon energy for low energy electrons. This is indicated by the fact that a different delayed coincidence curve was obtained for 0.340 Mev gamma coincidences with the M conversion electrons than for the N conversion electrons. These curves should have been identical if collection time effects were not present, but the centroid shift for the former was about 30 ± 10 nanoseconds greater than that of the latter. Also, the prompt curve in Figure 22 is delayed by 13 ± 9 nanoseconds with respect to a prompt curve obtained at an electron energy of 0.25 Mev, using the same experimental set-up

with the beta-gamma and conversion electron-gamma coincidences in Ir^{192}. At first sight, it may seem unreasonable that the difference in collection time between 3 kev and 4.4 kev electrons is about 30 nanoseconds, whereas, from the above, the collection time difference between 4.4 kev and 250 kev electrons is 13 ± 9 nanoseconds. However, it must be remembered that these are the electron energies before penetration of the thin VYNS window of the Geiger counter. As this window had a low energy cut-off for electrons of about 1.5 to 2 kev, a 3 kev electron would lose a large fraction of its energy in passing through the window, whereas a 4.4 kev electron would lose a much smaller fraction. Also, the Geiger counter used was an end-window type with a glass bead on the end of the counter wire. It is felt that the glass bead may have effectively "shielded" a portion of the counter volume between the window and the wire, thus tending to discriminate against low-energy electrons which could not travel very far through the counter gas. It should be pointed out that this dependence of collection time on energy would not affect the relative displacements of the curves in Figure 22 as the data for these curves were being obtained simultaneously with electrons of the same energy. The only parameter which was different for these two curves was the energy of the coincident gamma radiation. Experience with the same gamma detector operated in the same coincidence circuitry but with a resolving time of 12 nanoseconds showed no observable time shift for a change in energy from 0.100 Mev to 0.340 Mev. Hence, it is assumed that any such effect, if present, between energies of 0.275 and 0.340

Mev is negligible compared with the observed shift of 28 ± 15 nanoseconds in Figure 22. This quantity represents the mean life of the 4.8 kev level and thus the half-life is 19 ± 10 nanoseconds.

4.2.7 Additional Determinations of Transition Intensities

Once the structure of the level scheme is known, it is possible to obtain from coincidence work some intensity data which would not otherwise be available. For example, the 0.100 Mev transition depopulates the 0.1048 Mev level, which is fed by a 1.09 Mev beta group, a 0.240 Mev transition and some higher energy transitions. The beta spectra in coincidence with the K and L conversion lines of the 0.100 Mev transition show beta groups with end-point energies of 1.09, 0.850 and perhaps ~ 0.40 Mev (see Figure 16). As the 0.240 Mev transition is the only mode of decay from the 0.3449 Mev level to the 0.1048 Mev level and the 0.3449 Mev level is not fed by gamma transitions, the ratio of intensities of the 1.09 and 0.850 Mev beta groups in this coincidence spectrum must be the ratio of intensities of the 1.09 Mev beta group and the 0.240 Mev transition. This ratio is measured to be 0.60 ± 0.10 and the total probability per decay of the 0.240 Mev transition is 0.031 ± 0.014. Hence, the 1.09 Mev beta group makes up 0.019 ± 0.010 of the total decay. This group is too weak to be found in the Fermi analysis of the total beta continuum, as it is surrounded by several groups which have much greater intensities. This measured intensity for the 1.09 Mev beta group may be too large, since the conversion lines of the weak 0.0980, 0.0986 and 0.1019 Mev transitions were not resolved from the 0.100 Mev conversion lines.

The coincidence experiment discussed above also provides a check on some of the data presented earlier in this chapter. When spectrometer number 2 is set to focus a conversion line from the 100 kev transition, the peak counting rate is

$$N_o f_{100} \mathcal{K}_{100} \omega_2 \mathcal{E}_2 \qquad (7)$$

The nomenclature is the same as that used in section 3.3.2 and the subscripts on f and $\mathcal{K}$ here refer to the transition energy. In this section, a factor $\mathcal{E}$ is explicitly included to take into account any decrease in counting rate on the low energy conversion peaks due either to a detection efficiency less than unity or to a reduction in peak height caused by source thickness. The area under the coincidence beta spectrum with end-point energy of 850 kev is

$$N_o f_{240} (f_{100}/f_s) \mathcal{K}_{100} \omega_2 \mathcal{E}_2 \omega_1 \eta_1 \qquad (8)$$

f_s is the sum of the probabilities of transitions which depopulate the 0.1048 Mev level. It is seen that (8)/(7) gives the ratio f_{240}/f_s since ω_1 and η_1 are known. From the coincidence experiments, $f_{240}/f_s = 0.35 \pm 0.08$. This quantity is actually the ratio of f_{240} to the total population of the 0.1048 Mev level. From Table II and the decay scheme, this value is found to be

$$f_{240}/(f_{717} + f_{637} + f_{240} + \delta_{1090}) = 0.32 \pm 0.10$$

The good agreement between these independent measurements tends to confirm the intensity data and proposed level structure presented earlier in this chapter.

In a similar manner, coincidence experiments with the 0.163, 0.168 and 0.177 Mev doublets provide an independent means of obtaining some intensity data. For instance, consider the beta-gamma experiment with the 170 kev photopeak (see Figure 18). Suppose spectrometer number 1 counts gammas and number 2 scans the beta spectrum. The area under the single channel beta spectrum in number 2 is

$$\int \frac{N_2}{p}\, dp = N_o \omega_2 \eta_2 \tag{9}$$

At first we shall neglect internal conversion in expressions for photon intensities and ignore transitions depopulating the levels at 0.168 Mev other than the 0.163 and 0.168 Mev doublets. Then the partial coincidence beta spectrum with end-point energy of 0.850 Mev has an area

$$N_o (f_{177.1} + f_{176.5}) 2\omega_1 \epsilon_1 \omega_2 \eta_2 \tag{10}$$

Here ϵ_1 is the efficiency of the NaI(Tl) detector for the unresolved gammas in the 170 kev photopeak. The coincidence partial beta spectrum with an end point of 1.03 Mev has an area

$$N_o (\delta_{167.7} + \delta_{168.4}) \omega_1 \epsilon_1 \omega_2 \eta_2 \tag{11}$$

where $\delta_{167.7}$ and $\delta_{168.4}$ are the intensities of the beta groups feeding levels at 167.7 and 168.4 kev, respectively.

The factor $\omega_1 \epsilon_1$ can be found from an electron-gamma coincidence experiment using the same geometry for the NaI(Tl) counter. In this case the internal K-conversion peak height for the 0.177 Mev transition in spectrometer number 2 is

$$N_o(f_{177.1}\mathcal{K}_{177.1} + f_{176.5}\mathcal{K}_{176.5})\omega_2^1\varepsilon_2^1 \qquad (12)$$

The rate of coincidences between this conversion peak and the gamma photopeak is

$$N_o(f_{177.1}\mathcal{K}_{177.1} + f_{176.5}\mathcal{K}_{176,5})\omega_2^1\varepsilon_2^1\omega_1\epsilon_1 \qquad (13)$$

Thus it is seen that the ratio

$$\frac{(10)(12)}{(9)(13)} = 2(f_{177.1} + f_{176.5})$$

These experiments result in a value for $f_{177.1} + f_{176.5}$ of 0.06 ± 0.02, in good agreement with the value of 0.063 ± 0.012 given in Table II. Extending the above expressions to correct for the reduction of photon intensities due to internal conversion results in only a small change in the above value, as the new terms added tend to cancel out. The exact amount or direction of this correction is difficult to predict without more detailed knowledge of the decay, but the net effect is probably not greater than ten

or fifteen per cent of the value quoted above. Including the presence of the 76 kev transition depopulating the level at 167.7 kev would affect expressions (10) and (11) by about 5% and 10%, respectively, and thus would lower the above value by approximately 5%.

It is seen that the quantity (11)/(10) gives the ratio of the number of betas feeding the two levels at about 168 kev to the number of 177 kev gammas feeding these levels. In the experiment discussed above, (11)/(10) = 0.284 ± 0.04, indicating that the ratio of betas to 177 kev gammas is 0.57 ± 0.08 and hence the sum of the intensities of the two beta groups is 0.034 ± 0.011. If one calculates from the decay scheme and Table II the intensities of gammas feeding into and out of this pair of levels, it is found that a beta intensity of $\sim 9\%$ would be required to complete the balance. However, the gamma spectra in coincidence with the K-conversion lines of the 0.163 and 0.168 Mev transitions contain some transitions in the energy region from 0.55 to 0.80 Mev. These transitions are not shown in the decay scheme, but they are known to feed one or both of the levels at about 0.168 Mev. Their estimated intensity is 0.04 ± 0.02 which accounts for a large portion of the discrepancy discussed above.

4.3 Discussion

The decay scheme presented in Figure 19 has been proposed to explain the results obtained during the course of the present work.

The levels at excitation energies of 0.0048 Mev, 0.0696 Mev, 0.1048 Mev, 0.345 Mev, 0.445 Mev, 0.740 Mev, 0.820 Mev and the existence of one level at about 0.168 Mev have been established on the basis of both energy fit and coincidence experiments. The levels at 0.0658 Mev, 0.0915 Mev, 0.209 Mev, 0.324 Mev and the existence of the doublet at 0.168 Mev were added by Geiger and Graham (1962) on the basis of precise energy measurements of conversion electrons.

The intensities of the gamma transitions were obtained by measuring α_K for the 0.340 Mev transition and comparing the conversion electron intensity to the total beta intensity. The strengths of the low energy transitions were estimated from conversion electron intensities. The distribution of beta group intensities which would be required to satisfy the level scheme is in reasonable agreement with that obtained by a Fermi analysis of the beta spectrum. The only case where there is any discrepancy is the 0.750 Mev group which is found from the Fermi analysis to be 11 per cent, but the transitions depopulating the 0.445 Mev level add up to only 4.7 per cent of the decay.

The total intensity of all the transitions leading to the ground state and the 0.0048 Mev level, including the 1.195 Mev beta group, adds up to 95 per cent. Since this quantity depends on the normalization of the gamma intensities to the total beta intensity, it is subject to errors in the measurement of α_K for the 0.340 Mev transition and in the total beta continuum. It is also possible that the detector efficiency was less than 100 per cent for the conversion electrons below 60 kev which make up an appreciable fraction of the intensity feeding the two lowest levels. In view of these uncertainties, it is considered that

the beta and gamma intensity scales are consistent.

The beta intensities and corresponding log ft values for the various beta groups are shown on the decay scheme. The log ft values are insufficient to give much indication of the level spins in Sm^{151}. In some cases this is so because only lower limits are established. In other cases, even though the log ft values may be well known, this does not determine the type of beta transition uniquely. For instance, the 0.850 Mev beta group has a log ft value of 6.8. This could be either a first forbidden or an allowed hindered transition (see Table IX of Mottelson and Nilsson, 1959). It is known from section 4.2.5 that the levels at 0.0048 Mev, 0.0696 Mev, 0.1048 Mev and 0.209 Mev have the same parity as the ground state, whereas the levels at 0.821 Mev, 0.445 Mev, 0.345 Mev and one level at 0.168 Mev have the opposite parity. Thus, if the 0.850 Mev beta group is first forbidden, the 1.195 Mev, 1.13 Mev and 1.09 Mev groups must be either allowed or second forbidden. The log ft values for these groups range from 7.8 to 8.5 which do not seem reasonable for either allowed or second forbidden transitions. The more logical choice is that the 0.850 Mev group is an allowed hindered transition and then the above three groups could be first forbidden. This implies that the 0.38, 0.45 and 0.75 Mev beta groups, with log ft values of 6.6, 7.0 and 7.6, respectively, are also allowed hindered. It also implies that the ground states of Pm^{151} and Sm^{151} have opposite parities.

The recently published data of Harmatz et al. (1962) are shown in Table IV and in Figure 23. It is seen that these data further

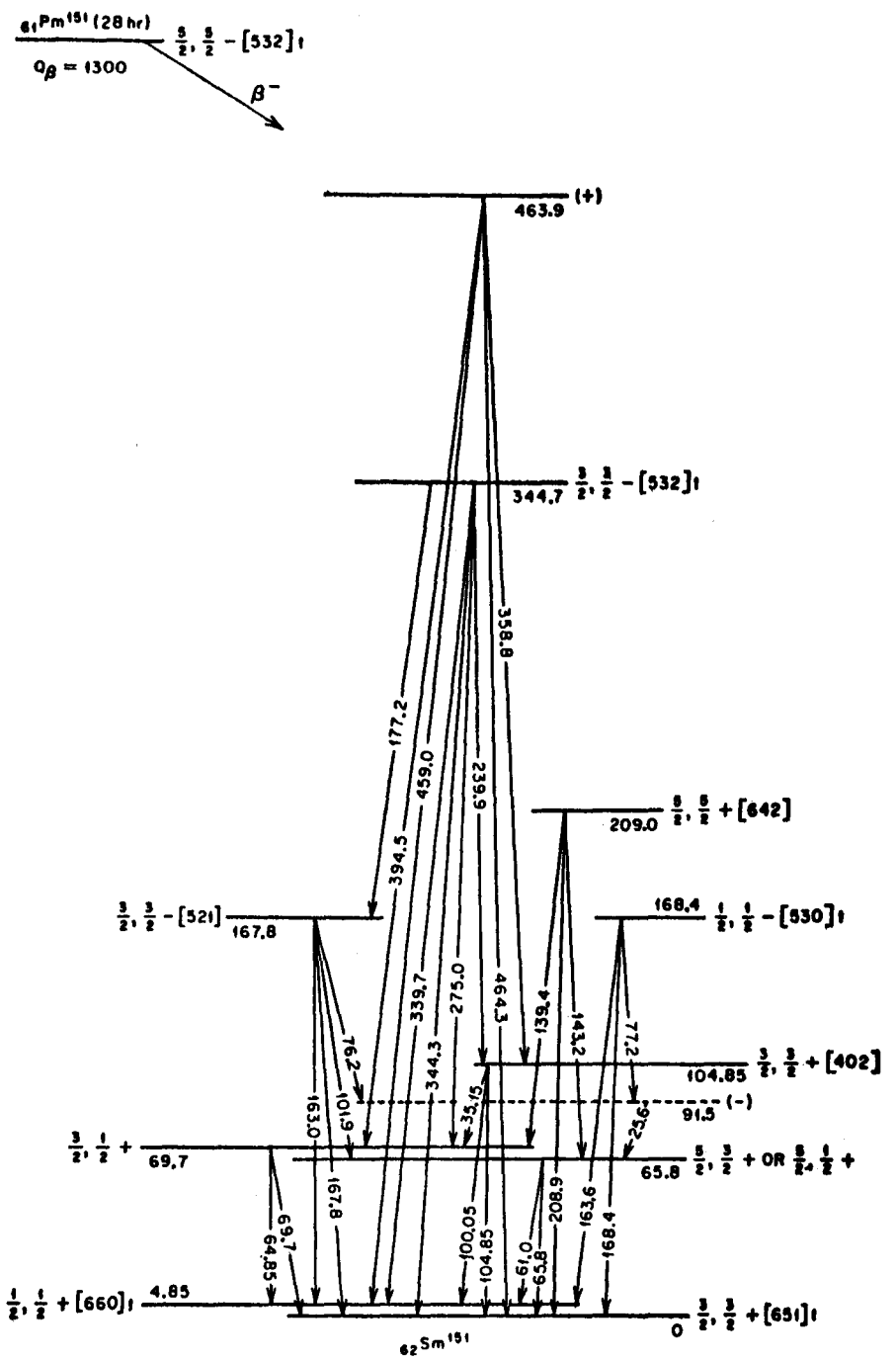

Fig. 23. Sm^{151} level scheme proposed by Harmatz et al. (1962)

TABLE IV

Internal conversion electron data from the work of Harmatz et al. (1962)

Transition energy (keV)	K	L_I	L_{II}	L_{III}	M	N	Remarks[a,b]
25.6		*d*	~60[e]	*d*	~60	15	*E*1
35.15		~10	70	80	35	10	*M*1/*E*2 = 2
58.6[e]			25	25	*d*		*E*2
61.0			~13	13	*w*		*E*2
64.85	>1000	400	*w*	*d*	100	30	*M*1
65.8	>700	~280[d]	70	60	80	20	*M*1/*E*2 ≈ 30
69.7	>300	85	~8	*d*	25		*M*1
76.2	>100	~17	105	115	70	12	*E*2
77.2	20	*d*					
89.0[e]	8	*w*					
100.05	1000	<250[d]		*w*	50	15	*M*1
101.9	80	13	*c*	~6	*w*		*E*1
104.85	~1250[d]	210	17	7	50	12	*M*1
105.8[e]	~15						
109.6[e]	~10	*w*					
112.05[e]	~12						
139.4	<250[d]	~20			*w*		
143.2	27	8					
149.6[e]	~8						
156.25[e]	20	~6		*w*			
163.0	14	*c*					
163.6	200	30	*c*	~5	*d*		*E*1
167.8	175	23		*d*	*d*		
168.4	130	19		*d*	*d*		
177.2	390	58	*c*		18		*M*1
186.4[e]	~5	*w*					
188.1[e]	~5	*w*		*w*			

Energy (keV)	K	L_I	L_{II}	L_{III}	M	Remarks[a,b]
208.9	120	20	*c*		6	*M*1
219.5[e]	*w*					
232.35[e]	70	13				*M*1
236.8[e]	15	*d*				
239.9	45	~9		*d*		
251.1[e]	*w*					
257.5[e]	*w*					
275.05	55	8		*w*		
280.0[e]	~11[d]	*w*				
290.8	3.3					
323.7[e]	9					
339.65	100	15		*w*		
344.4	11	*w*				

Energy (keV)	K	Energy (keV)	K	Energy (keV)
358.8	*w*	447.3[e]	3.5	547.0
394.5	~5	459.0		555.5[e]
422.9[e]	~5	464.3		715.3[e]
433.6[e]	~4.5	467.8[e]		833.4
440.1	~5	498.1[e]		838.2
445.0	12	542.0		850.7[e]

[a] Multipole assignments are based in *K*/*L* and *L*-subshell ratios.
[b] Intensity data are normalized to 1250 units for the most prominent line. "*w*" indicates weak line.
[c] Conversion line is partially resolved.
[d] Conversion line is a composite of two different lines
[e] Not placed in decay scheme.

verify the level structure proposed in Figure 19. In addition, they provide relative conversion electron intensities and multipolarities for some of the transitions which were not resolved in this laboratory. These multipolarities are consistent with the parity assignments of Figure 19, with one exception. Harmatz et al. (1962) suggest that both of the levels at 0.168 Mev have parity opposite to that of the ground state. However, Ewan (1962) has shown that the two levels at 0.168 Mev do not have the same parity. From the work of Harmatz et al. it is seen that their parity assignment for the 0.1677 Mev level is based on the multipolarities of three transitions, whereas that of the 0.1684 Mev level is based on the multipolarity of only one transition. As the 0.1677 K and 0.1684 K peaks have approximately the same intensity but the 0.1635 K peak is much stronger than the 0.1629 K, it is seen that the relative intensities and "average" values of α_K in Table II are consistent with the assumption that the 0.1629 and 0.1677 Mev transitions are E1, while the 0.1635, 0.1684 and 0.1771 Mev transitions are E2 + M1. This means that the 0.1684 Mev level would have the same parity as the ground state, whereas the 0.1677 Mev level would have opposite parity.

At the present time, no direct measurements of the spin, magnetic dipole moment or electric quadrupole moment of the ground state of Sm^{151} have been made. Hence, any assignments of the spin and parity of this state are necessarily based on speculation. If one investigates the trends in nuclear properties with mass numbers, it is seen that this nuclide poses a difficult problem from the theoretical point of view. It is well known that a sudden increase in the deformation of nuclei is found as the mass number increases through the value $A \sim 150$. To

be more exact, the sudden increase in deformation is found between neutron numbers 88 and 90, nuclides with 90 neutrons usually having a large deformation, whereas those with 88 neutrons have a relatively small deformation (Mottelson and Nilsson, 1959)), The nuclide Sm^{151} has 89 neutrons and therefore is in the transition region between the above two cases.

The Nilsson model of the deformed nucleus (Nilsson, 1955) has had great success in explaining the level schemes of many nuclei with large permanent deformations. However, Sm^{151} is just on the edge of the region where large deformations are found so it is not certain that the Nilsson model can be expected to explain the level structure shown in Figure 19. Perhaps an extension of the Davydov-Filippov model, such as has been worked out by Hecht and Satchler (1962) should really be used in the present case, since this theory is intended to be applicable even in the transition regions from small to large deformation. On the other hand, the experimental data available are insufficient to make unique spin and parity assignments to the complex of levels identified. Thus, one cannot proceed from either a secure experimental or a secure theoretical base to make interpretations. One fact, obvious from the large number of low-lying excited states, is that collective motions must play an important part in the interpretation of the level scheme.

The ground state spin of Pm^{151} has been measured to be 5/2 (Cabezas et al.1961). The Nilsson diagram (Figure 3 of Mottelson and Nilsson, 1959) shows that there are two possible particle states with spin 5/2 for the 61st proton. For a deformation $\delta > 0.2$ the odd

proton should be in the 5/2 5/2 - [532] orbital, whereas for $\delta < 0.2$ it is expected to be in the 5/2 5/2 + [413] orbital. (Quantum numbers used here are JK π [N $n_3 \Lambda$] as in section 2.3.) Harmatz et al. (1962) have assigned the 5/2 5/2 - [532] orbital to the ground state of Pm^{151} because there are 90 neutrons and therefore the deformation is probably quite large.

It is seen from the decay scheme in Figure 19 that in the present work the 5/2 5/2 + [413] orbital has been assigned to the ground state of Pm^{151}. This decision was made on the basis of the magnetic dipole and electric quadrupole moments which have been measured by Budick (1962) to be 1.8 ± 0.2 nm. and 2.9 ± 0.4 barns, respectively. The top half of Figure 24 shows the expected values of the electric quadrupole moment calculated as a function of the deformation δ, for both weak coupling and strong coupling cases. The cross-hatched area indicates the experimental value of 2.9 ± 0.4 barns. In view of the fact that Pm^{151} has many low-lying levels and appears to have a rotational band based on the ground state (Schmid and Burson, 1959), it seems logical to assume that this nucleus approaches the strong coupling limit. Hence, the quadrupole moment measurement indicates that the deformation is probably in the region of $\delta \sim 0.3$.

The lower half of Figure 24 shows the theoretical values of the magnetic dipole moment for the 5/2 5/2 + [413] and 5/2 5/2 - [532] orbitals calculated from the Nilsson model. Again, the cross-hatched area indicates the experimentally observed value. It is seen that neither orbital has a dipole moment which agrees with the experimental measurement for a deformation of ~ 0.3, but the 5/2 5/2 + [413] orbital

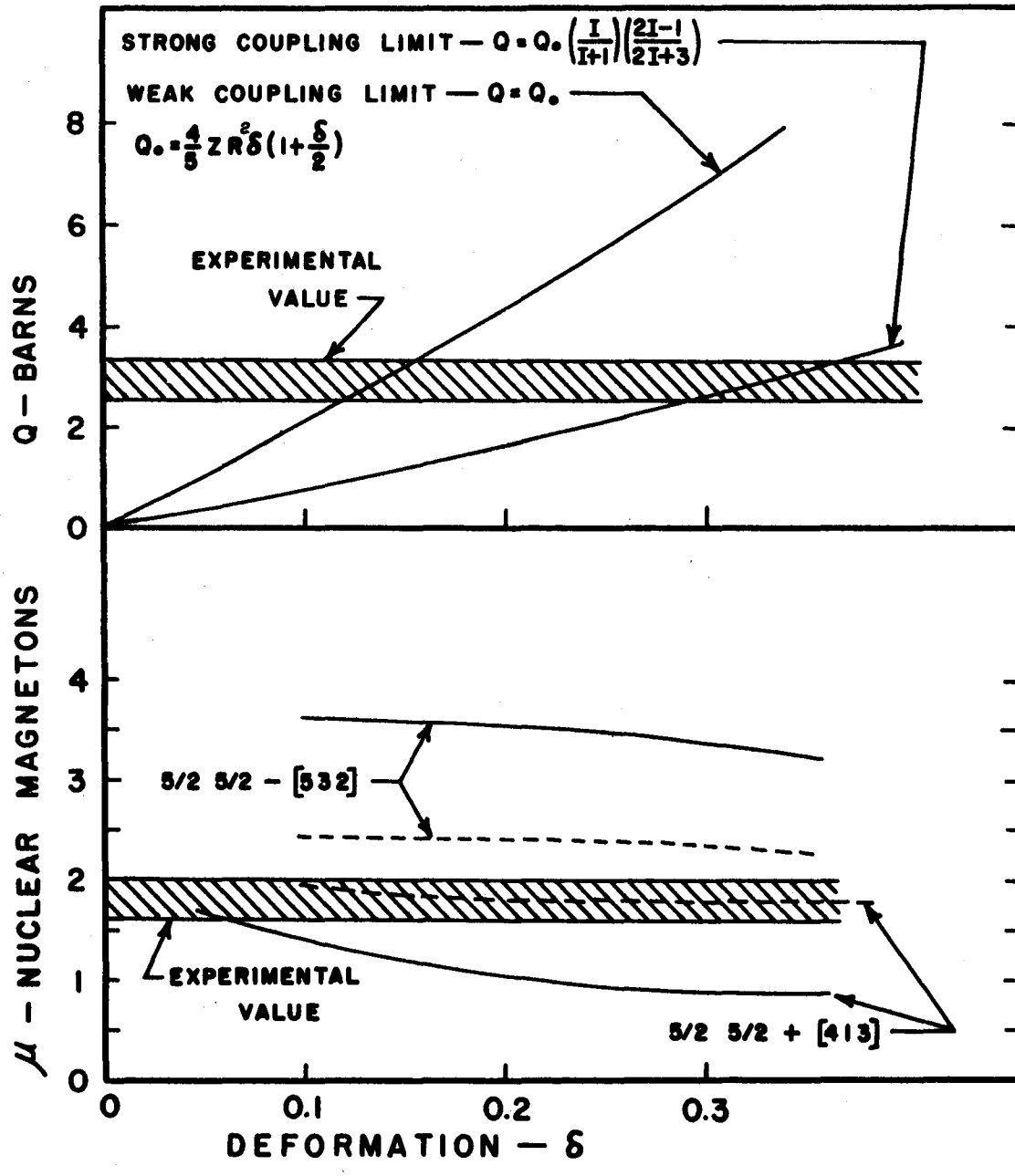

ELECTRIC QUADRUPOLE AND MAGNETIC DIPOLE MOMENTS FOR Pm^{151}

FIGURE 24

would fit the experiment for small deformations. It is noted, however, that the solid lines in the diagram represent extreme "single particle" limits and if any quenching of the intrinsic proton moment takes place the values for the 5/2 5/2 + [413] orbital would be raised and those for the 5/2 5/2 - [532] orbital would be lowered. The maximum possible variation which can be attributed to such quenching is shown by the dashed lines in Figure 24 where the calculations have been carried out assuming no anomalous proton magnetic moment (i.e. using a spin g-factor of 2). It is seen that such a strong measure as this would bring values for the 5/2 5/2 + [413] orbital into an agreement with experiment but would not do so for the negative parity orbital. In view of the discrepancies between the various values of magnetic dipole moments found in the literature, it is also possible that the experimental value of 1.8 nm is slightly too large.* Since, in general, the 5/2 5/2 + [413] orbital is closest to the experimental value, it has been chosen for the ground state of Pm^{151} in the present work. The fact that neither of the orbitals agrees well with the experimental measurement could be an indication that the simple Nilsson model is not really applicable to this nucleus. For instance, a deviation from

---

*Lindgren (1962), for instance, discusses some of the difficulties in interpretation of the experimental data which give rise to uncertainties in the quoted values for the moments. Budick (1962) has actually measured the ratio of the magnetic moments of Pm^{151} and Pm^{147} and used the atomic beam measurement of 3.2 nm for Pm^{147} to get the value of 1.8 nm for Pm^{151}. However, Stapleton et al. (1961) have measured the Pm^{147} magnetic moment to be 3.0 ± 0.3 nm and Klinkenberg et al (1960) obtain a value of 2.7 ± 0.3 nm from optical spectroscopy. If one of these lower values is used, the experimental value for the magnetic moment of Pm^{151} would be reduced by the same proportion.

axial symmetry could have an effect upon the magnetic moment. Unfortunately, the calculations of Newton (1960) do not go to high enough values of Z to settle this point.

If the ground state parity of Pm^{151} is even, then that of Sm^{151} must be odd, because it was shown earlier in this section that the two must be opposite. The ground state spin of Sm^{151} must be 3/2, 5/2 or 7/2 because it decays to the spin 5/2 state of Eu^{151} by means of an allowed or first forbidden beta transition (log ft = 7.5). Thus, the choice is narrowed down to the Nilsson orbitals with spin 3/2, 5/2 or 7/2 and odd parity. The orbitals which best satisfy these conditions are the 3/2 3/2 - [521] and 5/2 5/2 - [523]. Further away from the N = 89 position in the Nilsson diagram is the 3/2 3/2 - [532] orbital. The assignment of any of these orbitals to the ground state of Sm^{151} differs from the choice of Harmatz et al. (1962) who have assigned the 3/2 3/2 + [651] orbital to this level from analogy with isotone Gd^{153} and with odd-A Z = 89 isotopes.

From the above discussion, it is seen that the problem of a spin and parity assignment for the ground state of Sm^{151} is still unsettled and that assignments to excited levels are therefore speculative in nature. However, from their multipolarity measurements, Harmatz et al. (1962) have set up a possible spin sequence, assuming the ground state to be 3/2 + as mentioned above. They have then proceeded to suggest possible assignments for some of the levels on the basis of the Nilsson model. These assignments, which can be seen in Figure 23, have been given with due consideration for the trends of the Nilsson orbitals in neighbouring nuclides. In general, it is seen that these assignments,

although not necessarily unique, are consistent with the observed transition intensities and mixing ratios. There are only one or two curious circumstances which might be pointed out. For instance, it is unusual that no levels with spin 7/2 are found. There should be an abundance of 7/2 levels in rotational bands based on the 3/2 and 5/2 states. The beta transitions from spin 5/2 Pm^{151} to 7/2 levels in Sm^{151} should be comparable in intensity to those which feed 3/2 and 5/2 states and stronger than the transitions feeding states with spin $\frac{1}{2}$.

It is also noted that the $\frac{1}{2}$ + [660] orbital is a case with $K = \frac{1}{2}$ and hence may have a disturbed ordering of the levels in the rotational band due to the Coriolis term (see section 2.2). Calculations based on Nilsson's model show that, for $0.1 < \delta < 0.3$, the decoupling parameter, a, has a value between 6 and 7. This value is so large that one would expect the 5/2, or perhaps even the 9/2, level in the rotational band to have the lowest energy. In the decay scheme shown by Harmatz et al. (1962) this orbital is assigned to the level at 4.8 kev and the level with spin $\frac{1}{2}$ has the lowest energy.

One more interesting point is that the 0.0762 Mev E2 transition has an intensity approximately 18% as great as the 0.1678 Mev E1 transition depopulating the same level. Estimates of the probabilities for single particle transitions indicate that the E1 transition should be approximately 10^6 times as fast as the E2 transition. It is logical to assume that the observed enhancement is due to collective motions and that the 0.0915 and 0.1678 Mev levels are part of the same rotational band.

The assignments shown on the level scheme in Figure 19 are suggested with the above difficulties in mind. Following Harmatz et al. (1962) the levels at 0.0658 and 0.0697 Mev are assumed to be rotational levels based on the ground state and the 0.0048 Mev level, respectively. The M1 character of the 0.0649, 0.0658 and 0.0697 Mev transitions and the E2 character of the 0.610 Mev transition are explained very nicely by assuming the spin sequence I, I-1, I+1, I for the first four levels. It is seen that the 0.0256 Mev transition feeding the 0.0658 Mev level is E1 and that no competing transitions to the levels at 0, 0.0048 or 0.0697 Mev are observed. This suggests a spin of I + 2 for the positive parity level at 0.0915 Mev.

It was shown earlier in this section that the only negative parity Nilsson orbitals which were logical choices for the ground state of Sm^{151} were 3/2 3/2 - [521], 3/2 3/2 - [532] and 5/2 5/2 - [523]. From the above discussion, it is seen that the first two of these would result in a spin of 7/2 for the 0.0915 Mev level. As there are no Nilsson orbitals with spin 7/2 predicted, it seems more logical to choose the 5/2 5/2 - [523] orbital for the ground state, in which case the 0.0915 Mev level is 9/2 + . If one assumes that this is the 9/2 level based on the $\frac{1}{2}$ + [660] orbital and that the level at 0.1678 Mev is the 5/2 + member of the same rotational band, the available multipolarity data for these two positive parity states can be explained nicely. Also, from the work of Harmatz et al., the gamma intensity feeding the 0.0915 Mev level is somewhat greater than the estimated intensity of the 0.025 Mev transition. Thus, any beta group which feeds the 0.0915 Mev level is probably quite weak. This would be expected if the level

were 9/2 + as the beta transition would be second forbidden.

If the above assignments are correct, the spins of several other states can be predicted. The 0.1048 Mev level must be either 3/2 - or 5/2 - because of the M1 transitions to the ground state and 0.0048 Mev level. In view of the fact that no transition to the 7/2 - level at 0.0658 Mev has been found, the choice of 3/2 - seems most probable. The level at 0.3239 Mev decays by E1 and M1 transitions to the ground state (5/2 -) and 0.0915 Mev level (9/2 +), respectively, and hence must be 7/2 +. The 0.1684 Mev level feeds the 0, 0.0048, 0.0697 and 0.0915 Mev levels and thus has a spin of either 5/2 or 7/2. This may be the 7/2 + member of the rotational band based on the 0.0048 Mev level. Similarly, levels at 0.2090, 0.3449 and 0.4445 Mev must have spins of 3/2 or 5/2.

If one examines the decay from the 0.3449 Mev level, strong E1 transitions are found to the 0.0048 and 0.0697 Mev levels. The fact that these transitions are considerably stronger than the E1 ground state transition is further evidence that the levels at 0.0048 and 0.0697 Mev may be members of a rotational band. It is an easy matter to calculate the relative intensities of single particle transitions from a given state to the various levels in a rotational band because the dependence on the initial and final spins can be absorbed into a geometrical factor which does not depend on the nuclear properties. Following Preston (1962) the reduced transition probability (see section 1.3) can be written

$$B = (J_i \lambda K_i K_f - K_i \mid J_f K_f)^2 \left| \langle K_f \mid 0 \mid K_i \rangle \right|^2$$

It is seen that the only dependence on the J's occurs in the Clebsch-Gordan coefficient. Hence, for given values of K's and J's, the ratios of the transition intensities are simply ratios of Clebsch-Gordan coefficients. Such ratios have been calculated for the 0.340 and 0.275 Mev transitions assuming the most probable values of J and K for the 0.3449 Mev level. The calculations have also been made for different J and K assignments for the 0.0048 and 0.0697 Mev levels. The results are given in the following table where the energy dependence of the transition rates has also been included.

Assumed J and K for the level at						$\frac{T(E1)_{340}}{T(E1)_{275}}$
0.3449 Mev		0.0697 Mev		0.0048 Mev		
J	K	J	K	J	K	
3/2	3/2	5/2	3/2	3/2	3/2	2.82
5/2	3/2	5/2	3/2	3/2	3/2	1.95
5/2	5/2	5/2	3/2	3/2	3/2	4.40
3/2	3/2	3/2	1/2	1/2	1/2	2.35
3/2	1/2	3/2	1/2	1/2	1/2	9.4
5/2	5/2	7/2	5/2	5/2	5/2	4.70
7/2	5/2	7/2	5/2	5/2	5/2	1.02
5/2	3/2	7/2	5/2	5/2	5/2	0.75

The experimental value for this ratio is 3.3 ± 0.4 which not only suggests that the 0.3449 Mev level is 3/2 3/2 but tends to confirm the assignments already made to the 0.0048 and 0.0697 Mev levels.

Another pertinent experiment which should be considered is a gamma-gamma angular correlation measurement by Chery (1962). The angular correlation patterns have been measured for the "65" - 275, "100" - 240 and "165" - "175" kev cascades. It is now known that each one of the photopeaks considered would include several transitions and thus it may be difficult to determine which cascade is responsible for any anisotropy which may be found.

It is customary to write $w(\theta) = 1 + A_2P_2(\cos\theta) + A_4P_4(\cos\theta)$ where $w(\theta)$ is the probability that the cascading gamma rays will be emitted at angle θ to each other, the A's are constants and the $P(\cos\theta)$ are Legendre polynomials. Chery (1962) gives the following values for A_2 and A_4 for the three cascades measured.

Cascade	A_2	A_4
"65" - 275	0.090 ± 0.011	-0.078 ± 0.011
"100" - 240	0.080 ± 0.017	0.062 ± 0.018
"165" - "175"	0.180 ± 0.080	-0.057 ± 0.081

The third cascade is largely made up of the 0.1771 and 0.1677 Mev dipole transitions. With the spin sequence 3/2,5/2,5/2 shown in Figure 19 for this cascade, one would expect $A_2 = -0.043$ (Ferentz and Rosenzweig (1955)) which does not agree with the measured value of 0.180 ± 0.080. The 0.1771 - 0.1629 Mev cascade, which would also be included in this measurement, would have a spin sequence 3/2,5/2,3/2 for which $A_2 = +0.14$

but this should not change the pattern very much as the 0.1677 Mev transition is much stronger than the 0.1629 Mev transition. The experimental value would be better explained by assuming J = K = 5/2 for the 0.3449 Mev level (which is not quite as probable on the basis of the E1 intensity ratios discussed earlier). Then the spin sequence would be 5/2,5/2,5/2 for which A_2 = 0.18. However, it is difficult to estimate how much weight should be put on the angular correlation experiments when there is the possibility of other interfering transitions. For instance, it is noted that the first two cascades above have very large values for A_4 but, since these are all dipole transitions, A_4 should be zero. In view of the fact that the experimental values for these two cascades do not agree with the well-substantiated multipolarity results, the data for the third cascade may be questioned, as they are subject to similar experimental difficulties. Thus, although there is some doubt, it seems most likely that J = K = 3/2 for the 0.3449 Mev level and the 3/2 3/2 + [651] orbital has been assigned to this state.

In view of the lack of knowledge which still exists concerning spin values for other states, it seems pointless to make further assignments of orbitals. It is seen, however, that there are many Nilsson particle states in the region and only a few of them have been used in Figure 19.

An examination of the trends of single particle states in neighbouring nuclides (see, for example, Table XXXI of Harmatz et al. (1962)) shows that the assignments suggested in Figure 19 are not unreasonable if one considers that Sm^{151} may not be strongly deformed

and that the deformation may be different for the various intrinsic states. The choice of spins and paritics in Figure 19 overcomes some of the weak features present in the decay scheme given by Harmatz et al. (1962). However, there is not enough evidence as yet to say which, if either, of the two schemes is correct and there still may be some questions which neither scheme explains well. For instance, there is still no good explanation for the fact that the E1 transition from the 0.3449 Mev level to the 0.00485 Mev level is enhanced more than an order of magnitude over the E1 ground state transition.

Whereas it is not yet possible to make unique spin and parity assignments for the levels in Sm^{151}, the future looks bright. Mr. Keith Eastwood of the Atomic Beams Group at this university has undertaken to measure the spin and magnetic moment of the Sm^{151} ground state. Also, when the complete results of Geiger and Graham (1962) and Ewan (1962) become available, it is certain that multipolarities will be known for more of the transitions. The additional information from these sources should remove most of the ambiguities discussed above.

SUMMARY

The transitions in Sm^{151} following the beta decay of Pm^{151} have been studied by internal and external conversion techniques. In addition, a series of coincidence experiments were performed with a double lens coincidence spectrometer. A decay scheme containing 39 transitions and 14 levels has been proposed. The levels at excitation energies of 0.0048, 0.0697, 0.1048, 0.345, 0.445, 0.741 and 0.821 Mev and the existence of one level at about 0.168 Mev have been established on the basis of both the energy fit and coincidence experiments. The levels at 0.0658, 0.0915, 0.209 and 0.324 Mev and the existence of the doublet at 0.168 Mev were added by Geiger and Graham (1962) on the basis of precise energy measurements of conversion electrons.

The strengths of the beta groups feeding various levels were obtained by Fermi analysis of the beta spectrum or by coincidence measurements. In general, the values obtained are found to give a good balance of intensities feeding into and out of each level. The total decay energy of Pm^{151} is 1.195 ± 0.010 Mev.

One of the interesting features of this decay scheme is a level at 0.0048 Mev. The conversion electrons of the ground state transition from this level have been observed and the half-life of the state has been measured to be 19 ± 10 nanoseconds.

Finally, speculations are made concerning the possible interpretation of the levels on the basis of the Nilsson model. These suggestions are compared with similar conjectures reported in a recent article by Harmatz et al. (1962).

APPENDIX A

SOURCE PREPARATION

For the study of beta spectra and internal conversion lines, it is necessary to have "thin" sources in order to reduce the amount of energy lost by the electrons in escaping from the source material. The actual thickness which can be tolerated increases with electron energy. In many studies, the source thickness places a lower limit on the energy of electrons which can be used in a given experiment. Fortunately, the nuclear reactions used to produce Pm^{151} make it possible to prepare carrier-free sources by an ion exchange separation. A vacuum sublimation technique can then be used to deposit the active material on the source holder in what, theoretically, could be a monatomic layer.

For the sources used in the present study, approximately 3 to 5 mg. of Nd, enriched to 95.65 percent Nd^{150}, were irradiated in the McMaster reactor at a flux of 1.5×10^{13} $n/cm^2/sec$ for periods of from 8 to 70 hours. Neutron capture resulted in Nd^{151} which decayed to Pm^{151} by beta emission with a half life of 12 minutes. Hence, about two hours after the end of irradiation essentially all of the Nd^{151} had decayed to the 27.5 hr. Pm^{151}. After removal from the reactor, the quartz capsule containing the sample was broken under 6N HCl and the contents were dissolved by heating. The solution was evaporated to dryness, re-dissolved in water and placed on an ion exchange column containing Dowex 50, 400 mesh, cation resin. This column was 0.3 cm in diameter and 10 cm long. It

had previously been washed with a solution of NH_4Cl and rinsed with water. After making sure that the Nd^{151} had had time to decay to Pm^{151} the material was eluted from the column with alpha-Hydroxy-isobutyric acid with a pH of 4.2. The activity in the solution which dripped from the bottom of the column was monitored with an end window counter and as the different elements came down, at different times, they were collected in different beakers. The Pm was thus separated from the other activities amongst which were found Tb^{160}, Gd^{159}, Eu^{152m}, Sm^{153} and Nd^{147}.

The solution containing Pm was then acidified with HCl and placed on a second column containing Dowex 50W, 100 - 200 mesh, cation resin. After washing with distilled water and 1.5N HCl the Pm was eluted from the column with double distilled 6N HCl. This solution was placed under a heat lamp and evaporated until only a small drop of liquid remained. For most of the early sources, this drop was transferred with a pipette to a VYNS or mylar source holder.

For later sources, intended for experiments with low energy electrons, much thinner sources were made by a vacuum sublimation method. The apparatus for this process is shown in Figure 25. The small drop containing the Pm^{151} activity was placed in an indentation in the flat tungsten filament and dried with a heat lamp. The vacuum system was pumped down to a pressure of about 10^{-3} mm of Hg and pulses of current applied to the filament. As the material sublimed from the hot filament, some of it was deposited on the source holder which consisted of 800 gm/cm^2 aluminum foil, masked to limit the size of the source.

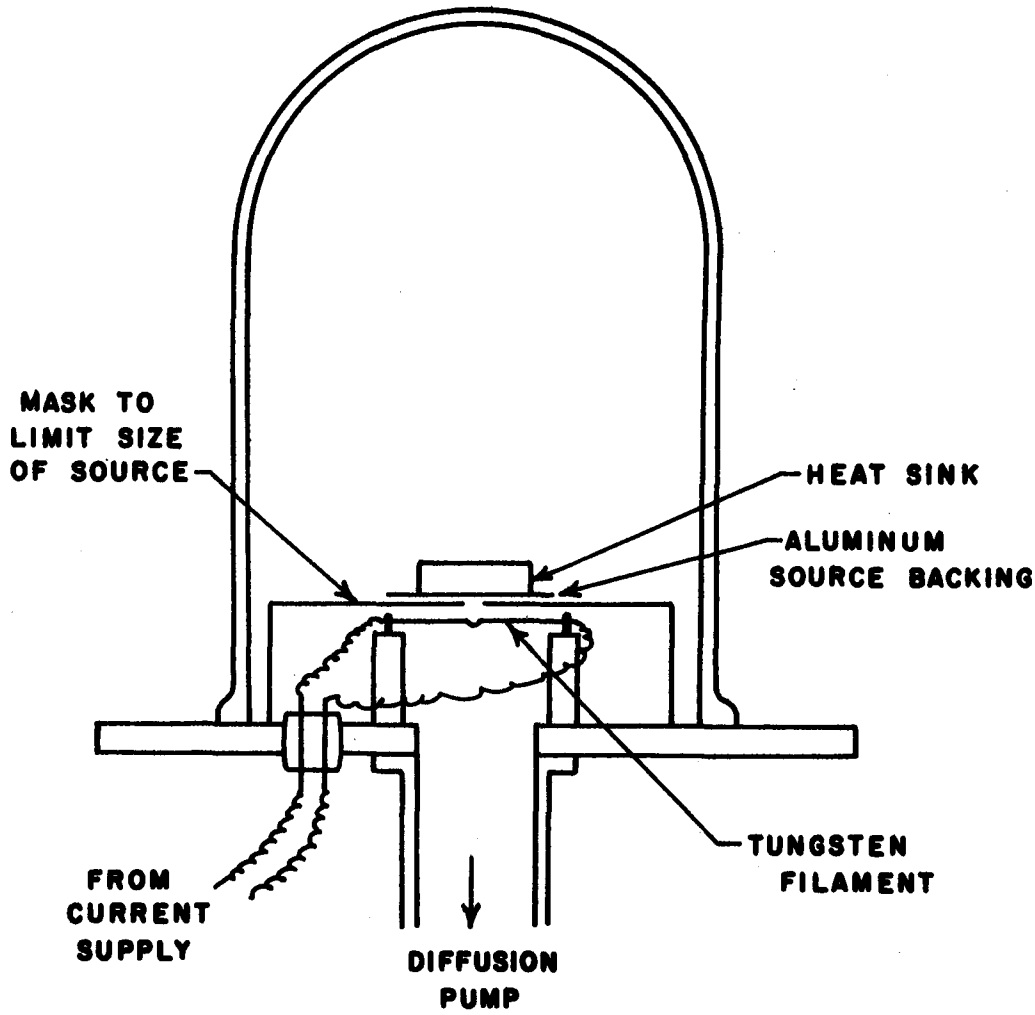

APPARATUS FOR PREPARATION OF SOURCES BY VACUUM SUBLIMATION

FIGURE 25

It was found that the drop of material invariably contained, in addition to the Pm, a small amount of inactive material which, if allowed to remain mixed with the activity, seriously increased the source thickness. However, it was found to have a lower sublimation temperature than the Pm and thus a separation could be effected on this basis. The voltage of the pulses applied to the filament was gradually increased until the filament glowed with a reddish-yellow heat with each pulse. At this temperature, the unwanted inactive material sublimed. A new source holder was then installed and the voltage of the pulses again increased until the Pm sublimed at a white heat. In this manner sources were obtained which were so thin that they could not be seen. It was found necessary to pulse the current to the filament in order to avoid melting the aluminum source holder. Periods of about one second on and ten seconds off were found to be satisfactory. The Timer and power supply circuits which were used for this purpose are shown in Figure 26.

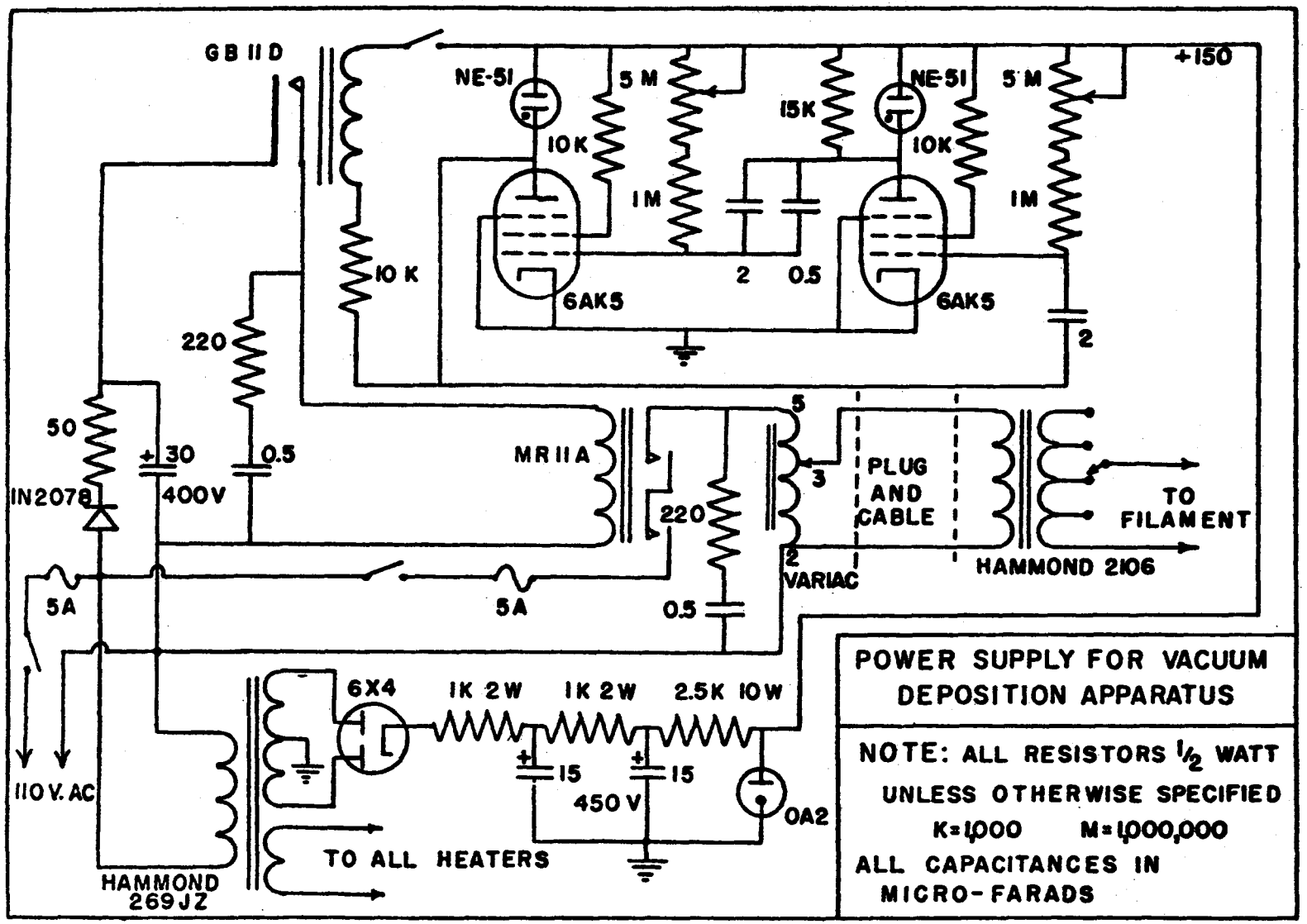
GB II D
NE-51
5 M
10K
1M
10 K
6AK5
220
50
±30
400V
0.5
IN2078
MR II A
220
5
3
2
VARIAC
PLUG AND CABLE
TO FILAMENT
HAMMOND 2106
5A
5A
0.5
15K
NE-51
5 M
10K
1M
2
0.5
6AK5
2
+150
6X4
1K 2W
1K 2W
2.5K 10W
15
15
450 V
0A2
110 V. AC
TO ALL HEATERS
HAMMOND 269JZ
POWER SUPPLY FOR VACUUM DEPOSITION APPARATUS
NOTE: ALL RESISTORS 1/2 WATT
UNLESS OTHERWISE SPECIFIED
K=1,000 M=1,000,000
ALL CAPACITANCES IN MICRO-FARADS

FIGURE 26

APPENDIX B

GEIGER COUNTER FOR LOW ENERGY ELECTRONS

The anthracene crystal-photomultiplier assembly normally used as a detector in the Gerholm spectrometer was unsatisfactory for low energy electrons because the signal was masked by photomultiplier noise. Whereas the 18 kev K-conversion line of the 65 kev transition could be found with this detector, the efficiency was only 20 to 30%. For electron energies below 30 kev, it was not possible to obtain a "plateau" in the single channel discriminator bias curve. Thus, when it was decided to look for the conversion electrons from the 4.8 kev transition, a more efficient detector was required.

For this purpose the Geiger counter shown in Figure 27 was constructed. The window of this counter had to be thin enough to transmit 3 kev electrons but strong enough to withstand a gas pressure of several centimeters of mercury. At the suggestion of J. S. Geiger, of the Chalk River Laboratories, the window was constructed of laminated VYNS films supported by an electroformed nickel grid. The grid used had a spacing of 100 lines per inch and an open area of 80%. VYNS films which had been formed on water and picked up with a wire hoop were allowed to stand for about a day. Ones which had not developed visible pinholes after this length of time were selected and laminated onto the nickel mesh in the dry condition.

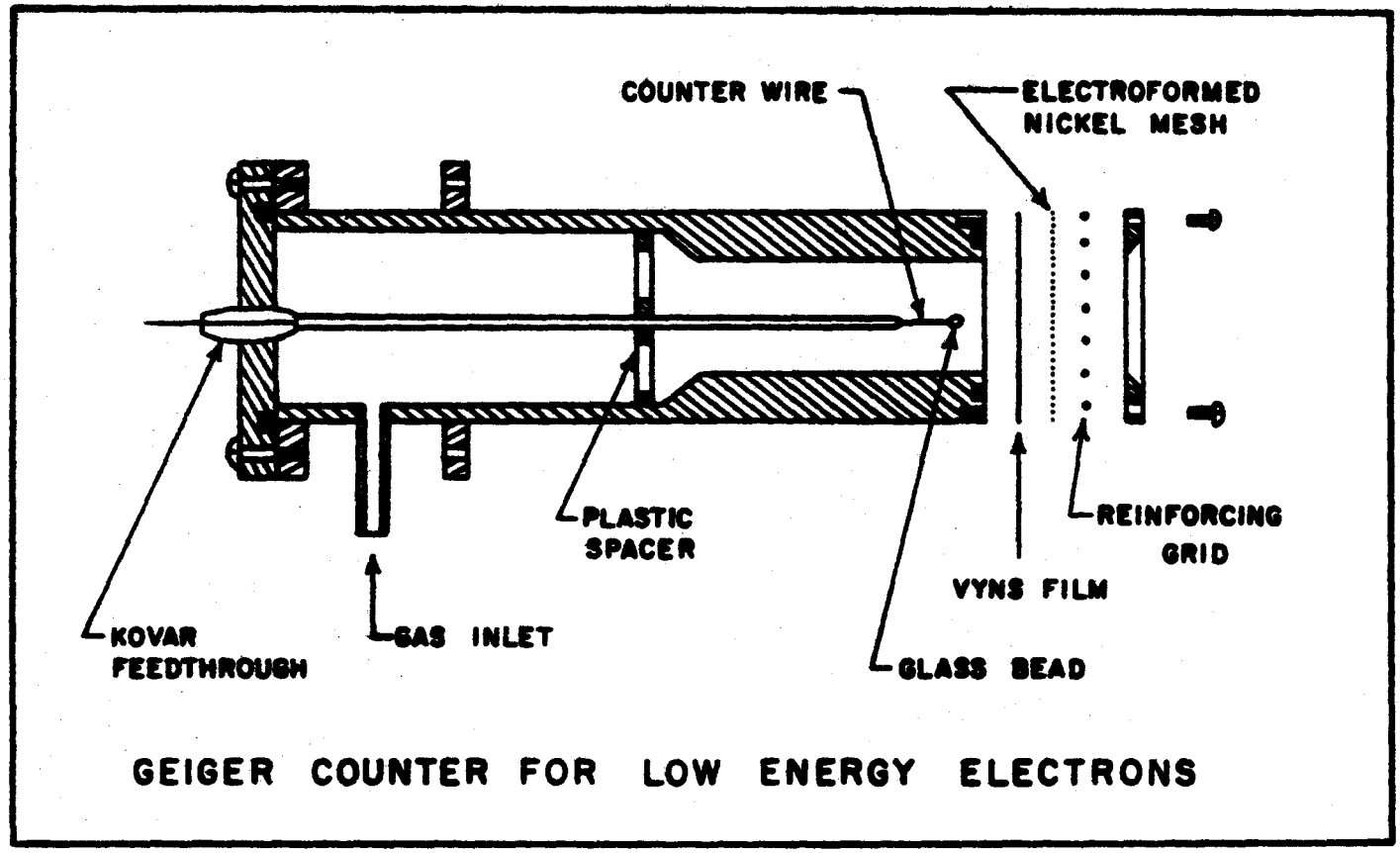
COUNTER WIRE
ELECTROFORMED NICKEL MESH
PLASTIC SPACER
REINFORCING GRID
VYNS FILM
KOVAR FEEDTHROUGH
GAS INLET
GLASS BEAD
GEIGER COUNTER FOR LOW ENERGY ELECTRONS

FIGURE 27

Experience showed that four films usually gave first-order reinforcement of reflected light in the purple to blue region. According to Pate and Yaffe (1955) this corresponds to a film thickness of 30 to 35 μgm/cm^2. For the actual experiments, only two such films were used and hence the window thickness was estimated to be 15 to 18 μgm/cm^2.

The counter was mounted in the pole face of the spectrometer in such a manner that the window was in the position normally occupied by the anthracene crystal. A filling of 1 part ethanol to 3 parts Argon (by volume) at a total pressure of 8 cm of Hg was usually used. Coincidence experiments with this detector were limited to a resolving time of about 300 nanoseconds due to the inherent time jitter in the counter.

It was found that this detector had some undesirable features and if the experiment were repeated some modifications would be made. One problem was the difficulty encountered in getting a window which did not leak. Most of the windows would allow some of the counter gas to escape, so that after a few minutes the pressure in the counter would be reduced. This necessitated a gradual reduction in the counter voltage in order to stay on the "plateau." This problem could be overcome by using a thicker VYNS window and applying post-acceleration to get the electrons through the extra window thickness.

Another worthwhile modification would be the removal of the glass bead on the counter wire. As mentioned in section 4.2.6, it was felt that the glass bead tended to "shield" part of the window area and increase the collection time for low-energy electrons. Better performance should result if a simple wire loop were used in place of this bead.

REFERENCES

Alaga, G., Alder, K., Bohr, A. and Mottelson, B. R. (1955) Kgl. Danske Vidensk. Selsk. Mat.-Fys. Medd. 29, No.9

Alaga, G. (1957) Nuclear Phys. 4, 625.

Artna, A. (1961) Ph.D. Thesis, McMaster University, Hamilton, Ontario.

Bay, Z. (1950) Phys. Rev. 77, 419.

Bell, R. E., Graham, R. L. and Petch, H. E. (1952) Can. J. Phys. 30, 35.

Belyaev, S. T. (1959) Danske Vidensk. Selsk. Mat.-Fys. Medd. 31, No.11.

Budick, B. (1962) University of California Report UCRL -10245.

Burke, D. G., Law, M. E. and Johns, M. W. (1963) Can. J. Phys. 41, 57.

Burson, S. B. and Schmid, L. C. (1958) Argonne National Laboratory Report No. 5937.

Cabezas, A. Y., Lindgren, I. and Marrus, R. (1961) Phys. Rev. 122, 1796.

Chery, R. (1962) Nuclear Phys. 32, 319.

Davydov, A. S. and Filippov, G. F. (1958) Nuclear Phys. 8, 237.

Davydov, A. S. and Rostovsky, V. S. (1959) Nuclear Phys. 12, 58.

Ewan, G. T. (1962) Private Communication.

Feenberg, E. and Trigg, G. (1950) Rev. Mod. Phys. 22, 399.

Ferentz, M. and Rosenzweig, N. (1955) Argonne National Laboratory Report No. 5324.

Fermi, E. (1934) Z. Physik 88, 161.

Frey, W. F., Hamilton, J. H. and Hultberg, S. (1962) Ark. Fys. 21, 383.

Geiger, J. S. and Graham, R. L. (1962) Private Communications.

Geiger, J. S., Graham, R. L. and Merritt, J. S. (1963) Bull. Am. Phys. Soc. Series II, 8, No.1

Gerholm, T. R. (1956) Ark. Fys. 11, 55.

Goldhaber, M., Grodzins, L. and Sunyar, A. W. (1958) Phys. Rev. 109, 1015.

Habib, E. (1961) Ph.D. Thesis, McMaster University, Hamilton, Ontario.

Hans, H. S., Saraf, B. and Mandeville, C. E. (1955) Phys. Rev. 97, 1267.

Harmatz, B., Handley, T. H. and Mihelich, J. W. (1962) Phys. Rev. 128, 1186.

Hatch, E. N. and Boehm, F. (1957) Phys. Rev. 108, 113.

Haxel, O., Jensen, J. H. D. and Suess, H. E. (1949) Phys. Rev. 75, 1766L.

Haxel, O., Jensen, J. H. D. and Suess, H. E. (1950) Z. Physik 128, 295.

Hecht, K. I. and Satchler, G. R. (1962) Nuclear Phys. 32, 286.

Johns, M. W., Waterman, H., MacAskill, D. and Cox, C. D. (1953) Can. J. Phys. 31, 225.

Kerman, A. K. (1956) Kgl. Danske Vidensk. Selsk. Mat.-Fys Medd. 30, No.15.

Klinkenburg, P. F. A. and Tomkins, F. S. (1960) Physica 26, 103.

Konopinski, E. J. and Uhlenbeck, G. E. (1941) Phys. Rev. 60, 308.

Lindgren, I. (1962) Nuclear Phys. 32, 151.

Mayer, M. G. (1948) Phys. Rev. 74, 235.

Mayer, M. G. (1949) Phys. Rev. 75, 1969L.

Mayer, M. G. (1950) Phys. Rev. 78, 16.

Miller, W. F., Reynolds, J. and Snow, W. J. (1958) Argonne National Laboratory Report No. 5902.

Mottelson, B. R. and Nilsson, S. G. (1959) Kgl. Danske Vidensk. Selsk. Mat.-Fys Skr. 1, No.8.

Murray, G., Graham, R. L. and Geiger, J. S. To be published.

National Bureau of Standards (1952) "Tables for the Analysis of Beta Spectra," Applied Mathematics Series No.13, U.S. Government Printing Office, Washington, D. C.

Newton, T. D. (1960) Can. J. Phys. 38, 700.

Nilsson, S. G. (1955) Kgl. Danske Vidensk. Selsk. Mat.-Fys. Medd. 29, No.16.

Nuclear Data Sheets (1959) National Academy of Sciences, National Research Council, Washington 25, D. C.

Pate, B. D. and Yaffe, L. (1955) Can. J. Chem. 33, 15.

Pauli, W. (1934) "Rapports du Septieme Conseil de Physique Solvay, Brussels, 1933, "Paris: Gauthier- Villars et Cie.

Preston, M. A. (1962), "Physics of the Nucleus," Addison-Wesley Publishing Co., Inc., Reading, Mass., U. S. A.

Ramberg, E. G. and Richtmyer, F. K. (1937) Phys. Rev. 51, 913.

Reines, F. and Cowan, C. L. (1953) Phys. Rev. 90, 492.

Reines, F. and Cowan, C. L. (1959) Phys. Rev. 113, 273.

Rose, M. E. Goertzel, G. H., Spinrad, B. I., Harr, J. and Strong, P. (1951) Phys. Rev. 83, 79.

Rose, M. E. (1958), "Internal Conversion Coefficients," North Holland Publishing Co., Amsterdam.

Rutledge, W. C., Cork, J. M. and Burson, S. B. (1952) Phys. Rev. 86, 775.

Sargent, B. W. (1925) Proc. Roy. Soc. A. 109, 541.

Schmid, L. C. and Burson, S. B. (1959) Phys. Rev. 115, 178.

Siegbahn, K. and Svartholm, N. (1946) Nature 157, 872.

Sliv, L. A. and Band, I. M. (1956 and 1958), "Coefficients of Internal Conversion of Gamma Radiation," USSR Academy of Sciences, Moscow, Leningrad.

Stapleton, H. J., Jeffries, C. D. and Shirley, D. A. (1961) Phys.Rev.124, 1455.

Valentin, J. (1962) Compt. rend. 254, 858.

Van Name, F. W. (1949) Phys. Rev. 75, 100.

Weisskopf, V. F. (1951) Phys. Rev. 83, 1073L.

Wu, C. S., Ambler, E., Hayward, R. W., Hoppes, D. D. and Hudson, R.P. (1957) Phys. Rev. 105, 1413.